

Electrification of the heat treatment process for iron ore pelletization at LKAB

Master's thesis within the Sustainable Energy Systems programme

Erik Lindén and Emil Thureborn

MASTER'S THESIS 2019

Electrification of the heat treatment process for iron ore pelletization at LKAB

ERIK LINDÉN
EMIL THUREBORN



CHALMERS

Department of Space, Earth and Environment
Division of Energy Technology
CHALMERS UNIVERSITY OF TECHNOLOGY
Gothenburg, Sweden 2019

Electrification of the heat treatment process for iron ore pelletization at LKAB

ERIK LINDÉN
EMIL THUREBORN

© 2019.

Supervisors:

Fredrik Normann, Division of Energy Technology, Chalmers
Adrian Gunnarsson, Division of Energy Technology, Chalmers

Assistant supervisor:

Samuel Nordgren, LKAB

Examiner:

Fredrik Normann, Division of Energy Technology, Chalmers

Master's Thesis 2019
Department of Space, Earth and Environment
Division of Energy Technology
Chalmers University of Technology
SE-412 96 Gothenburg
Telephone +46 31 772 1000

Cover: Schematic illustration of a linear plasma torch.

Typeset in L^AT_EX
Printed by: Chalmers Reproservice
Gothenburg, Sweden 2019

Electrification of the heat treatment process for iron ore pelletization at LKAB
ERIK LINDÉN
EMIL THUREBORN
Department of Space, Earth and Environment
Division of Energy Technology
Chalmers University of Technology

Abstract

LKAB is a Swedish state-owned mining company that extracts and refines iron ore for the global steel industry. Their main product is iron ore pellets which accounts for around 83 % of LKAB's iron ore products. The straight-grate process is used for heat treatment of the pellets and is the most energy-intensive part of the refining process. The heat is supplied by fossil fuel burners with considerable emissions of greenhouse gases and pollutants such as nitrogen oxides, which should be reduced to comply with emission targets set by LKAB as well as the Swedish government.

This project investigates electrical heating alternatives in the form of plasma torches and microwaves to replace the fossil fuel burners, providing potential for a CO₂-neutral production process. The work focus on how process conditions are affected when switching to an electric heat source. Process performance is evaluated through product quality, energy efficiency, emissions of CO₂ and NO_x. Furthermore, new potential process optimization measures as a result of the implementation of electric heating are discussed. A previously established process model of the straight-grate process was used to establish a reference case and several new cases where modifications were made to simulate the implementation of electric heating. NO_x emissions from plasma torches were studied by reaction modelling in Chemkin and results were evaluated against data from previous practical experiments.

Results showed that electric heating through microwaves may supply energy at low temperature to the drying process, which would allow for a more compact drying zone and replacement of up to 1 MW of fossil fuels. However, the total power demand of the process increased by 15 - 20 %. To supply heat at the high temperature required in the firing zones, plasma torches have the potential to replace the entire fossil fuel demand and achieve a CO₂ neutral process. The implementation of plasma torches only had a slight effect on pellet quality and energy efficiency. Simulations regarding NO_x emissions from plasma torches when mixing hot plasma gases with air shows that the formation of NO_x may be higher than from a fossil fuel burner. The most important factor for determining the NO_x emissions is the gas residence time at high temperatures. Reburning using small amounts of natural gas was the most efficient NO_x reduction strategy with NO_x reduction of up to 65 %. Future work should be directed towards financial analyses of the implementation of electric heating and experimental tests to prepare for practical implementation.

Keywords: Electrification, heat treatment, iron ore, straight-grate, pelletization, microwaves, plasma torches, nitrogen oxides, LKAB.

Acknowledgements

First of all, we would like to express our sincere gratitude towards our supervisors Fredrik Normann and Adrian Gunnarsson. Without their continuous support and feedback throughout our many meetings, this project would not have been possible. Fredrik was the one who motivated us to work with this project and has been vital in steering the project in the right direction while Adrian has been a great help with understanding the process model.

Furthermore, we would like to thank our assistant supervisor Samuel Nordgren at LKAB for providing us with modelling data and sharing his experience of the process. We would like to give a special thanks to Rikard Edland for providing valuable insight and guidance regarding the Chemkin modelling and NO_x emissions. We also want to express gratitude to our friends Herman, Johanna, Rasmus and Tove for reading our report and providing valuable feedback. Finally, we would like to thank everyone in the Department of Energy Technology for providing such a pleasant working environment.

Erik Lindén and Emil Thureborn, Gothenburg, June 2019

Contents

List of Figures	xi
List of Tables	xiv
Nomenclature	xv
1 Introduction	1
1.1 Background	1
1.2 Aim	3
1.3 Limitations	3
2 Theory	4
2.1 Iron ore processing	4
2.2 Pelletization heat treatment processes	6
2.2.1 Straight-grate process	6
2.2.2 Grate-kiln process	7
2.2.3 Heat treatment chemistry	9
2.3 Microwave heating	10
2.3.1 Microwave interaction with matter	10
2.3.2 Heating mechanisms and properties	11
2.3.3 Previous microwave applications for iron ore pelletization	12
2.3.4 Potential for application of microwaves at LKAB	14
2.4 Plasma torches	15
2.4.1 Definition of plasma	15
2.4.2 Plasma generation	16
2.4.3 Types of plasma torches	16
2.4.4 Industrial plasma torches	18
2.4.5 Application of plasma torches for iron ore pelletization	19
2.5 Nitrogen oxides	21
2.5.1 Formation of thermal NO	21
2.5.2 NO _x emissions from iron ore pelletization	22
2.5.3 NO _x emissions from plasma torches	23
2.6 Process model	23
2.6.1 BedSim model	23
2.6.2 Matlab framework	25

3	Methodology	26
3.1	Reference case	27
3.1.1	Performance indicators	28
3.1.2	Process constraints	29
3.2	Microwaves	30
3.2.1	New process design A	32
3.2.2	New process design B	32
3.3	Plasma torches	33
3.4	Nitrogen oxide formation	34
3.4.1	Reactor models	34
3.4.2	Validation and sensitivity analysis	36
4	Results and discussion	37
4.1	Reference case	37
4.1.1	Performance indicators	40
4.1.2	Process constraints	41
4.2	Microwaves	42
4.2.1	Microwave case study	42
4.2.2	New process designs	46
4.3	Plasma torches	48
4.3.1	Plasma torch case study	48
4.3.2	Optimization of plasma torch case	52
4.4	Nitrogen oxide formation	53
4.4.1	No-mixing case	54
4.4.2	Mixing case (temperature profile)	55
4.4.3	Mixing case (energy equation)	56
4.4.4	Model validation	57
4.4.5	Sensitivity analysis	57
4.4.6	Working gases and NO reduction	59
5	Conclusions	61
5.1	Recommendations for future work	62
5.2	New process concept	64
	Bibliography	66
A	Process parameter calculations	I
A.1	Power requirement of microwaves	I
A.2	Evaporation rate	II
A.3	Gas moisture saturation	II
A.4	Pressure drop	III
A.5	Mean magnetite mass fraction	III
A.6	Mean bed temperature	III
A.7	Energy balance	IV
B	Nitrogen oxide plots	V
B.1	NO reactions	V

Contents

B.2	No-mixing case	VI
B.3	Mixing case (temperature profile)	VIII
B.4	Mixing case (energy equation)	X

List of Figures

2.1	Schematic illustration of the straight-grate process.	6
2.2	Schematic illustration of the grate-kiln process.	7
2.3	Illustration of microwaves interacting with matter.	10
2.4	Heating a homogeneous particle by (a) Convective/conductive heating, (b) Microwave heating.	11
2.5	Simplified illustration of the four fundamental states of matter.	15
2.6	Schematic illustration of a linear plasma torch.	17
2.7	Vertical cross section of a firing chamber in the straight-grate process.	20
2.8	Illustration of the calculation method used in the BedSim model.	24
3.1	Visualization of the working procedure in this project.	26
3.2	Schematic illustration of the connections between process zones in the reference case.	27
3.3	Illustration of how the calculations are performed in the simulation model. The red streams are left unconnected.	28
3.4	(a) Original UDD (b) UDD and microwave zone configuration.	30
3.5	Illustration of connections between process zones. Gas flows which are modified compared to the reference case are marked in red.	32
3.6	Schematic illustration of the process streams considered for an oil burner (a) and a plasma torch (b).	33
3.7	Reactor dimensions for the NoMix case (a) and for the MixTP and MixEE cases (b).	35
4.1	Pellet temperature throughout the process for the reference case. The markings on the x-axis shows where each zone ends.	38
4.2	Mass fraction of magnetite throughout the process for the reference case.	38
4.3	Gas temperature throughout the process for the reference case.	39
4.4	Temperature differences between connected process zones for the reference case.	40
4.5	Pressure drop over the bed throughout the process for the reference case.	41
4.6	Temperature in the top layer of the grate throughout the process for the reference case.	42
4.7	Reference case moisture content.	43
4.8	Microwave case moisture content.	43
4.9	Reference case temperature profile.	44
4.10	Microwave case temperature profile.	44

List of Figures

4.11	New process design moisture content.	46
4.12	New process design pellet temperature.	46
4.13	Pellet temperature throughout the process for the reference case and the plasma torch case.	49
4.14	Magnetite mass fraction throughout the process for the reference case and the plasma torch case.	49
4.15	Pellet temperature throughout the process for the plasma torch cases with increased flow rates.	50
4.16	Mass fraction of magnetite throughout the process for the plasma torch cases with increased flow rates.	51
4.17	Temperature profile for the NoMix case.	54
4.18	NO concentration for the NoMix case.	54
4.19	NO concentration for the MixTP case.	55
4.20	NO production for the MixTP case.	55
4.21	Temperature profile for the MixEE case.	56
4.22	NO production for the MixEE case.	56
4.23	Effect of plasma temperature on NO concentration.	58
4.24	Effect of mixing zone length on NO concentration.	58
4.25	Effect of air to plasma ratio on NO concentration.	58
4.26	Effect of air to plasma ratio on NO formation.	58
4.27	Effect of plasma gas flow rate on NO concentration.	59
4.28	Effect of plasma gas flow rate on NO formation.	59
4.29	NO mole fraction for common plasma working gases.	60
4.30	Effect of methane flow rate for the two reduction strategies.	60
5.1	Principal design of the new process concept for pelletization and direct- reduction of iron ore.	64
B.1	Temperature profile for the NoMix case.	VI
B.2	NO concentration for the NoMix case.	VI
B.3	NO mass flow for the NoMix case.	VI
B.4	NO production for the NoMix case.	VI
B.5	Species concentration for the NoMix case.	VII
B.6	Close-up of Figure B.5.	VII
B.7	Rate of production for the NoMix case.	VII
B.8	Close-up of Figure B.7.	VII
B.9	Temperature profile for the MixTP case.	VIII
B.10	NO concentration for the MixTP case.	VIII
B.11	NO mass flow for the MixTP case.	VIII
B.12	NO production for the MixTP case.	VIII
B.13	Species concentration for the MixTP case.	IX
B.14	Close-up of Figure B.13.	IX
B.15	Rate of production for the MixTP case.	IX
B.16	Close-up of Figure B.15.	IX
B.17	Temperature profile for the MixEE case.	X
B.18	NO concentration for the MixEE case.	X
B.19	NO mass flow for the MixEE case.	X

List of Figures

B.20 NO production for the MixEE case.	X
B.21 Species concentration for the MixEE case.	XI
B.22 Close-up of Figure B.21.	XI
B.23 Rate of production for the MixEE case.	XI
B.24 Close-up of Figure B.23.	XI

List of Tables

2.1	Annual operating costs for a 2 MW fuel oil burner and air plasma torch.	19
3.1	Selected performance indicators for the straight-grate process.	28
3.2	Process constraints considered for the straight-grate process.	29
3.3	Parameters used for the plasma torch case study.	33
4.1	Performance indicators for the reference case.	40
4.2	Process constraints for the reference case.	41
4.3	Pellet temperature and moisture content measured at the end of the UD- D/Micro section in the study by Athayde et al. [25].	43
4.4	Pellet temperature and moisture content at the end of the UDD/Micro section in the simulation model.	43
4.5	Performance indicators for REF and microwave case study.	45
4.6	Process constraints for the microwave case study.	45
4.7	Performance indicators for the new process designs.	47
4.8	Process constraints for the new process designs.	47
4.9	Calculated parameters for the plasma torch case study.	48
4.10	Performance indicators for the plasma torch case study.	50
4.11	Performance indicators for the plasma torch cases with increased flow rate.	51
4.12	Performance indicators for the optimization of the plasma torch case.	52
4.13	Comparison of NO concentration [ppm] between the experiments and the simulation models with different amounts of air in CO ₂ working gas.	57

Abbreviations & Nomenclature

Abbreviations

AC	Alternating current
AF	After-firing zone
C	Cooling zone
DC	Direct current
DDD	Downdraft drying zone
DRI	Direct-reduced iron
EAF	Electric arc furnace
EU	European union
F	Firing zone
FGR	Flue gas recirculation
LKAB	Luossavaara-Kiirunavaara Aktiebolag
Micro	Microwave zone
MixAdapt	Adapted mixing case
MixEE	Mixing case (energy equation)
MixTP	Mixing case (temperature profile)
NoMix	No mixing case
PFR	Plug flow reactor
PH	Preheating zone
REF	Reference case
RF	Radio frequency
SCR	Selective catalytic reduction
UDD	Updraft drying zone

Chemical substances

CaCO_3	Calcium carbonate
$\text{CaMg}(\text{CO})_3$	Dolomite
CaO	Calcium oxide
CH_4	Methane
CO_2	Carbon dioxide
CO_2eq	Carbon dioxide equivalent
Fe_2O_3	Hematite
Fe_3O_4	Magnetite
HNO_3	Nitric acid
MgO	Magnesium oxide
NO_x	Nitrogen oxide
O_3	Ozone

Variables

E_{tot}	Total energy consumption [kWh/ton _p]
F_{mag}	Magnetite content at the end of the grate [%]
I_a	Arc current [A]
P_t	Electric power of plasma torch [MW]
q	Power intensity [W/m^2]
Q_{el}	Power requirement from electricity [MW]
Q_{fossil}	Power requirement from fossil fuel sources [MW]
Q_p	Thermal power of plasma [MW]
r_{evap}	Evaporation rate [$\text{kg}/\text{m}^3/\text{s}$]
T_{bed}	Bed temperature at the end of the grate [$^{\circ}\text{C}$]
T_{fan}	Recuperation fan temperature [$^{\circ}\text{C}$]
T_{grate}	Grate temperature [$^{\circ}\text{C}$]
U_a	Arc voltage [V]
V_{gas}	Working gas flow rate [Nm^3/h]
Δp_{bed}	Pressure drop over the bed [Pa]
η_{th}	Thermal efficiency [-]

1

Introduction

1.1 Background

Some of the major challenges for modern society are global warming and the vast emissions of greenhouse gases and pollutants such as nitrogen oxides (NO_x). In the 2015 Paris climate conference, 195 nations agreed on guidelines for managing climate change. The nations decided to take action to keep the global temperature rise below 2 °C and pursue efforts to limit it to 1.5 °C. [1] In order to achieve this goal, Sweden has a vision of having zero net emissions of greenhouse gases to the atmosphere in the year 2050 as well as having a sustainable and resource-efficient energy supply [2]. International regulation is also an important tool in order to reduce NO_x emissions. According to the 2016 EU air pollution directive, NO_x emissions should be reduced by 42% until 2020 and by 63% until 2030 compared to the emission levels of 2015 [3].

LKAB (Luossavaara-Kiirunavaara Aktiebolag) is a Swedish state-owned mining company that mines and refines iron ore for the global steel market. The company was founded in 1890 and currently has over 4000 employees. LKAB mines around 80 % of all iron ore in the EU, making it the largest iron ore producer in Europe. In 2017, LKAB produced over 27.2 million ton iron ore products and iron ore pellets accounted for around 83 % of LKAB's iron ore deliveries. [4] As one of the largest industries in Sweden, operating several pellet plants, LKAB contributes significantly to greenhouse gas emissions. Due to this, LKAB is examining different methods to reduce their climate impact. LKAB's current goal is to reduce the emissions of carbon dioxide by 12 % per ton finished product until the year 2021, while simultaneously reducing the energy intensity by 17 % compared to 2015 levels [5]. HYBRIT is an initiative by the companies LKAB, SSAB and Vattenfall with the goal of producing the world's first fossil-free steel. The project aims to reduce CO_2 emissions throughout the entire steel production chain, where iron ore pelletization is an important part. [6]

LKAB's mines are located in the ore fields in the north of Sweden, mainly in Kiruna, Malmberget and Svappavaara. The ore deposits are located several hundred meters below ground and the iron ore is extracted in large underground mines. [7] The two main types of mineral found in the deposits are magnetite (Fe_3O_4) and hematite (Fe_2O_3). The iron ore is then processed in processing plants, where the ore is sorted and concentrated in several steps before being pelletized. The pelletization process involves forming the iron ore into small round balls called green pellets and subjecting these to a heat treatment process that oxidizes and sinters the pellets. The finished pellets are then transported by rail to the ports and shipped to customers all around the world for steel production. [8]

The focus of this project is the heat treatment of the iron ore pellets which is the most energy intensive part of the pelletization process. The two most common processes for heat treatment are called the grate-kiln and straight-grate processes. The grate-kiln process uses a travelling grate for drying, preheating and cooling and a rotating kiln for sintering, while the straight-grate uses a travelling grate for the entire process. The grate-kiln process is more suitable for pellets with a high magnetite content and achieves a more homogeneous temperature profile which leads to higher pellet quality. The straight-grate process can handle ores with higher hematite content and also achieves a lower fuel consumption than the grate-kiln process. [9]

Currently, fossil fuel burners are used in order to heat up the iron ore to the required temperature. A considerable amount of heat is also supplied from the iron ore itself through an exothermic oxidation reaction. In order to reduce CO_2 -emissions and lower the running costs, LKAB has shown interest in investigating the effects of replacing the current burners with electric heating technologies such as plasma torches and microwaves. This leads to certain changes in the process conditions which might affect the quality of the finished pellets. Another potential problem is that plasma torches operate at extremely high temperatures which leads to the formation of NO_x .

This project is a part of a collaboration between LKAB and the Division of Energy Technology at Chalmers University of Technology. During the collaboration, a simulation model has been developed and experimental tests have been performed in order to verify the model. So far most of the research has been towards improving the energy efficiency of the processes. This project builds on previous work and adapts it for operation with electric heating. Furthermore, the NO_x emissions from plasma torches are studied through reaction modelling in Chemkin.

1.2 Aim

The aim of this project is to make an assessment of the possibilities for utilizing electricity to supply the required energy for the heat treatment in the iron ore pelletization process at LKAB. More specifically the work will focus on:

- Supplying the high-temperature heat requirement using plasma torches in the straight-grate process
- Finding possible application areas where microwaves could provide low-temperature heat input to the straight-grate process
- Evaluating how the implementation of electric heating affects process conditions, energy efficiency, emissions (CO_2 and NO_x) and quality of the finished pellets
- Finding new potential for process optimization as a result of the implementation of electric heating

1.3 Limitations

The heat treatment in the straight-grate process is dominated by convective heat transfer between heated gases and the iron ore pellets while the grate-kiln process receives an important contribution to the heat treatment via radiation from a large open flame. The suggested electric heating alternatives do not provide radiation properties similar to fossil fuel flames. Therefore, this report will focus on the straight-grate process since it is most suited for the first assessment of electric heating implementation. The other limitations of this project include:

- The only electric heating technologies that will be studied are plasma torches and microwaves
- The theoretical potential of replacing fossil fuel burners with electric heating will be investigated but the practical aspects of implementation will not be studied
- No cost evaluations or in-depth economic analysis of the suggested changes to the straight-grate process will be performed

2

Theory

2.1 Iron ore processing

Iron ore deposits are found with varying concentrations of the two main minerals magnetite and hematite. In the LKAB mines, magnetite is the dominating mineral with content in the range of 80-100 % [10]. When extracting iron ore from the mines, holes are drilled in the ore body which are then filled with explosives. A blast is initiated which separates smaller pieces of ore from the main ore body. The ore contains waste rock and impurities which must be removed to produce high quality iron ore pellets. The first step in the refining process is to pass the ore through crushers to reduce the size of the ore pieces to around 10 cm in diameter. [7]

The crushed ore is then transported to a sorting process where the ore is separated from the waste rock. The iron ore can be separated from waste rock using magnetic separators due to the magnetic properties of magnetite ore. The ore passes through the sorting process several times. Between every passing, the ore is crushed into even smaller pieces. The iron ore enters the sorting process with an iron content of around 45 % and leaves at around 62 %. [8] The separated ore needs further removal of impurities to provide a high quality end product. Therefore, the ore enters the concentration process where it is ground into fine particles. The finely ground iron ore is then mixed with water to form a slurry. The iron content is increased to around 68 % during this process. Different additives are then introduced to the slurry depending on the product specification and pellet type that is to be produced. The final step in the concentration process is to reduce the water content of the slurry by filtering. The slurry is then ready for pelletizing.

A clay mineral additive, bentonite, is added to the slurry at the pelletizing station. Bentonite is a binder which allows the slurry to form round balls called green pellets. These are approximately 10 mm in diameter and are formed by rolling the slurry in large rotating drums. The pellets are then heat treated to reduce the moisture content and oxidize the magnetite to hematite. The reason for this is to produce a high quality product as well as to increase the strength of the pellets so that they can withstand the stresses imposed on them during transportation from LKAB's facilities to the customers. The heat treatment consists of three main steps executed in the following order; drying/pre-heating, sintering and cooling. The two most common processes for the heat treatment of iron ore pellets are the straight-grate process and the grate-kiln process, described in Section 2.2.1 and 2.2.2 respectively.

The finished pellets are mainly used for steel production in blast furnaces or through direct-reduction. These processes typically require iron ore in a form that allows formation of a bed through which gas can flow with low resistance and this is the reason for shaping the iron ore into spherical pellets. LKAB is not directly involved in the steel production but a brief description of these processes are given here in order to explain how the pellets are used.

A blast furnace is a vertical shaft furnace that produces liquid metals by the reaction of a mixture of metallic ore, coke and limestone introduced from the top with a flow of hot air introduced from the bottom. Blast furnaces produce crude iron from iron ore pellets by a reduction process under elevated temperature where the iron oxides are reduced by carbon monoxide into its elemental form. [11] Crude iron contains a high proportion of carbon, typically around 4 %, and can be further processed into steel by reducing the carbon content and adding different alloys that give the steel its unique properties [12].

The direct-reduction process uses a similar arrangement as the blast furnace, where iron ores are fed from the top and a reducing gas is fed from the bottom. The difference is that the reduction process occurs in solid phase at temperatures below the melting point (800 - 1200 °C). The reducing gas is usually syngas which is a mixture between hydrogen gas and carbon monoxide that can be produced from natural gas. The direct-reduction process is very energy efficient and requires significantly less fuel than a traditional blast furnace. The end product from the process is direct-reduced iron (DRI), so called sponge iron. This is often directly processed to steel in an electric arc furnace (EAF) to take advantage of the heat from the reduction process. [13]

2.2 Pelletization heat treatment processes

This section describes the heat treatment which is a major part of the pelletization process. The straight-grate and the grate-kiln processes are both used by LKAB to provide heat treatment to the iron ore pellets. The working principles of these processes and the chemical reactions taking place in the pellets are explained in this section.

2.2.1 Straight-grate process

The straight-grate process consists of a continuously moving grate with a pellet bed resting on the grate, with no mixing occurring in the pellet bed. The straight-grate system performs the drying, firing and cooling in the same machine. A schematic illustration of the straight-grate process based on LKAB's MK3 unit is presented in Figure 2.1. The straight-grate consists of several different process zones called updraft drying (UDD), downdraft drying (DDD), preheating (PH), firing (F), after-firing (AF) and cooling zones (C1 and C2). As can be observed, the hot process gas is recycled to increase the energy efficiency of the process while the exhaust gases leaves the process through a stack.

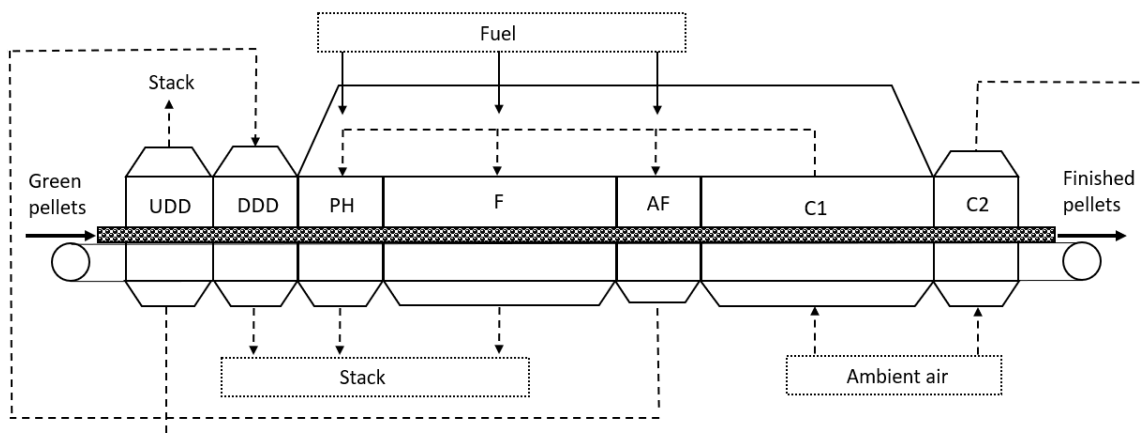


Figure 2.1: Schematic illustration of the straight-grate process.

The green pellets are introduced on top of a layer of already treated pellets called the hearth layer, which has the purpose of protecting the grate from thermal stresses when it is travelling through the firing zones. In the first two zones (UDD and DDD), the pellets are dried by a cross flow of recirculated process gas. In the UDD zone the gas from the C2 zone flows through the bed from below and in the DDD zone the gas from the AF zone flows from above. The reason for switching from updraft to downdraft drying is to achieve a more homogeneous evaporation rate and reduce the risk for recondensation of water in the bottom layer. [14] Moderate gas temperatures are used in the drying zones since too high temperatures will cause the pellets to dry too fast, eventually causing cracking of the pellets due to the build up of pressure generated by steam inside the pellets [10].

The PH, F and AF zones are called the firing zones and the main purpose of these zones is to increase the temperature for the sintering process. Sintering is a diffusion-driven process where the particles in the pellets partly fuse together, increasing their mechanical strength. Oxidation of magnetite into hematite occur simultaneously with the sintering process. The oxidation is an exothermal reaction which means that it releases heat. Approximately 60% of the thermal energy needed for pellet production comes from the oxidation of magnetite, which reduces the need for addition of external fuel [10]. In the PH zone, most of the water content has been evaporated and the pellet temperature begins to increase. The majority of the oxidation takes place in the F and AF zones under high temperatures.

All of the firing zones are supplied by recirculated gas from the C1 zone which needs to be heated even further to 1000 - 1300 °C. In the current MK3 unit, 4 natural gas burners and 12 oil burners are used for the additional energy supply. These are located in downcomer pipes on the sides of the pellet bed. The hot gas then flows in a downdraft direction through the bed. The exhaust gas from the firing zones has a reduced oxygen content since oxygen is consumed during the combustion and oxidation reactions.

The hot pellets coming from the firing zones then needs to be cooled down to below 100 °C to facilitate product transport. This is achieved in the cooling zones by blowing ambient air in an updraft direction through the bed. The gas flow is heated in the cooling zone and distributed throughout the process as a heat carrier. The magnetite may not be fully oxidized when entering the cooling zone meaning that some oxidation may take place in the beginning of the cooling zone as well. [14]

2.2.2 Grate-kiln process

The grate-kiln process is a widely used heat treatment process alongside the straight-grate process. The grate-kiln process consists of three distinct sections, the drying and preheating section, the rotating kiln and the cooling section, as can be seen in Figure 2.2.

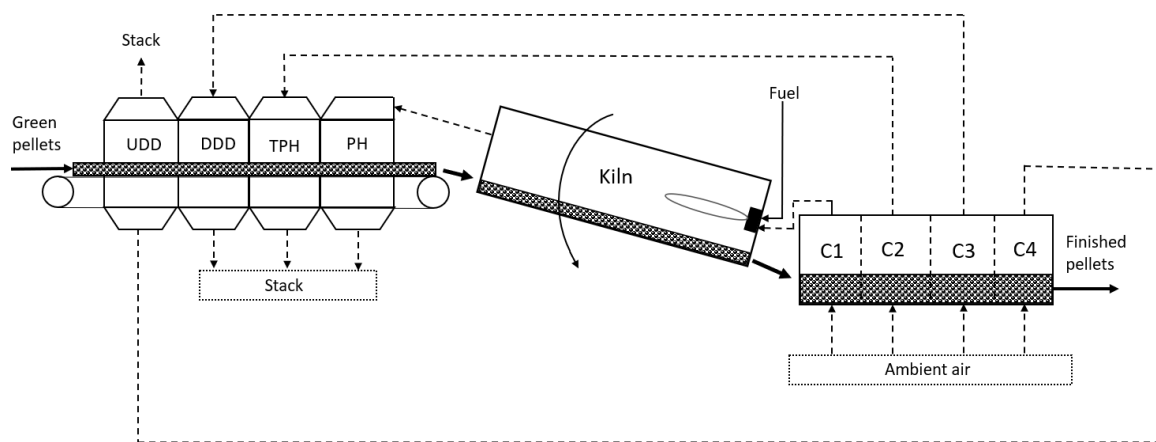


Figure 2.2: Schematic illustration of the grate-kiln process.

The green pellets first enter the drying section which is a travelling grate where the pellets are dried and preheated using recirculated cooling air and combustion gases, similar to the straight-grate process. The pellets then enter the rotating kiln where they are sintered at high temperature, up to 1300 °C. The rotational movement of the kiln mixes the pellets and thereby provides an even temperature distribution in the pellet bed. This leads to more homogeneous sintering and results in a higher quality product compared to the straight-grate process. Coal is the primary fuel used for heat generation. The heat is transferred to the pellets via one large flame inside the rotating kiln, burning in the opposite direction of the pellet flow. The radiation from the flame provides an important contribution to the heat transfer in the kiln. The pellets then leave the rotary kiln and enter the cooling section. The cooling unit is a circular container rotating along a vertical axis. Figure 2.2 shows a simplified sketch of the cooling unit where it looks like a travelling grate, which is not the case in reality. The pellets travel one lap in the rotating cooler while being cooled with ambient air flowing through the bed. The pellets are then ready for storage and transportation to customers.

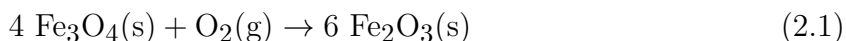
The grate-kiln process is best suited for iron ore with high magnetite content since hematite ore produces more fines when mixed in the rotating kiln and gives larger radiation losses [15]. The complexity of implementing plasma torches in the grate-kiln process lies in replacing the large flame and the radiation heat transfer contribution that it provides since a plasma flame does not provide the same radiation properties. It is therefore likely that large process modifications must be made to implement the plasma torches and maintain sufficiently good pellet quality. In the straight-grate process the majority of the heat transfer to the pellets occur via convection, which means that changing the energy source has a larger potential for success with smaller process modifications.

Since the implementation of plasma torches is more complex in the grate-kiln process compared to the straight-grate process, the straight-grate process is better suited for a first assessment of the implementation of electric heating. This is why the grate-kiln process is not the focus of this report. If implementation of electric heating is successful in the straight grate process, further studies will most likely focus on converting the grate-kiln process to electric heating as well.

2.2.3 Heat treatment chemistry

There are four main reactions that are of importance for the iron ore pelletization process; evaporation of water, oxidation of magnetite, calcination of calcium carbonate and decomposition of dolomite. In the beginning of the process, liquid water is trapped inside the pellets and the moisture content is around 9 wt%. The water evaporates when the temperature is increased through the drying and preheating zones. Assuming atmospheric pressure, the enthalpy of evaporation is 2256 kJ/kg. [15]

Oxidation of magnetite is the most important reaction in the heat treatment of iron ore pellets. In this reaction, magnetite in the pellets reacts with oxygen from the air to form hematite, see Reaction 2.1. The oxidation reaction is exothermic and the enthalpy of reaction is -119 kJ/mol. The reaction starts at a temperature of 200 - 300 °C but does not reach maximum conversion efficiency until around 1100 °C [16].



The reaction will undergo two stages before the final stable hematite structure is formed. In the first stage, the reaction is governed by kinetics and a growing hematite shell will form around a magnetite core. In the second stage, the reaction is governed by mass transfer and oxygen will begin to diffuse inward to complete the reaction. If a temperature of 1200 °C is exceeded the oxidation rate drops and dissociation of hematite back to magnetite will occur. [17]

Calcium carbonate from limestone additives reacts into calcium oxide and carbon dioxide, as described by Reaction 2.2. The calcination reaction is endothermic, and the enthalpy of reaction is +182 kJ/mol. Due to the small amount of limestone in the pellets, the total heat demand of the reaction is relatively small. The reaction starts at around 600 °C and reaches full conversion efficiency at around 900 °C [18].



Dolomite is another additive and will decompose into calcium oxide, magnesium oxide and carbon dioxide as described by Reaction 2.3. This reaction is also endothermic, having a reaction enthalpy of +296 kJ/mol. Similarly to calcium carbonate, the concentration of dolomite is low resulting in a small heat demand. The reaction normally occurs at temperatures between 600 - 760 °C [19].



2.3 Microwave heating

Microwaves consist of non-ionizing electromagnetic radiation within the frequency interval of 300 MHz to 300 GHz. Electromagnetic radiation consists of an electric field and a magnetic field which oscillate in a wave motion as they travel through space. Some materials absorb the electromagnetic energy, converting it to thermal energy. This process is commonly used to heat food in microwave ovens. The following sections describe the process of heating materials using microwaves and evaluates possible applications for the straight-grate pelletizing process.

2.3.1 Microwave interaction with matter

Materials behave in three principal ways when in contact with microwaves. The incoming microwaves are either reflected, absorbed or transmitted through the material as illustrated in Figure 2.3. Materials can show one dominant mode of interaction or a combination of the three, depending on the material properties. [20]

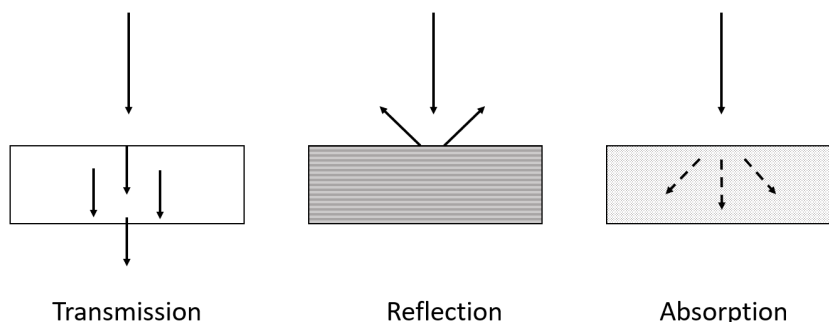


Figure 2.3: Illustration of microwaves interacting with matter.

Transmissive materials are invisible to microwave radiation and have no effect on the propagating electromagnetic wave. Such materials are often used for supporting functions in a microwave heating context such as physically holding the object to be heated in place. Materials which reflect microwaves are often used for guiding the microwaves in desired direction and protecting the surroundings. Materials with good conductive properties, such as metals, are often used for this purpose. Materials that absorb electromagnetic energy are the only ones which are able convert it into thermal energy [20].

It should be noted that a material can show different properties in an electromagnetic field depending on its particle size. Metals for example, show reflective properties when present in bulk but do not show the same behaviour in powder form. For example, microwaves have successfully been used for sintering of metal powder [21]. Materials with reflective properties can create electrical discharge in the form of arcing when subjected to microwave radiation. Under certain conditions, electrons can become concentrated at the surface and edges of the metal due to the penetration of electromagnetic waves. At a certain point, the energy is discharged in the form of an electric arc. [22]

Magnetite, which is the main component of the green pellets produced at LKAB, shows good properties for absorption of microwave radiation [20]. The green pellets consist of about 10% water which also is a good microwave absorber. This provides good prerequisites for heating these pellets using microwaves. Hematite is also a good absorber of microwaves which means that the properties for heating using microwaves are still good after drying and conversion to hematite. However, arcing has been observed at high temperatures which could lead to equipment malfunction [20].

2.3.2 Heating mechanisms and properties

The mechanisms of heating by microwave radiation and conventional heating differ significantly. In conventional heating the thermal energy is transferred to the surface of the material and spreads inwards by the mechanisms of radiation, convection and conduction. When using microwaves, heat is generated within the material, resulting in rapid heating. This is illustrated in Figure 2.4.

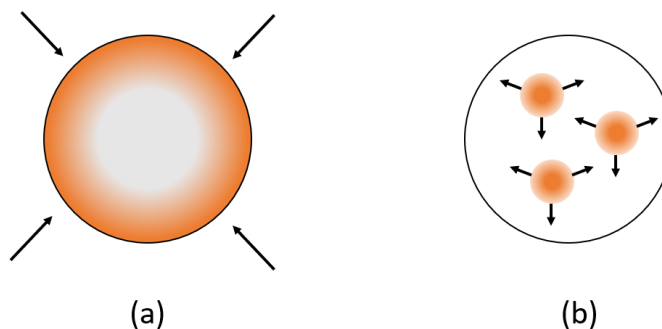


Figure 2.4: Heating a homogeneous particle by (a) Convective/conductive heating, (b) Microwave heating.

Since microwave heating is selective, non-homogeneous materials can heat unevenly. The heat distribution in the volume depends on the dielectric and conductive properties of the materials in the volume. In some cases certain areas can achieve significantly higher temperatures than others. This is referred to as thermal runaway [20]. The thermal expansion properties of different materials in a particle can cause micro cracks, especially in a rapid heating process with large local variations such as thermal runaway [23].

The conversion from electromagnetic radiation into thermal energy is a process where the dielectric properties of the material is of great importance. Dielectric materials containing polarized molecules will respond to the oscillating electrical component of the electromagnetic radiation. The water molecule is a typical example of a polarized molecule which reacts to changes in the electric field surrounding it. The polarized molecules align themselves to the electric field, causing increased motion of the molecules. The increased motion leads to increased kinetic energy of the molecules which is then converted into thermal energy through friction and collisions with other molecules. The thermal energy then spreads throughout the material by conduction, driven by thermal gradients. [20]

The dielectric heating is also connected to the ionic conduction properties of the material. The ionic conduction mechanism is driven by mobile charge carriers, such as electrons and ions, moving inside the material as a response to the oscillating electrical field. This creates an electrical current through the material. The materials resistance to electric conduction causes the material to heat. [24] The magnetic component of the electromagnetic field contributes to heating by eddy current loss and hysteresis loss which provides a considerable contribution to the heating of ferrous materials [24].

2.3.3 Previous microwave applications for iron ore pelletization

Studies have been performed on the implementation of microwave technology in iron ore pelletization. Two studies performed by Maycon Athayde et al. [23] [25] has investigated effects of implementing microwave technology in the drying section of the iron ore pelletization process.

In early 2018, there was a study published by Athayde et al. [23] investigating kinetic parameters of the iron ore pellet drying process assisted by microwave technology. In this study, green pellets were produced from hematite ore and sieved into three size categories with average diameters of 10.75, 13.5 and 15.25 mm having a moisture content of 10 %. Samples of 100 g were subjected to microwave radiation for 180 s with intervals of 30 s using a turnable-tray microwave oven normally used for heating food. The frequency used was 2.45 GHz and the power levels used were 300, 600 and 1000 W. The tests were conducted at temperatures lower than 500 °C.

Results showed that the dryout time was much faster when using microwaves instead of convective heating. The drying activation energy was halved when using microwaves compared to convective heating. When drying the pellets, an intense heating rate was observed in the beginning of the drying phase. The heating rate slowed down as the moisture content of the pellets decreased which indicates that the moisture content is an important parameter for the ability of the pellets to absorb microwave energy. The dryout time was slower in small pellets than in large pellets. This was likely due to the large surface area to volume ratio which leads to large heat loss to the surroundings.

Effects on pellet quality was assessed by evaluating the crushing strength of the pellets after drying with microwaves. Results showed strength levels varying between 0.6-2.5 kg/pellet which is considerably lower than conventional methods. Pellets gently dried in a conventional oven at 105 °C showed a crushing strength of 5.2 kg/pellet. The loss in strength was likely due to micro cracks found in the hematite and goethite, which is another iron oxide found in these pellets. Cracks were observed in the mantle as well as the core of the pellets. Differences in heating rate and linear expansion of the different materials in the pellet was thought to cause these cracks.

Observations of the pellet structure using a scanning electron microscope (SEM) revealed hematite reduction to magnetite. This reduction occurs at temperatures much higher than the 500 °C that was supposed to be the upper temperature limit of the experiments. This was considered as thermal runaway, difficult to detect with the temperature measuring equipment used.

Later in 2018, another study was published by Athayde et al. [25]. This time evaluating a novel drying process assisted by microwave technology for iron ore pelletization. The effect of combining microwaves and traditional convective heating was evaluated against the traditional processing technique using only convective heating. The tests were performed using a pot grate in lab scale simulating a travelling grate furnace. The pot grate simulates the drying process of the straight-grate initiating the process with an UDD section followed by a DDD section. The UDD mode introduced an airflow with an inlet temperature of 290 °C during 175 seconds before switching to the DDD mode which introduced an airflow with an inlet temperature of 280 °C during 340 seconds. The microwaves were used only during the UDD operation mode at a frequency of 915 MHz and a constant power supply of 10 kW. Green pellets were produced using iron ore dominated by hematite mineral. The majority of the pellets had a diameter between 9-16 mm. The moisture content was adjusted to batches of 10 % and 10.3 %.

The results showed a rapid heating process when microwaves were used compared to purely convective heating. Maximum heating rates of 1.5 °C/s were observed with an average of 0.79 °C/s while purely convective heating showed an average heating rate of only 0.14 °C/s. The surface layers of the pellet bed showed considerably higher temperatures when using microwaves. At 60 mm depth the temperature reached 115 °C compared to 71 °C in the purely convective case. The lower layers showed no change in temperature for the two cases. This is believed to be due to low penetration depth of the microwaves. All the electromagnetic energy was consumed in the higher layers.

Results from moisture measurements in different levels of the bed at the end of the UDD section showed that purely convective flow increased the moisture content in the upper layers of the bed by 0.08 - 0.36% compared to initial levels due to recondensation of moisture. The microwave assisted drying process decreased the moisture content in the higher layers by 0.12 - 0.8% compared to initial levels, which was a considerable improvement. The lower layers showed similar results for both microwave assisted drying and purely convective drying, probably due to the low penetration depth of the microwaves.

Thermal imaging of the top layer of pellets in the pot grate showed energy concentrations in the center of the bed in the microwave assisted drying case. This was caused by the oscillating behaviour of the microwaves which created areas with higher power density than others, resulting in local variations in temperature. The pellet samples were checked for micro cracks which were not found in any sample, implying that the heating rate was sufficiently low to avoid this problem.

The study showed promising results for using microwaves to assist the convective drying technique resulting in dryer pellets which are less inclined to cluster, deform and clog the voids in the pellet bed. This allowed for a lower pressure drop through the bed and provided the possibility of using higher temperature gas in the DDD stage since the lower moisture content makes micro-cracks due to steam expansion inside the pellet less likely to occur.

2.3.4 Potential for application of microwaves at LKAB

This section evaluates the potential for application of microwaves in the pelletizing process at LKAB, using the theoretical knowledge about microwave behaviour in combination with knowledge about the straight-grate process conditions.

The potential of using microwave energy for the straight-grate process lies in the areas where heating is required. This would be in the drying zones or the sintering zones. Microwave heating has shown rapid heating rates, low penetration depth and arcing at high temperatures in earlier studies [23] [20]. These properties are not beneficial for the sintering process, but could potentially be a good complement to the convective heating in the drying zones.

Traditionally, the drying process begins with an updraft zone. The layers which are subjected to the highest static load, i.e. the lower layers in the bed, are dried first to increase the mechanical strength of the pellets and thereby reducing the occurrence of deformation and clogging. Some of the moisture that evaporates in the lower layers of the bed will recondense in the middle and higher layers as the gas cools down when passing through the bed, reducing its ability to retain moisture. As a result, the moisture content of the pellets in the middle and higher layers of the bed can increase to levels above the initial moisture content. This is acceptable to some extent, but there is a limit where over-wetting of the pellets results problematic deformation and clogging of pellets. At a certain point, the flow must switch to downdraft to avoid over-wetting of the middle and higher layers. This effectively dries the higher layers but the drying process of the middle and low-middle layers of the bed is slow.

Microwaves could be used in the updraft zone to eliminate the recondensation of moisture in the higher layers by heating the bed from both sides i.e. convective heating from below and microwave heating from above. This provides potential for extending the updraft section and decreasing the size of the downdraft section which would result in a faster drying process for the low-middle layer and could thereby lead to a faster drying process overall. A faster drying process with less problems related to deformation and clogging of pellets is beneficial since it could provide potential for increased production rate and a higher quality end product. The possibilities of modeling the microwave energy contribution to the drying process using the straight-grate simulation model is further investigated in this project.

2.4 Plasma torches

This section introduces the theory required to understand the operation of industrial plasma torches. It includes a description of the basic principles of plasmas and plasma generation, common types of plasma torches and how they can be applied to the straight-grate process.

2.4.1 Definition of plasma

Plasma is one of the four fundamental states of matter (solid, liquid, gas and plasma). A plasma can be described as a highly ionized form of gas. Plasmas generally consists of ions, electrons and neutral species, see Figure 2.5. The positive and negative charges compensate each other making the overall plasma electrically neutral. [26] Plasmas can be generated artificially by heating or subjecting a gas to a strong electromagnetic field. Positively charged ions are then created by separation of electrons from the atomic nuclei and the ionized gaseous substance becomes increasingly electrically conductive. The high temperature in combination with high reactivity makes plasma an effective way to achieve high heat transfer rates and chemical reactions. [27]

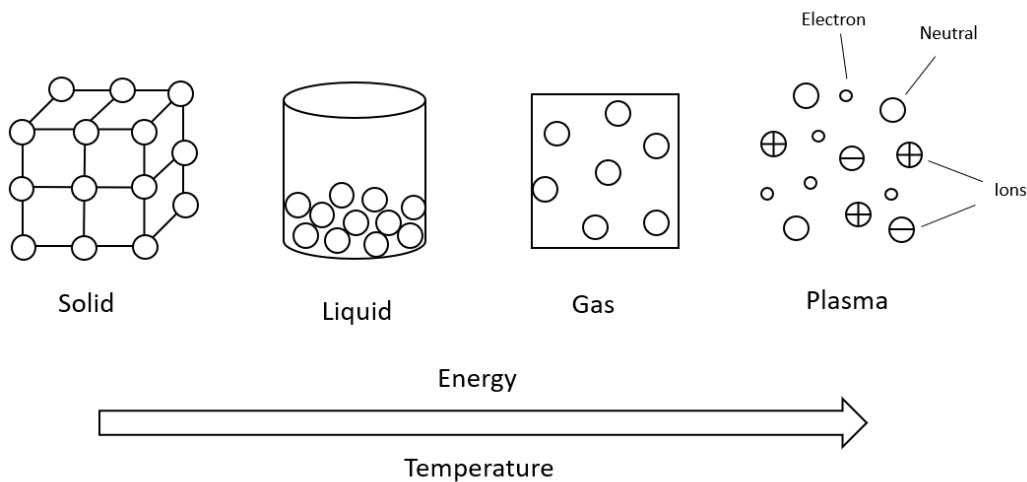


Figure 2.5: Simplified illustration of the four fundamental states of matter.

Plasmas can generally be classified in two categories, thermal and non-thermal plasmas. Thermal plasmas are atmospheric pressure plasmas where the ions and electrons are in local thermodynamic equilibrium, meaning that they have the same temperature. Non thermal plasmas, also called cold plasmas, are plasmas where the ions stay at low temperature while the electron temperature is much higher. Plasmas can also be classified according to the degree of ionization, which can be described by the electron density (the amount of electrons per unit volume). The degree of ionization depends on the surrounding environment, mainly the temperature and pressure. The plasma used in most technical applications are thermal plasmas with a relatively low degree of ionization. [26]

2.4.2 Plasma generation

A plasma generating device is used to convert electrical energy to thermal energy. The most common way to produce a thermal plasma is to heat a gas using an electric arc. When an electrical arc is established in the presence of a gas, the gas will be partly ionized and become electrically conductive [28]. This occurs through a collision process between electrons from the electric arc and particles of the gas. The electrons are accelerated by the electric field and acquires kinetic energy that will be transferred to thermal energy through the collisions.

The electric arc is a self-sustaining discharge with a high current density and a voltage drop of a few Volt. The arc needs to be stabilized in order to remain in steady state by creating and maintaining boundary conditions. A plasma torch is a device for stabilizing the electric arc. Stabilization involves constricting the arc, cooling the outer layers and defining the path for the arc. Free burning arcs are stabilized by natural convection while other arcs require external stabilizing mechanisms such as gas or liquid flow stabilization. [27]

Gas flow stabilization is the most simple stabilization method and involves a flowing external layer of gas surrounding the arc column. The flow can be either axial or vortex depending on how the gas is injected. In order to get a stable arc, the gas flow rate and the electric power of the plasma torch needs to be balanced. The choice of working gas is mainly based on gas enthalpy, reactivity and cost. The most common working gases used in plasma torches are argon, nitrogen, helium, air and hydrogen [29]. If a high energy content is desirable, diatomic substances such as nitrogen or helium should be used due to the dissociation reaction prior to ionization. If an inert gas atmosphere is required, the preferred working gas is usually argon. Reactive gases such as hydrogen, oxygen and nitrogen can be used to provide reducing or oxidizing effects to the plasma. [27]

The primary source of electricity used to generate the plasma can be direct current (DC), alternating current (AC) and radio frequency (RF). DC is the most common since when compared to AC, there is usually less flicker and noise, a more stable operation, better control, lower electrode consumption and lower energy consumption. [29]

2.4.3 Types of plasma torches

A plasma torch produces low temperature plasma, normally between 5 000 and 30 000 K. Most plasma torches consist of two electrodes between which an electric arc burns, a chamber restricting the gas flow and a section for introduction of the working gas. [30] Industrial plasma torches normally operate with power levels from 20 kW up to around 8 MW [31].

There are many classifications of plasma torches depending on the configuration and geometry. The terms transferred and non-transferred are used to describe the positions of the electrodes. In a non-transferred plasma torch both of the electrodes are located inside the torch and the arc is established between them. In a transferred plasma torch, one of the electrodes is located outside the torch. This is usually the work piece or the material that needs to be heated and the arc is then established between the torch and the work piece. A thermal plasma torch is an example of a non-transferred plasma torch while applications of transferred plasma torches include plasma arc welding and cutting. [26]

The most widely used plasma torch type is the linear non-transferred DC plasma torch with gas stabilization. A schematic illustration of this type of plasma torch is presented in Figure 2.6. In the linear torch design both of the electrodes are situated along the same line. It consists of the negatively charged internal electrode (cathode) and the positively charged output electrode (anode). [30] The cathode is usually formed as a rod while the anode is shaped in the form of a nozzle. The most common electrode materials are tungsten and copper. Other materials can also be used such as graphite, steel, molybdenum and silver. [27]

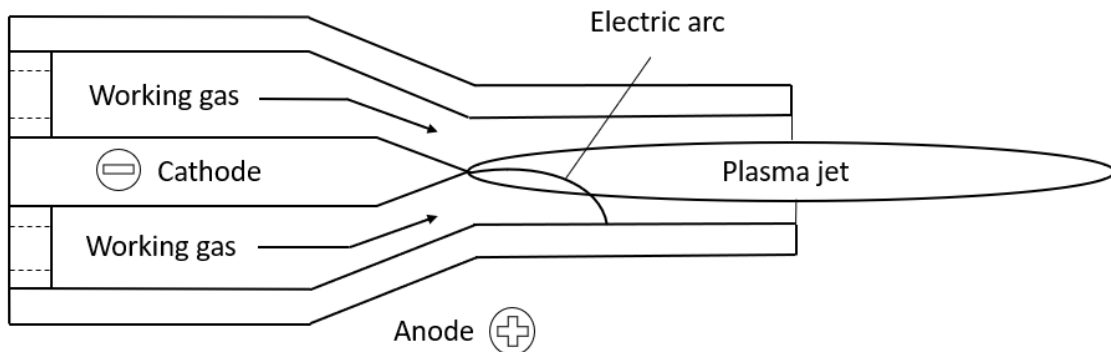


Figure 2.6: Schematic illustration of a linear plasma torch.

The electric arc is ignited between the internal and output electrodes. The closing section of the arc moves along the channel through the effect of the working gas flow, increasing the length of the arc. [30] A high velocity and high temperature flame is produced called plasma jet which can be up to a few inches long. When the gas exits the torch, it recombines into its neutral non-ionic state, but maintains its superheated properties [32]. The electrodes are separated by an electric insulator through which the working gas is supplied. From now on the term "plasma torch" will be used to describe this type of plasma torch.

The total power supplied to the plasma torch by the energy source is given by the product of arc current and arc voltage according to Equation 2.4. A part of the total energy is lost due to heating of the electrodes which are cooled by water in order to avoid overheating and to reduce electrode consumption. The lost energy exits the torch with the cooling water. The ratio of heating power transferred to the plasma and the torch power represents the thermal efficiency of the plasma generation process, see Equation 2.5.

$$P_t = U_a I_a \quad (2.4)$$

$$\eta_{th} = \frac{Q_p}{P_t} \quad (2.5)$$

The thermal efficiency varies a lot between different plasma torch manufacturers and technologies. Most industrial plasma torches operate with an efficiency of 50 - 70 % but an efficiency of over 90 % is possible [32].

2.4.4 Industrial plasma torches

Plasma torches have been used in the industry since the 1950s and the use continues to increase every year [31]. The use of plasma torches in industrial processes was originally motivated by the need of a heating source that could reach temperatures over 2000 °C and could be used inside of a reactor [28].

Technological advancements has made plasma torches an ideal solution for many chemical, mechanical and metallurgical processes. The plasma can be used both as heat source and a reagent in various industrial processes. A good example of a plasma torch application in the industry is metal melting. Destruction of hazardous waste using plasma torches has also become a big area of research.

The main advantages of plasma torches compared to other alternatives are the high temperature in the plasma jet, the high energy density of the plasma and the possibility to use different plasma gases depending on the desired application. Replacing fossil fuel burners with plasma torches can also lead to lower operating costs and greenhouse gas emissions. Other advantages include controlled process chemistry, small installation sizes and rapid start-up and shut-down features. The use of electrical energy as a heating source results in a decoupling of the heat source from the oxygen flow rate. This can be useful in applications where a certain oxygen level is desired [33].

The operation of conventional oil burners produces large amounts of greenhouse gases due to the combustion of fossil fuels. Increased concerns for climate impact makes solutions that can contribute to the reduction of greenhouse gas emissions more interesting. With increasing oil prices, there has also been a growing interest in technologies that can help replacing expensive fuels with more economic alternatives such as electricity. This makes plasma torches an interesting option since they use electricity as the primary energy source instead of fossil fuels.

The operating costs for a typical 2 MW fuel oil burner have been compared with a 2 MW air plasma torch by Pyrogenesis [33]. As can be seen in the table 2.1 below, there is a significant potential for reduction of operating costs. A cost reduction of around 23% is achieved in this example. Cost reductions become even higher when considering applications such as iron ore pelletization, cement kilns and metallic ore roasters since these type of plants can have a large number of burners.

Table 2.1: Annual operating costs for a 2 MW fuel oil burner and air plasma torch.

Costs	Fuel oil burner	Plasma torch
Fuel oil cost (\$ 0.5/l)	\$ 923 000	\$ 0
Electricity cost (\$ 0.03/kWh)	\$ 9000	\$ 600 000
Replacement parts cost	\$ 0	\$ 38 000
Total cost	\$ 932 000	\$ 638 000

Replacing fossil fuels with electricity represents a great potential to reduce greenhouse gas emissions. However, the degree of reduction depends on how the electricity is produced. Electricity produced by renewable energy sources such as hydro, wind and solar power have very low emissions, while electricity produced in coal or natural gas power plants have much higher. A fuel oil burner emits around 115 kg CO₂eq per GJ of heat while a plasma torch powered by electricity produced by hydropower only emits around 1 kg CO₂eq per GJ. Retrofitting a 2 MW plasma burner in place of fuel oil burner leads to a yearly reduction of over 7 000 tonnes of CO₂eq in this case. For a pelletizing plant with a thermal input of around 40 MW, a reduction of over 140 000 tonnes would be possible.

2.4.5 Application of plasma torches for iron ore pelletization

The heat treatment process for iron ore pelletization in the straight-grate process requires additional heating to reach the temperatures needed for the oxidation and sintering processes. The recirculated air from the cooling zone is heated by several smaller burners before reaching the firing zones (PH, F and AF). Direct exposure to the radiation from the burner flames should be avoided since it can cause overheating of the top pellet layers. Because of this, the burners are placed in separate enclosures which protects the bed from most of the radiation. The burners are currently located in downcomer pipes that exits on the sides of the tunnel-shaped firing chamber.

Under the assumption that the effect of radiation is negligible, implementing plasma torches in place of fossil fuel burners should be relatively straightforward. The plasma torches can be arranged in a similar way to the current oil burners. An example of a plasma torch installation is shown in Figure 2.7. Recirculated air from the cooling zone is mixed with extremely hot gas from the plasma torch before entering the firing chamber where it oxidizes the pellets.

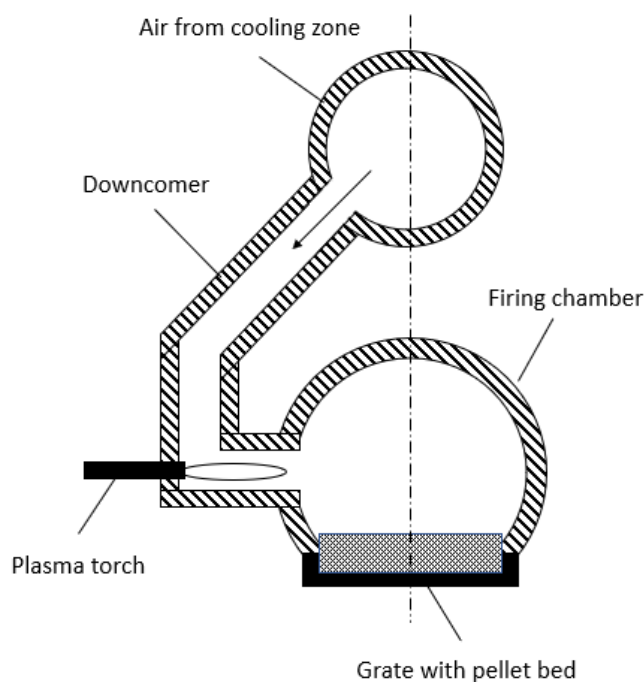


Figure 2.7: Vertical cross section of a firing chamber in the straight-grate process.

The main difference when introducing plasma torches is that there will be no combustion reaction in the firing zones which changes the process gas composition. The combustion reaction consumes oxygen and produces water vapor and carbon dioxide. Secondly, there is an additional working gas flow used to produce the plasma. This will slightly increase the flow rate of the process gas and may also change its composition. The changed composition will affect the properties of the process gas and its ability to oxidize the pellets. The process gases are also used to dry the pellets in the DDD zone, and drying with a wet gas is not very efficient. If the process air is heated by electricity instead of combustion, it will contain less water vapor as it enters the drying zone and can provide a higher drying efficiency.

Finally, the temperature of the plasma jet will be significantly higher than the temperature of the burner flame. Higher temperatures could potentially lead to undesired effects such as production of thermal NO_x . This problem will be discussed further in the following chapter. Another potential problem is hot gas zones caused by lack of mixing which leads to thermal stresses and uneven oxidation of the pellets. The mixing process is important in order to achieve a homogeneous process gas but will not be studied in this project.

2.5 Nitrogen oxides

Nitrogen oxides are molecules that are composed of nitrogen and oxygen atoms. The nitrogen oxides that contribute to atmospheric pollution are nitric oxide (NO), nitrogen dioxide (NO₂) and nitrous oxide (N₂O). The term "NO_x" is used to describe NO and NO₂, while N₂O is generally not included.

Anthropogenic activities are the main cause of increased levels of NO_x in the atmosphere. Most of the NO_x is formed in combustion processes where nitrogen from the air or the fuel reacts with oxygen and forms NO_x. A majority of the NO_x emissions in developed countries originate from the transport sector and the industrial sector. [34] The emissions of NO_x is considered to be a global problem. NO_x is considered to be toxic and can cause lung diseases in humans. However, the main problems with NO_x are the secondary effects, including acid deposition and formation of tropospheric ozone. [35]

Acid deposition can be in the form of wet deposition (acid rain) or dry deposition (gas and particles). When released to the atmosphere, NO_x will react with water vapor to form nitric acid (HNO₃). This can be transported over long distances before being deposited as acid rain, resulting in acidification of land and water. Acidification is harmful to vegetation and wildlife and has caused severe environmental problems in many parts of the world. [36]

Ozone (O₃) can be formed through a reaction between an oxygen molecule and an oxygen radical. The levels of oxygen radicals are increased by decomposition of NO₂ by sunlight, thereby increasing the formation of ozone. The ozone that is located close to the ground is called tropospheric ozone. Ozone in the upper atmosphere is vital for protecting the earth from harmful UV-radiation. However, tropospheric ozone is hazardous since it harms the human respiratory system and causes damage to vegetation and crops. Ozone is also a component of the so called "smog" that is a common problem in large cities. [37]

2.5.1 Formation of thermal NO

The formation of NO_x is dominated by NO at high temperatures but the emitted NO usually converts to NO₂ at lower temperatures. Therefore, the focus of this work will be the production and reduction of NO rather than NO₂.

The formation of NO is a complex process and consists of many intermediate reactions but it is common to divide the reactions into three main mechanisms; thermal, fuel and prompt NO. Thermal NO is formed through the reaction between nitrogen and oxygen from the air which normally occurs at very high temperatures. Fuel NO is formed by oxidation of nitrogen from the fuel with oxygen from the air. Finally, prompt NO is formed by the reaction between nitrogen from the air and hydrocarbon radicals from the fuel.

Out of these three mechanisms, only thermal NO will be relevant to plasma torches since the other two mechanisms requires combustion of fuel. The formation of thermal NO can be described by the Zeldovich reactions [38], Reaction 2.6 - 2.8.



These reactions are only important at high temperatures since N_2 contains a triple bond that requires a large amount of energy to break. The rate of formation for thermal NO usually becomes important relative to the other NO reactions at a temperature of over 1500 °C. The reaction rate is also determined by the concentrations of O_2 , N_2 and NO. [35] The formation of NO is limited by reaction 2.6, where nitrogen molecules reacts with oxygen radicals producing NO and nitrogen radicals. The nitrogen radicals will then be consumed immediately by reaction 2.7, producing more NO and oxygen radicals. The activation energy of reaction 2.6 is approximately 318 kJ/mol. The total amount of thermal NO produced also depends on the gas residence time at high temperatures. Strategies to reduce thermal NO will usually focus on reducing the O_2 concentration and removing temperature peaks.

2.5.2 NO_x emissions from iron ore pelletization

The iron ore industry is a substantial emitter of NO_x in Sweden. Iron ore pelletization plants normally has a heat input of around 40 MW and will probably have to comply with emission limits for medium to large size combustion plants. However, very limited research has been carried out on NO_x mitigation measures for these type of plants since the combustion conditions differ significantly from conventional combustion systems.

It is important to maintain high oxygen levels in the process gas to ensure a high degree of oxidation. Therefore, a large volumetric flow of air is required in the firing zones. Relating the air flow to the fuel flow, an air-to-fuel ratio of 4-6 is obtained. This is significantly higher than in conventional combustion, where the air-to-fuel ratio is approximately 1.

Implementation of flue gas cleaning systems such as selective catalytic reduction (SCR) is considered to be less efficient and more costly and the proportional cost for the environmental benefit is still being discussed in the industry. NO_x mitigation is usually only considered in cases where environmental regulations are otherwise not likely to be met. There is therefore incentive to develop cost efficient measures to reduce NO_x emissions from this type of plants. [35]

2.5.3 NO_x emissions from plasma torches

One of the major technical issues with the use of thermal plasma torches is the nitrogen oxides that can be generated in the high temperature plasma which may limit the plasma torch in its various applications. An electric arc operating in an oxidizing gas atmosphere, in combination with high plasma temperatures, leads to formation of NO_x. The plasma bulk temperature is normally 5000 - 6000 K, while the maximum temperature in the plasma jet can be up to 10 000 K [39].

The NO_x formation in plasma torches has not been studied extensively since most research has focused on NO_x emissions from conventional fuel combustion, where temperatures usually are below 2000 °C. One study has been made on plasma torches applied to an electric arc furnace [40]. These trials did not confirm any influence of the electric parameters of the plasma torch on the formation of NO_x. The influence was not detectable due to other more dominant parameters, including the composition of the furnace atmosphere.

Two common methods for industrial NO_x reduction are flue gas recirculation (FGR) and staged combustion. FGR involves extracting flue gases and mixing it with combustion air in order to lower the oxygen content of the combustion air as well lowering the combustion temperature. Staged combustion is a reduction strategy that works by injecting additional fuel in a secondary combustion zone. This creates a fuel rich reburning zone where NO_x is destroyed through reactions with hydrocarbon radicals. These two reduction strategies could probably also be applied to plasma torches with some modifications. For example, a study by Uhm et al. [39] showed that NO_x generated by a plasma torch can be disintegrated in a fuel-burning atmosphere with an exponential decrease in terms of methane flow rate.

2.6 Process model

A process model has been developed during the previous Chalmers-LKAB collaboration that can be used to simulate the straight-grate and grate-kiln processes. The model is based around LKAB's in-house bed simulation software BedSim. A Matlab framework has been built around BedSim in order to perform additional calculations and make the model more user friendly. The process model is a good tool for evaluating the effects of modifying variables and changing the process configuration.

2.6.1 BedSim model

The BedSim model simulates the pellet bed throughout the process. The BedSim code is confidential and can not be accessed in this project. Because of this, BedSim will be used as a "black-box" model, where a given input generates an output, but no changes can be made to the calculations inside the model. BedSim has been validated against small scale lab tests and has been proven to give accurate results regarding the gas and bed properties.

The model performs calculations for chemical reactions as well as mass and heat transfer between the process gas and the bed. The calculation approach used in BedSim is to divide the bed in a number of vertical elements. These elements moves through the process with given time steps, where each time step represents a position along the grate. The calculations are performed for every time step and the results are used as input for the calculations in the next time step. The elements are also divided in horizontal layers in order to account for changes in properties throughout the height of the bed. A number of points in the hearth layer and the grate itself are also included. The calculation approach in BedSim is presented in Figure 2.8.

The resolution in the time and height direction can be defined by the user depending on the desired accuracy. However the total time for the process cannot be specified directly, instead it will be calculated based on input parameters such as production rate, zone areas and bed height. Running and evaluating data from BedSim is quite complicated and time consuming. It can be hard to keep track of different cases when varying input parameters and analyzing the results requires a lot of manual work.

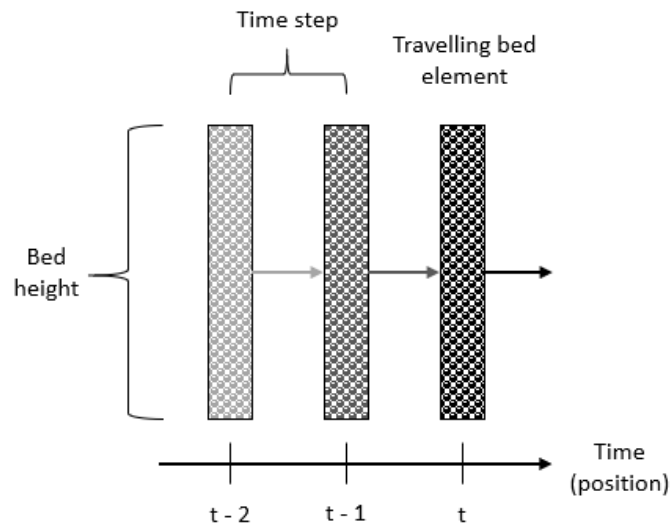


Figure 2.8: Illustration of the calculation method used in the BedSim model.

2.6.2 Matlab framework

The Matlab framework has been developed in previous projects in order to make BedSim more user friendly and simplify the analyzing work. Additional calculations are also performed in the Matlab framework such as mass and energy balances and calculations of energy consumption. The framework was originally developed for the grate-kiln process but has since then been adapted for the straight-grate process.

The input data needed for BedSim is provided in an Excel sheet and can be classified into general and zone-specific data. General data are constant parameters such as bed depth, pellet radius and production rate. Zone-specific data are parameters such as gas flow rate, area and temperature that changes between process zones. The output data from BedSim is provided in a number of CSV files, where each row represents a time step and each column represents a vertical position in the bed. The Matlab framework imports this data and sorts it based on output variable, bed layer and process zone. The output data is then visualized through a number of plots and certain important performance indicators are presented to the user.

Another important feature of this framework is the ability to connect gas streams between process zones. When two zones are connected, iterations are performed in order to achieve the same temperature in the outlet of the first zone as in the inlet of the second zone. This significantly increases the simulation time due to the increased complexity of the system.

Global mass and energy balances are carried out in order to make sure that the model handles the data correctly. The balances compares the predefined input values with the simulated output values and returns the difference. The mass balance is solely based on mass flows, while the energy balance is based on mass flows, temperatures and specific heat of the different compounds. The energy generated or consumed by the chemical reactions is calculated from the change of mass of the pellet bed and the heat of reaction.

3

Methodology

The work in this project was based on a previously established methodology developed in the Chalmers-LKAB collaboration. An important part of the work has been to continue the development of the straight-grate process model and to adapt it for operation with plasma torches and microwave heating. NO_x emissions from plasma torches have also been investigated through reaction modelling. Figure 3.1 shows an illustration of the working procedure of this project.

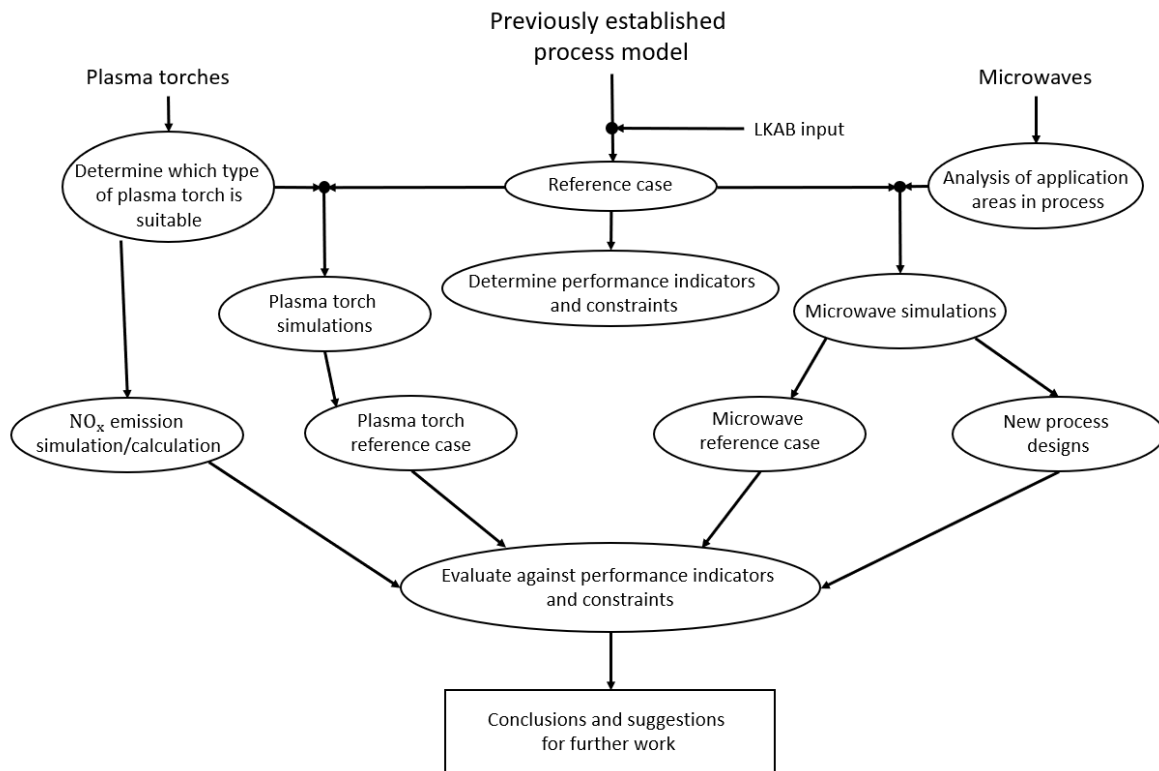


Figure 3.1: Visualization of the working procedure in this project.

3.1 Reference case

The reference case (REF) was based on information provided by LKAB for the process in the MK3 straight-grate unit. The input data used in the reference case have been used by LKAB for an earlier pot-furnace campaign but is not available in the public version of this report.

In the real MK3 unit described in Section 2.2.1, a large recuperation hood is used to lead the flow from the C1 zone to the firing zones (PH, F and AF). The problem with this configuration is the difficulty to control the amount and direction of air into the firing zones. In order to be able to make alterations to the process, more detailed sectioning was required where each cooling zone was connected to a specific firing zone.

The reference case therefore has 14 process zones instead of 8, where the F, AF and C2 zones were divided into two zones while the C1 zone was divided into five zones. The finer sectioning makes it possible to match the temperature profiles between the cooling and firing zones. An illustration of the connections between the process zones in the reference case can be seen in Figure 3.2.

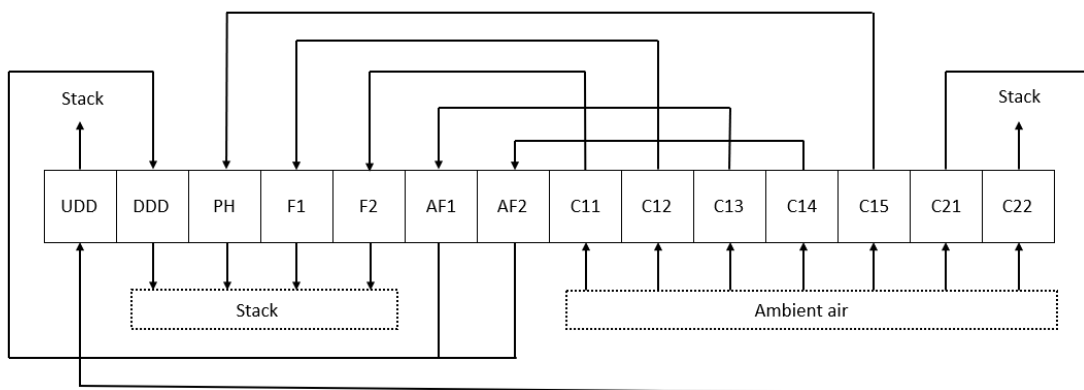


Figure 3.2: Schematic illustration of the connections between process zones in the reference case.

The model works by defining input data for the incoming flows and calculating output data for the outgoing flows. The flow rates between connected zones were matched in the input file. However, no process zones were directly connected in the simulation model, since this significantly increased the complexity of the system as well as the simulation time. Instead, the temperature differences between the flows from the C1 zone to the firing zones were accounted for in the energy calculations. Here the energy required to heat up the air to the desired temperature was calculated. This leaves the flows from C21 to UDD and AF to DDD. These were left unconnected but the results were monitored in order to make sure that the temperature differences between outgoing and incoming flows were not too large. The calculation approach used in the simulation model is visualized in Figure 3.3.

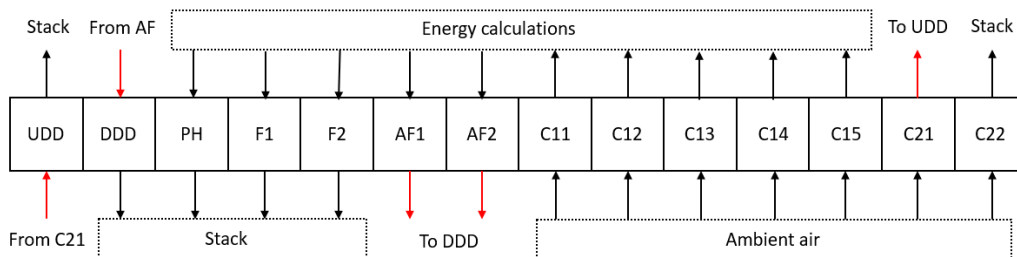


Figure 3.3: Illustration of how the calculations are performed in the simulation model. The red streams are left unconnected.

3.1.1 Performance indicators

The performance of the reference case served as a baseline for comparisons between different process designs. The performance indicators selected in this study are presented in Table 3.1.

Table 3.1: Selected performance indicators for the straight-grate process.

Indicator	Description
$F_{\text{mag,mean}}$ [%]	Mean magnetite content at the end of the grate
$F_{\text{mag,max}}$ [%]	Maximum magnetite content at the end of the grate
$T_{\text{bed,mean}}$ [°C]	Mean temperature of bed at the end of the grate
$T_{\text{bed,max}}$ [°C]	Maximum temperature of bed at the end of the grate
Q_{fossil} [MW]	Power requirement from fossil fuel sources
Q_{el} [MW]	Power requirement from electricity
E_{tot} [kWh/ton _p]	Total energy consumption per ton of pellets produced

The first parameters were the magnetite content, F_{mag} , and the bed temperature, T_{bed} , at the end of the process. The mean and maximum value of these parameters were used for assessing the pellet quality. The magnetite content was the main indicator of pellet quality used in this study since other parameters such as pellet strength and deformation could not be simulated in the model. The magnetite content represents the share of the pellets that have not been oxidized to hematite, meaning that a low magnetite content at the end of the process is desirable. The temperature of the finished pellets is also important since a too high temperature can lead to problems with material handling equipment when the pellets are prepared for transport. Higher temperatures also cause an increased amount of dust from the pellets. It is generally positive to achieve a more homogeneous bed where all of the pellets have a similar magnetite content and temperature and due to this a lower maximum temperature and magnetite content was also desirable.

The final three performance indicators were power requirement from fossil fuel, Q_{fossil} , and electricity, Q_{el} , as well as the total energy consumption, E_{tot} . These were the primary indicators used to evaluate the energy efficiency of the process. With a constant production rate, the energy consumption increases linearly with total power. The energy calculations only consider the energy required to heat the process gas, the electricity used to drive fans and other process equipment is not included. The calculations also do not consider the thermal efficiency of the burners. The calculations of the performance indicators are presented in Appendix A.

3.1.2 Process constraints

The operation of the straight-grate process is limited by certain physical constraints that had to be considered when making changes to the process. The constraints have been determined by LKAB and are presented in Table 3.2. The difference between performance indicators and constraints is that the constraints have a clearly defined limit.

Table 3.2: Process constraints considered for the straight-grate process.

Constraint	Limit	Description
Δp_{bed} [Pa]	8000	Maximum pressure drop over the bed
T_{fan} [°C]	400	Maximum recuperation fan temperature
T_{grate} [°C]	500	Maximum grate temperature
r_{evap} [kg/m ³ /s]	2.5	Maximum evaporation rate

The maximum grate temperature is used to limit the thermal expansion of the grate material which can cause the conveyor to break. This is an important constraint since it restricts the amount of heat that can be sent through the grate. The temperature of the gas flow through the recuperation fans cannot be higher than 400 °C to avoid thermal stresses to the fan blades. These fans are located after the firing and C2 zones. It is known that BedSim overestimates the temperature from the AF zone. In the real process, there is a leakage of air under the bed from the C1 zone which significantly lowers the temperature in the AF2 zone.

The pressure drop over the bed is limited since an increased pressure drop leads to higher power consumption for the process fans in order to force the flow through the bed. Finally, the evaporation rate is limited since too fast evaporation of the water inside the pellets leads to a build up of pressure that can cause the pellets to crack. Both the limit for the pressure drop and the evaporation rate were determined by taking the current maximum for the reference case and adding a margin of 10 %. This was chosen based on recommendations from LKAB. The maximum fan and grate temperature can be checked directly from the simulation output, while the pressure drop and evaporation rate need to be calculated. These calculations are presented in Appendix A.

3.2 Microwaves

The methodology of evaluating the potential for implementing microwave heating in the straight-grate process was to use the reference case, described in Section 3.1, in the simulation model and modify it to fit the characteristics of applying microwave heating in the UDD zone. A microwave case study was constructed focusing on recreating the trends in the moisture and temperature profiles of the pellets observed in the study performed by Athayde et al. [25] in an attempt to anchor the model in experimental results. The results from the study by Athayde et al. are presented in Section 2.3.3. It is important to note that some of the parameters that might be affected by microwave implementation such as thermal runaway, heating rate, crushing strength of the pellets and decreased pellet deformation and clogging cannot be measured with the simulation model and therefore these must be analyzed in practical tests.

The microwave heating was simulated via convective heat transfer in a downdraft flow direction. In reality, the microwave heating and updraft drying would be in the same zone, heating the bed from above and below simultaneously. In the simulation model however, these two modes of heating had to be in separate zones due to their opposite flow direction. Small microwave sections were placed evenly distributed across the length of the UDD zone according to Figure 3.4, to approximate the behaviour of the two zones being merged together. The simulation model could handle a maximum of 20 process zones and since the reference case has 14 zones in total, there was room for three UDD zones and four microwave zones. A larger amount of microwave zones would provide more accurate results although the trends of using microwaves and UDD in combination were still captured with this relatively small amount of microwave zones.

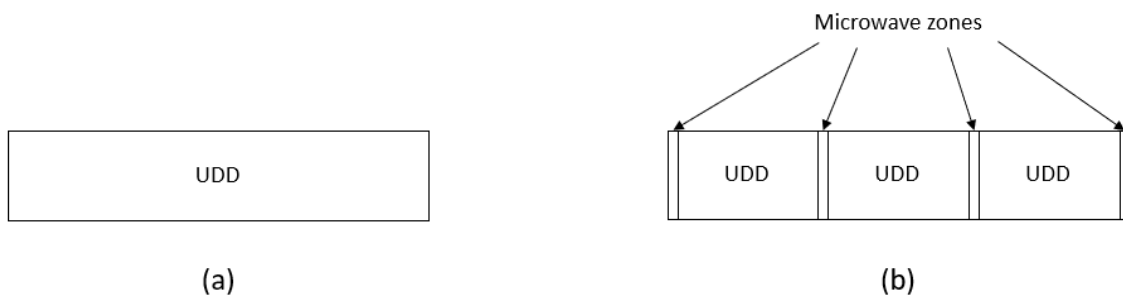


Figure 3.4: (a) Original UDD (b) UDD and microwave zone configuration.

The configuration of the microwave zones that most accurately correlated with the moisture and temperature profile found in the study by Athayde et al. [25] was established by a trial and error approach using the simulation model. The zone area, position, gas flow and gas temperature in the microwave zones were changed until the model showed results similar to the study.

The microwave zones were constructed to provide a very rapid change in temperature and moisture content of the upper layers. The rapid change was necessary for the lower layers of the bed to remain unaffected through the microwave zone to as large extent as possible. The performance of the microwave case study was then evaluated against the performance indicators and process constraints described in Section 3.1.1 and 3.1.2 respectively.

The amount of evaporated water in the UDD section increased when implementing microwave heating compared to using only convective heating. It was therefore of interest to investigate if the gas flowing through the UDD zone could transport the extra moisture away. The simulation model accounts for moisture saturation in the gas but since the UDD zones and microwave zones had to be separated when simulating the process, it was necessary to calculate what moisture content the gas would have had when exiting the UDD zone if the UDD zones and microwave zones were combined into one. This was done by adding the moisture content of the gas leaving the microwave zones to the gas leaving the UDD zones. Calculations were performed according to Equation A.4 and A.5 and results were manually compared to the maximum moisture carrying capacity of dry air at different temperatures to evaluate if the modeling results overestimate the moisture carrying capacity in the UDD/Micro zone.

The power requirement for microwave generation was estimated using the study by Athayde et al. [25] as a baseline. Since the modeling of the microwave heating in the simulation model was constructed to mimic the results of the pellet moisture and temperature gradients from the study by Athayde et al. it was considered reasonable to extrapolate the power requirement used in these experiments and apply it to the real process. The power intensity, q_{potgrate} , for the experiments performed by Athayde et al. was calculated according to Equation A.1 and was then used to calculate the power requirement for the LKAB process according to Equation A.2. Losses were included in the calculations but the magnitude of the losses in the microwave generation equipment and to the surroundings was unknown and therefore the estimation of the power requirement should be regarded as a rough estimation.

New process designs were developed with a trial and error approach with the focus of improving the performance indicators with modifications enabled due to microwave implementation while complying with the process constraints. Some general guidelines for modifications to the drying zones were found while experimenting with the simulation model. It was possible to increase the energy input in the UDD zone without exceeding the process constraints. The DDD zone showed much less room for increased energy input with the evaporation limit being the limiting constraint.

3.2.1 New process design A

The new process design A was focused on exploring the possible benefits of lengthening the UDD section while avoiding recondensation in the higher layers of the bed by implementing microwaves. It has a larger UDD/Micro zone and a smaller DDD zone compared to the reference case. The UDD size was increased to 29 m² from its previous 21 m² and the DDD size was decreased to 16.5 m² from its previous size of 31.5 m². Resulting in a 7 m² reduction in total grate area.

Due to the change in size of these zones, their respective gas flows were also modified as can be seen in Figure 3.5, where the lines marked in red indicate modifications compared to the reference case. The reasoning behind the configuration in Figure 3.5 was to re-use as much as possible of the energy in the streams available to increase the energy input per square meter of grate primarily in the UDD/Micro section but also a slight increase in the DDD zone until the evaporation rate constraint limit is reached. The temperature in the DDD zone is the same as the reference case but the mass flow of gas per square meter of grate is slightly increased. The gas flow from C22 which was previously sent to the stack is redirected to the UDD/Micro zone which increases the mass flow through the UDD/Micro zone heavily and reduces the temperature since it contains lower grade heat.

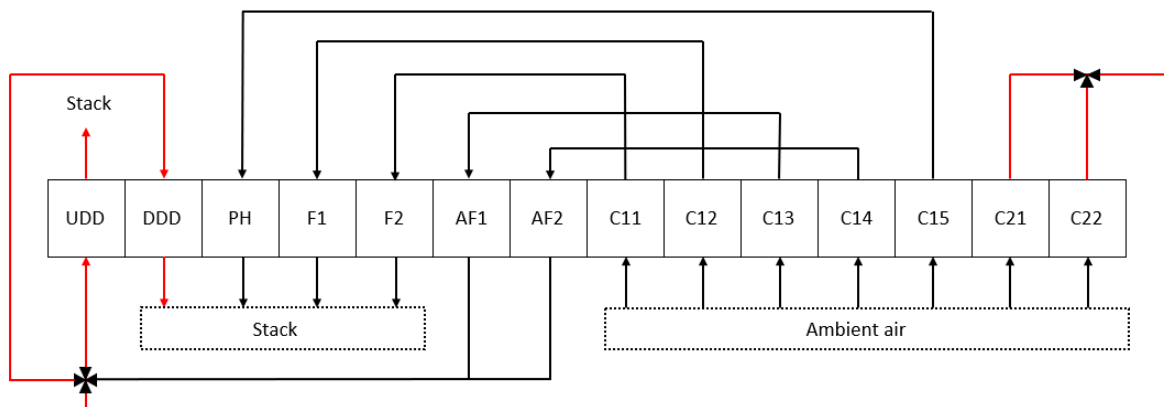


Figure 3.5: Illustration of connections between process zones. Gas flows which are modified compared to the reference case are marked in red.

3.2.2 New process design B

The new process design B was an extension of design alternative A. It was possible to reduce the magnetite content of the pellets by increasing the size of the first cooling zone, C11. The size of C11 was increased by 7 m² compared to design alternative A, making the total area of all zones equal to the reference case. The increased size of C11 results in a decrease in the gas flow per square meter of grate. Other than that, all input parameters are the same as the input parameters of design alternative A.

3.3 Plasma torches

To study the effect of implementing plasma torches in place of fossil fuel burners in the straight-grate process, a plasma torch case study was established. As mentioned in Section 2.4.5, the main differences when introducing plasma torches is the lack of combustion reaction and the addition of working gas flow into the process gas. An overview of the process streams considered for the oil burner and the plasma torch is presented in Figure 3.6.

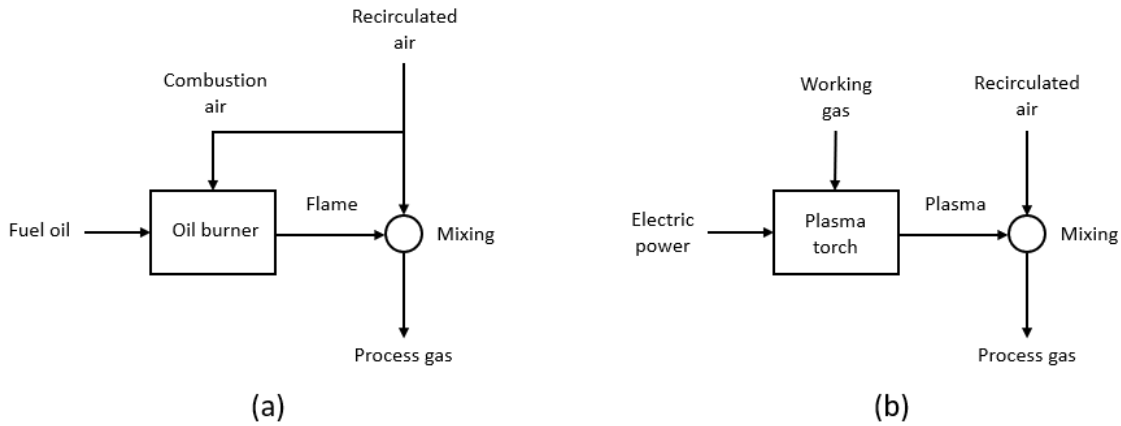


Figure 3.6: Schematic illustration of the process streams considered for an oil burner (a) and a plasma torch (b).

To calculate the flow rate and composition of the process gas in the firing zones, certain parameters for the plasma torches had to be specified. These include torch power, thermal efficiency and working gas flow rate. The parameters used for the plasma case study are based on a 2 MW industrial plasma torch from Westinghouse [32], presented in Table 3.3. This type of torch was chosen since it has a similar power level to the oil burners currently used in the MK3 unit.

Table 3.3: Parameters used for the plasma torch case study.

Parameter	Value	Description
P_t [MW]	2	Torch net electric power
U_a [V]	1000	Arc voltage
I_a [A]	2000	Arc current
η_{th} [%]	85	Thermal efficiency
V_{gas} [Nm^3/h]	250	Working gas flow rate

When a simulation of the reference case had been run, the heating power required for each firing zone could be calculated from the gas mass flow and the enthalpy difference over the zone. The number of plasma torches and the corresponding working gas flow could then be found. By specifying the composition of the plasma working gas and the air from the cooling zone, the new composition of the process gas could be calculated. Using the increased flow rates and the new process gas compositions as input data, a new simulation could be run to simulate the operation of the process with plasma torches.

An initial comparison was made between the reference case and a case with plasma torch operation. Simulations were then performed with different working gases and flow rates to analyze how these parameters affected the process. The BedSim model can only take N_2 , O_2 , H_2O and CO_2 as input for the process gas. Therefore it was not possible to test common working gases such as argon and helium. The working gases that were used in the simulations were air, N_2 , O_2 and CO_2 . The base case had a working gas flow of $250 \text{ Nm}^3/\text{h}$ per plasma torch, but higher flow rates were also used.

3.4 Nitrogen oxide formation

The quantities of NO_x produced from a plasma torch can be qualitatively estimated by reaction modelling in Chemkin based on established gas phase reaction kinetics. A common type of reactor model used for combustion modelling is the one-dimensional plug flow reactor (PFR). In the PFR a temperature profile can be defined and the reactions are calculated at different distances from the reactor inlet. This can be used to obtain a detailed analysis of the chemistry at different positions in the reactor. Even though no combustion occurs in a plasma torch, the same calculation approach should still be applicable.

The idea was to start with a simplified model and to gradually make it more complex. This gave an improved understanding of the underlying mechanisms and chemical reactions that contribute to the formation of NO_x . Since many parameters of the torches are unknown, the study is of a qualitative nature instead of a quantitative, where the focus is to find general trends rather than definite values of NO_x emission levels. The results can then be used as guidelines for future implementation of plasma torches when choosing operating conditions and torch type for a certain application.

3.4.1 Reactor models

In order to study the production of NO in a plasma torch applied to the straight-grate process, a PFR was used to represent the heating in the plasma gas channel and the subsequent cooling of the plasma gas when it mixes with air. The two reactor models that were used are illustrated in Figure 3.7. Since the exact dimensions, gas flows and temperature profiles of the torches were not available, reasonable values were chosen based on previous knowledge from the literature study. Due to this, most of the parameters were subject to sensitivity analysis in order to study their effect on the results.

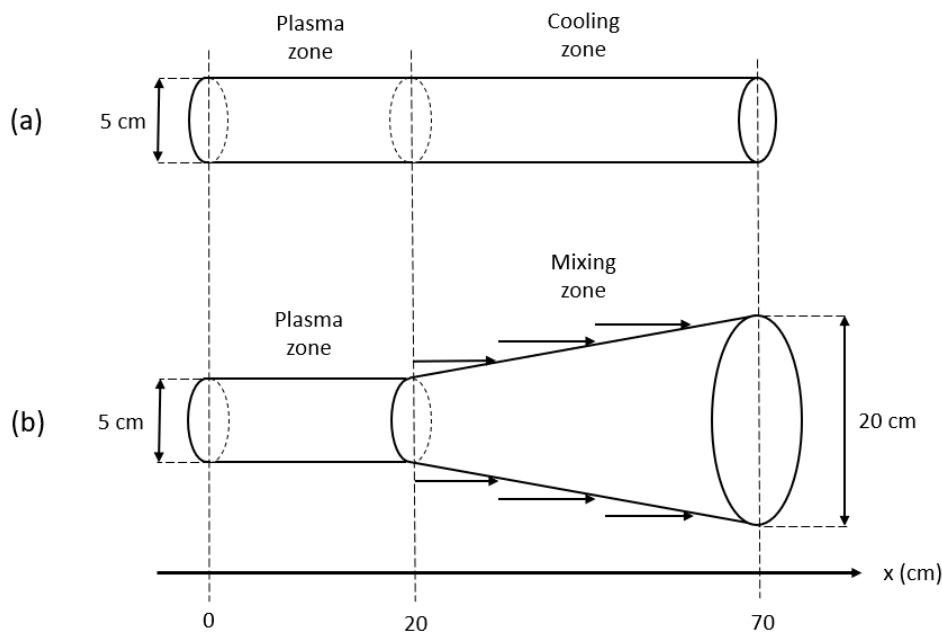


Figure 3.7: Reactor dimensions for the NoMix case (a) and for the MixTP and MixEE cases (b).

The reactor in (a) is a simplified model with a constant cross-section and no mixing. This model was used to study the amount of NO produced directly when the electric arc heats the plasma gas in the no-mixing case (NoMix). The plasma zone is the part of the reactor located inside the torch, where the plasma is heated up to the maximum temperature and maintains this temperature until the start of the cooling zone. The temperature then decreases linearly to the outlet temperature. The inlet temperature is 25 °C, the plasma temperature is 5000 °C and the outlet temperature is 1000 °C. The outlet temperature was chosen based on the temperature of the firing zones in the straight-grate process.

The reactor in (b) is a more complex model where mixing with air is considered. After the plasma zone, the reactor diameter increases linearly from 5 to 20 cm, at the same time as the mass flow increases linearly through successive mixing with air. This can be interpreted as a reaction zone extending from the outlet of the plasma torch, where no air is mixed with the plasma, towards the complete flow at the outlet. This model was used to approximate the amount of NO produced when the air is heated up by the plasma gas. Therefore, the working gas used in the plasma torch for these simulations was argon. Argon is an inert gas meaning that no NO will be produced in the plasma zone. In reality, the area of the outlet depends on the amount of mixing air, which affects the residence time of the gas in the reactor. However, this dependency was not considered in order to simplify the model.

Two versions of the mixing case were simulated, the mixing case with a defined temperature profile (MixTP) and the mixing case where the energy equation was solved to calculate the temperature profile (MixEE). In the MixTP case, the temperature profile was defined using the same temperature profile as the NoMix case. In the MixEE case, the inlet plasma and air temperatures were defined to 5000 °C and 1000 °C respectively and the resulting temperature profile was calculated by the program. The reactor was assumed to be adiabatic, meaning no heat flux out of the system. In both mixing cases, the plasma gas flow was 10 g/s and the total air flow was 100 g/s. The total residence time of the gas in the reactor was between 15-30 ms.

3.4.2 Validation and sensitivity analysis

In order to assess the reliability of the results, the simulation models were validated against experimental results from tests performed by Cementa [41]. In the experiments, a 250 kW plasma generator from ScanArc was used and the gas analysis was made with a Testo 350. NO_x and O₂ were detected with an electrochemical cell and the CO₂ was measured with IR-technique. The amount of NO_x was measured using CO₂ as working gas with different amounts of leakage air in the gas. Tests were made with 3, 6, 9 and 100 % air in the working gas. The results of the experiments showed that the NO_x concentration was rather proportional to the amount of air in the gas, and only air as working gas gave 1856 ppm NO_x.

The parameters chosen for variation in the sensitivity analysis were plasma gas temperature, mixing zone length, air to plasma ratio and plasma gas flow rate. These parameters were chosen since they were believed to have the largest influence on NO formation. For each case, all of the other parameters were held constant and only the studied parameter was varied. The upper and lower limits were determined by either reaching a very low NO concentration or problems with the model to reach convergence.

Two methods for NO reduction were studied through simulations, reburning (staged combustion) and reduction of the oxygen content of the mixing air through combustion. In the reburning simulations, different amounts of methane (CH₄) was added into the mixing zone at a distance of 10 cm from the end of the plasma zone in order to destroy NO through reactions with hydrocarbon radicals. In the oxygen reduction simulations, the composition of the mixing air was changed assuming complete combustion of methane before mixing with the plasma gas. These simulations were performed with a defined temperature profile according to the MixEE case. However, in practice, the additional combustion would cause a temperature increase, which might affect the NO reduction. The methane flow rate was varied between 0-5 g/s for both reduction strategies. The maximum amount of methane that could be combusted was around 5.8 g/s based on the amount of oxygen available.

4

Results and discussion

In this chapter, the results from the case studies are presented and analyzed. To begin with, the performance of the reference case is presented which serves as a baseline for comparisons between process designs. In the following sections, the results for the plasma, microwave and NO_x simulations are presented.

4.1 Reference case

One of the most important parameters is the pellet temperature since it affects the rate of oxidation and sintering. The pellet temperature for the reference case is shown in Figure 4.1. There is a major temperature difference between the top and bottom layers of the bed. For example, in the beginning of the PH zone, the top layer has reached over 1000 °C while the temperature in the bottom layer is almost unchanged. The reason for this is that the downdraft flow heats the upper layers first which also causes the oxidation to start there first.

In order for all the magnetite to oxidize, the pellet temperature needs to stay within a certain temperature interval for a sufficient amount of time. A higher temperature is generally better, but at over 1200 °C the reaction will slow down. This is the reason for the bump in the line for the bottom layer in Figure 4.2. In the end of the AF2 zone, the temperature becomes too high and the oxidation almost stops. But when the bed enters the cooling zone the temperature is reduced and the oxidation starts again for some time.

Figure 4.3 shows the gas temperature for the reference case. The inlet process gas temperature at the beginning and end of a zone is defined in the input file. The gas will then be cooled or heated by heat transfer with the bed. When the gas is supplied from above, the temperature will not change before reaching the bed. However, if the gas is supplied from below it will be heated up by the grate and the hearth layer before reaching the pellets.

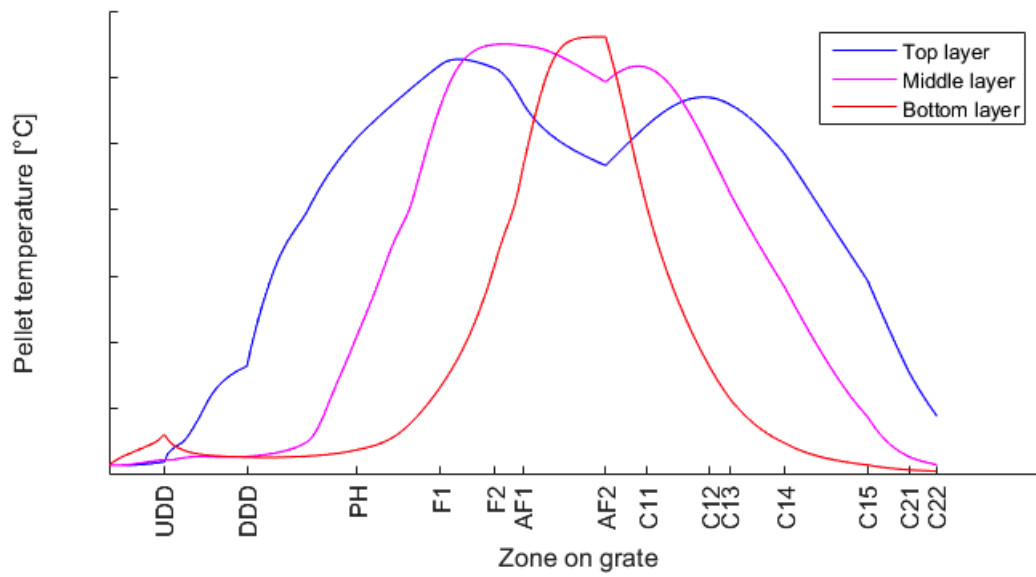


Figure 4.1: Pellet temperature throughout the process for the reference case. The markings on the x-axis shows where each zone ends.

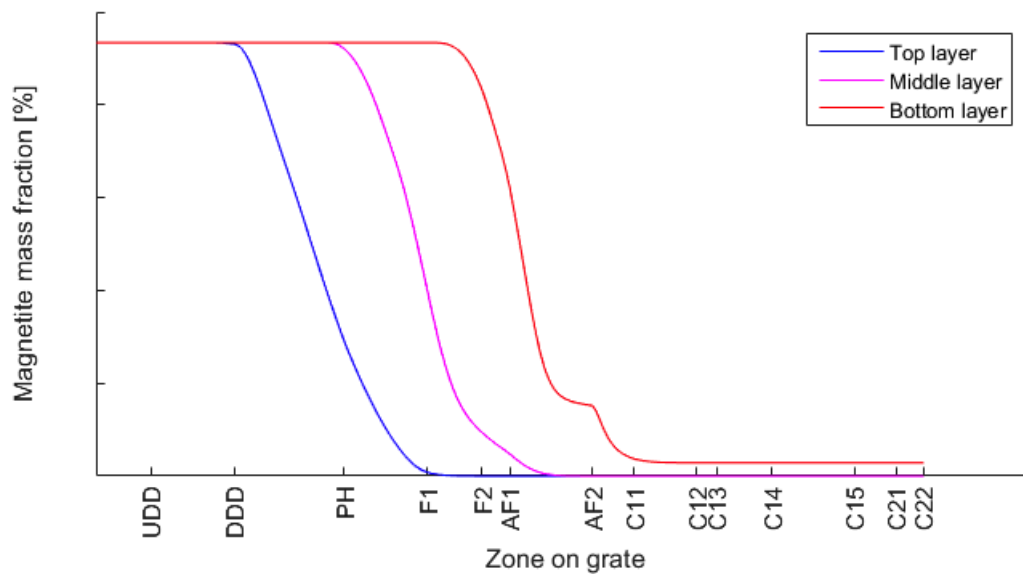


Figure 4.2: Mass fraction of magnetite throughout the process for the reference case.

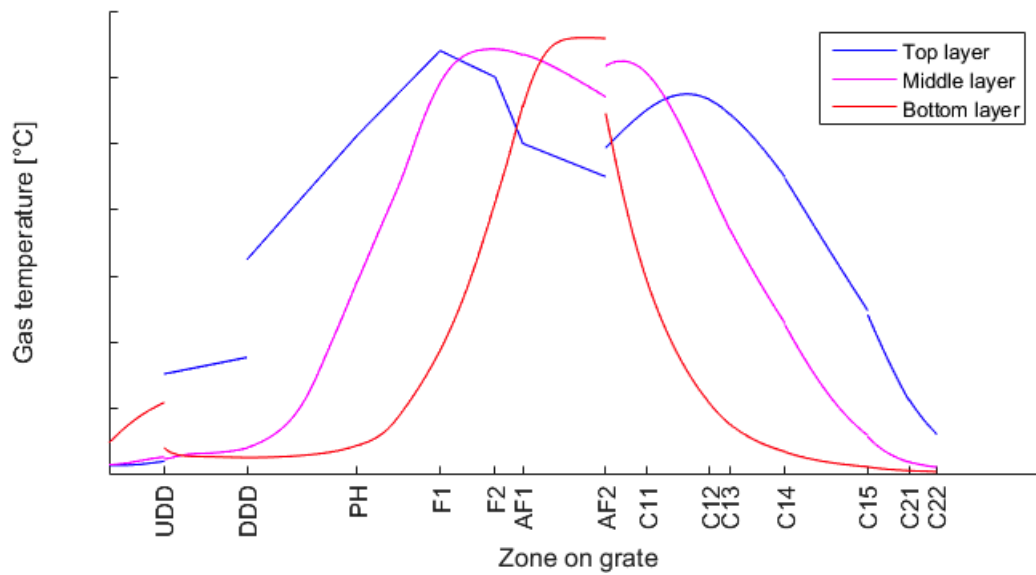


Figure 4.3: Gas temperature throughout the process for the reference case.

Figure 4.4 shows the temperature differences between connected process zones, i.e. the difference between the set temperature of the inlet gas to a heating zone and the calculated temperature of the outlet gas from a cooling zone. The calculated temperatures match the assumed inlet temperatures well except for the outlet of the AF zone which is much higher than the inlet of the DDD zone. It is known from previous studies that BedSim overestimates the temperature from the AF zone. In reality, there is a leakage of air from the cooling zone that results in a significantly lower temperature. This will therefore not be considered to be a problem. If the inlet temperature is higher than the outlet temperature, additional firing is required to increase the temperature. The heat demand is also determined by the gas mass flow in the zones.

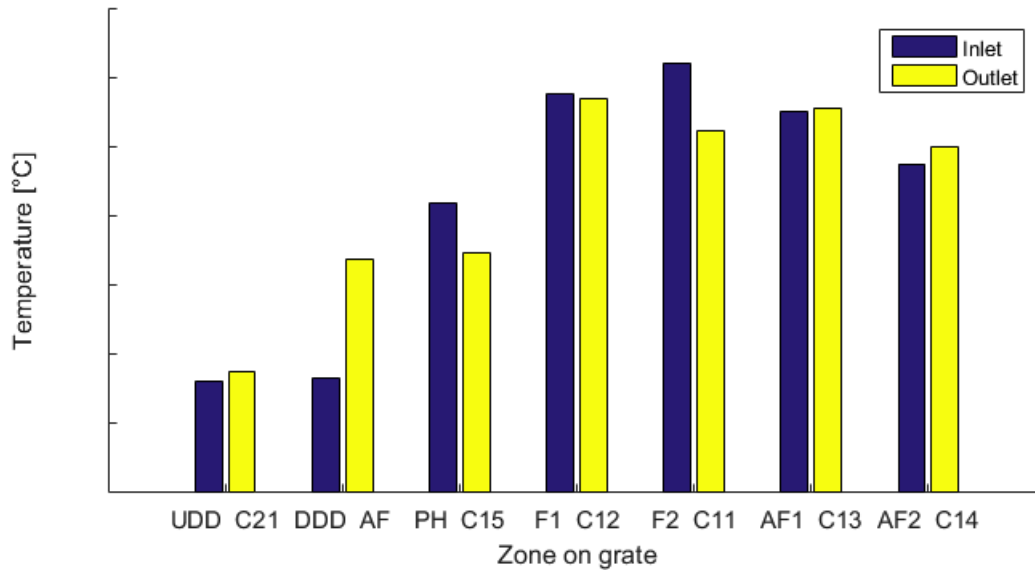


Figure 4.4: Temperature differences between connected process zones for the reference case.

4.1.1 Performance indicators

The performance of the reference case with regards to the chosen indicators is presented in Table 4.1. The maximum magnetite content at the end of the process occurs in the bottom layer while the maximum bed temperature occurs in the top layer. To improve the performance of the process, the focus is to decrease the magnetite content in the bottom layer. A slight increase in mean bed temperature is acceptable, but the temperature should be limited to below 100 °C. The power requirement can be decreased by reducing the temperature difference and the gas mass flow of the firing zones.

Table 4.1: Performance indicators for the reference case.

Indicator	Value
$F_{\text{mag,mean}}$ [%]	0.218
$F_{\text{mag,max}}$ [%]	2.857
$T_{\text{bed,mean}}$ [°C]	49.98
$T_{\text{bed,max}}$ [°C]	177.83
Q_{fossil} [MW]	15.06
Q_{el} [MW]	0
E_{tot} [kWh/ton _p]	33.46

4.1.2 Process constraints

The values of the process constraints for the reference case are presented in Table 4.2. As can be observed in Figure 4.5 and 4.6, both the maximum pressure drop and grate temperature occurs at the start of the first cooling zone, making this critical part of the process. This zone has a high pellet temperature and a large gas mass flow resulting in a high pressure drop. It is also reasonable that the highest grate temperature occurs at the transition between the firing and cooling zones.

Table 4.2: Process constraints for the reference case.

Constraint	Value	Limit
Δp_{bed} [Pa]	7260	8000
T_{fan} [°C]	348.1	400
T_{grate} [°C]	480.8	500
r_{evap} [kg/m ³ /s]	2.329	2.5

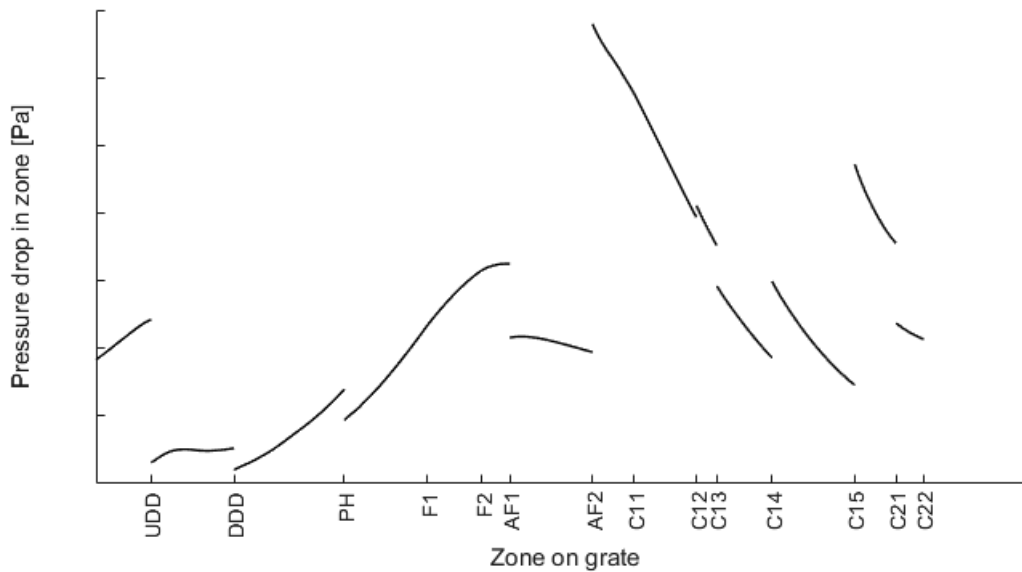


Figure 4.5: Pressure drop over the bed throughout the process for the reference case.

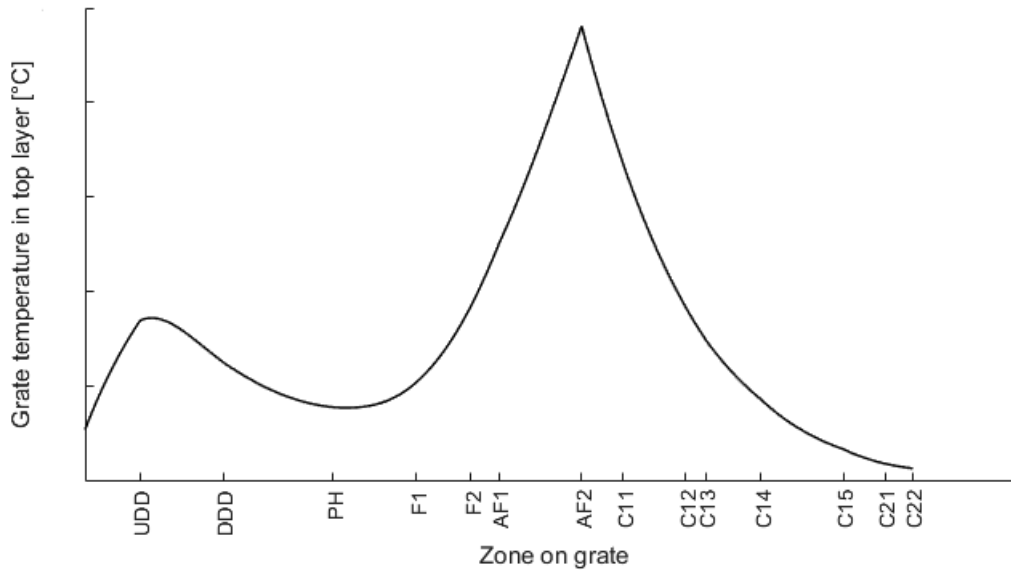


Figure 4.6: Temperature in the top layer of the grate throughout the process for the reference case.

4.2 Microwaves

This section presents the results from process simulations with microwaves, starting with the microwave case study and later presenting results from new process designs.

4.2.1 Microwave case study

The microwave case study has the addition of the microwave energy input in the UDD zone. Table 4.3 shows the measured values of pellet temperature and moisture content presented in the study performed by Athayde et al. [25] and Table 4.4 shows the values of pellet temperature and moisture content at the end of the UDD section for the reference case and the microwave case study from the process model. Measurements by Athayde et al. recorded a larger temperature difference between their reference case and microwave assisted case. The process gas used in these experiments was warmer which provides less of a cooling effect, leading to lower thermal gradients and less driving force for heat transfer between pellets and process gas resulting in higher pellet temperatures. It is also possible that the process model underestimates the temperature increase of the pellets affected by microwaves. However, the trends are similar and the values are reasonable in comparison which enforces the credibility of the results from the microwave case study.

Table 4.3: Pellet temperature and moisture content measured at the end of the UDD/Micro section in the study by Athayde et al. [25].

Depth [mm]	H ₂ O _{REF} [%]	T _{REF} [°C]	H ₂ O _{Micro} [%]	T _{Micro} [°C]
0	-	55	-	130
30	10.5	71	9.3	115
60	10.2	-	10.0	-
240	6.4	85	6.4	85
360	-	-	-	-

Table 4.4: Pellet temperature and moisture content at the end of the UDD/Micro section in the simulation model.

Depth [mm]	H ₂ O _{REF} [%]	T _{REF} [°C]	H ₂ O _{Micro} [%]	T _{Micro} [°C]
0	8.7	39.6	6.5	79.3
25	8.8	40.2	7.4	61.7
76	8.8	41.5	8.2	47.6
203	8.4	46	8.3	44.7
305	6.9	56	6.9	53.5
418	0.7	122.3	0.6	112

Figure 4.7 and 4.8 gives a visual representation of the moisture content of the pellets in the drying zones of the reference case and the microwave case study. It can be seen that the moisture content in the higher layers of the bed in the UDD is decreased when microwaves are implemented, avoiding recondensation. The lower layers are virtually unaffected by the microwaves.

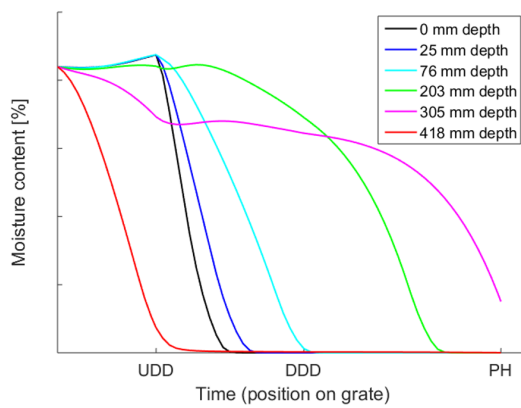


Figure 4.7: Reference case moisture content.

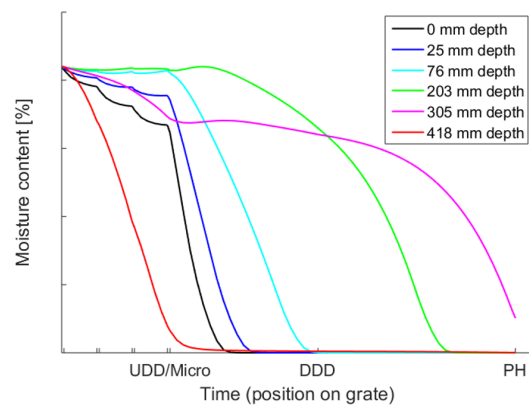


Figure 4.8: Microwave case moisture content.

Figure 4.9 and 4.10 shows the temperature profile of the pellets in the drying zones of the reference case and the microwave case study. The zone transitions between the microwave zones and the UDD zones are more prominent in the temperature profile than the moisture content as can be seen by comparing Figure 4.10 and 4.8. The pellet temperature reduces to almost the same level as the reference case before spiking again when switching to microwave mode. It is believed that the process model underestimates the temperature profile seen as an average across the whole UDD/Micro zone due to UDD being the dominating operational mode.

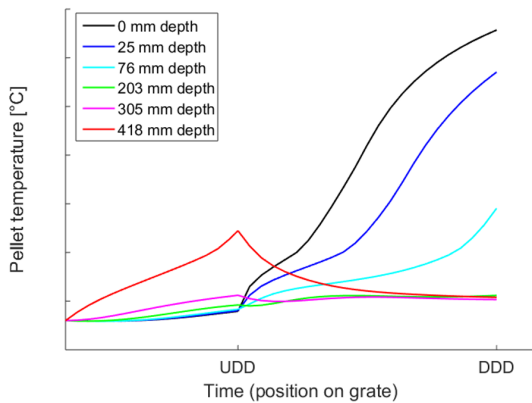


Figure 4.9: Reference case temperature profile.

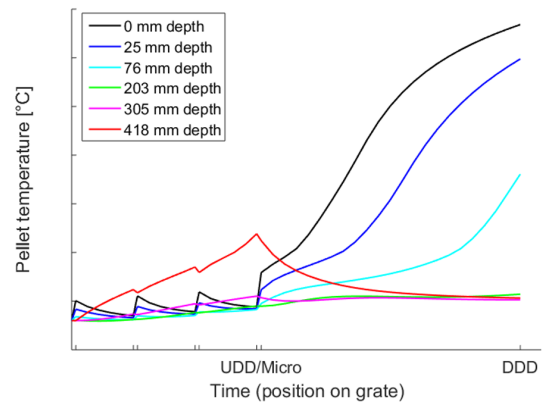


Figure 4.10: Microwave case temperature profile.

Calculations of the moisture content of the gas exiting the UDD/Micro section was performed according to Equation A.4 and A.5. Results showed that the gas is slightly over-saturated when exiting, implying that the process model overestimates the amount of moisture that can be transported from the UDD/Micro zone. However, the maximum moisture carrying capacity of air increases exponentially with temperature which implies that a small change in temperature has a large impact on the moisture carrying capacity of the gas. As previously mentioned, it is believed that the temperature profile of the pellets is underestimated by the process model in the microwave case study. Assuming that the gas is heated to a temperature close to that of the pellets when passing through would indicate that the ability of the gas to transport the moisture away is sufficient. Practical tests are necessary to further investigate this matter. However, it is a problem that can be managed by increasing the temperature of the gas exiting the UDD/Micro zone, increasing the mass flow of gas or a combination of the two.

The electric power requirement, Q_{el} , for microwave generation was calculated according to Equation A.2 and was found to be 5.36 MW for the microwave case study which has an UDD area of 21 m². This is a considerable amount of power in comparison to the power requirement for the whole process. Losses are included when calculating the power requirement for microwaves while there are losses for the oil burners which are not captured in the process model. It is known that LKAB uses 5 liters of oil per ton finished pellets in normal operation of the MK3 straight-grate unit which is the base for the reference case [14].

This amounts to a power requirement of 24.34 MW while the total power demand for the reference case calculated by the process model only amounts to 15.06 MW which is a considerable difference. This should be kept in mind when assessing the power requirement of the microwaves.

The performance indicators of the microwave case study are presented in Table 4.5, next to the performance indicators of the reference case. The power requirement is the most noticeable difference between the two cases while the rest of the performance indicators show only marginal changes. The power supplied from the microwaves, Q_{el} , has almost no impact on reducing the fossil power demand, Q_{fossil} . This is likely due to a lot of the heat supplied by the microwaves being absorbed by the gas flow leaving the UDD zone. It is a considerable energy loss source. The temperature of the gas flow leaving the UDD zone would likely be around, or even below, 100 °C assuming that it reaches approximately the same temperature as the pellets in the top layer of the bed. This is low-grade heat which has limited application areas.

Table 4.5: Performance indicators for REF and microwave case study.

Indicator	REF	Micro
$F_{mag,mean}$ [%]	0.218	0.206
$F_{mag,max}$ [%]	2.857	2.756
$T_{bed,mean}$ [°C]	49.98	50.62
$T_{bed,max}$ [°C]	177.83	179.56
Q_{fossil} [MW]	15.06	15.00
Q_{el} [MW]	0	5.36
E_{tot} [kWh/ton _p]	33.46	45.24

The values of the constraint parameters for the microwave case study lies well within the limits as can be seen in Table 4.6. The most noticeable change is the decrease in maximum evaporation rate. This maximum occurs in the higher layers of the bed at the start of the DDD section which is the same as for the reference case. Less moisture content in the pellets at this point seems to help reducing the maximum evaporation rate.

Table 4.6: Process constraints for the microwave case study.

Constraint	REF	Micro	Limit
Δp_{bed} [Pa]	7260	7265	8000
T_{fan} [°C]	348.1	349.6	400
T_{grate} [°C]	480.8	488.8	500
r_{evap} [kg/m ³ /s]	2.329	2.27	2.5

The results indicate that microwave implementation is ineffective without further design changes of the process since the total power requirement increases substantially with almost no reduction in fossil fuel demand while the remaining performance indicators are virtually unaffected.

4.2.2 New process designs

The results for the new process designs A and B are presented side by side in this section since there are many similarities in the configuration of the two cases, as described in Section 3.2.1 and 3.2.2.

The drying sections of process design A and B are the same meaning that Figure 4.11 and 4.12 applies for both cases. Figure 4.11 shows the moisture content of the pellets and Figure 4.12 shows the pellet temperature in the drying section of the process. When comparing these to the reference case in Figure 4.7 and 4.9, it can be seen that the increased energy input in the UDD/Micro section results in a quicker drying process and a higher temperature in the lower layers of the bed.

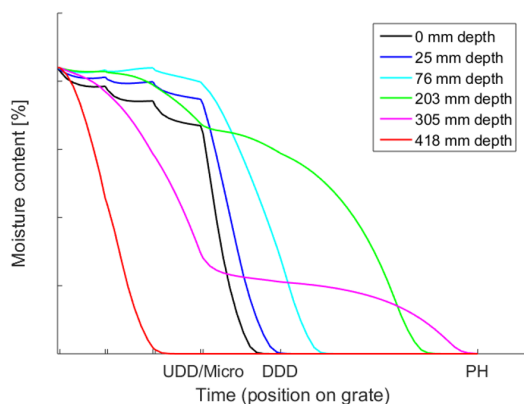


Figure 4.11: New process design moisture content.

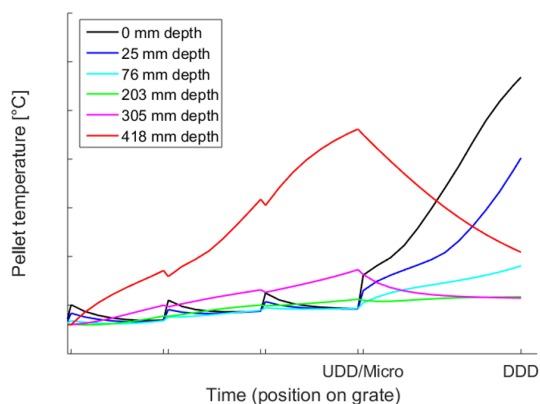


Figure 4.12: New process design pellet temperature.

The microwave energy input was kept constant even when changing the size of the UDD section in the new process designs A and B. The new process designs has an UDD area which is larger than the microwave case study. This leads to a lower power intensity from the microwaves in the UDD zone of the new process designs leading to the moisture and temperature profiles being conservative compared to the microwave case study. This choice was made since it was difficult to extrapolate the effect that the microwaves had on the moisture and temperature profiles and therefore being on the conservative side makes it possible to assume that cracking of pellets due to rapid moisture evaporation rates does not occur as a result of microwave heating since it was not observed in the study by Athayde et al. [25] where higher power intensity was used.

Performance parameters for design alternatives A and B are presented in Table 4.7. The total grate area, A_{grate} , differs between the designs and therefore it was added as an additional performance indicator. Design alternative A shows pellet outlet temperatures and magnetite content similar to the reference case with lower total grate area and higher total power demand. The fossil power demand, Q_{fossil} , is decreased by 0.51 MW compared to the reference case which is small in comparison to the increased power demand for electricity, Q_{el} .

Design alternative B shows the lowest magnetite content out of all design alternatives. This is due to the added grate area in the first cooling zone, C11, which results in a slightly slower cooling process and thereby a longer residence time in the temperature interval where magnetite conversion occurs. The fossil power demand is decreased by 0.98 MW compared to the reference case which is again, small in comparison to the increased power demand from electricity. It is clear that microwaves can replace a small amount of the high-temperature energy in the process by supplying heat in the low-temperature range which is otherwise covered by the high-temperature energy flows which must be added to the process for magnetite conversion and the sintering process. Implementation of microwaves decrease the energy efficiency of the process although it does provide potential for CO₂ reduction depending on how the electricity is produced. A financial analysis is needed evaluating if there is sufficient financial gain in reducing the grate area and fossil power demand to make design alternative A and B economically viable.

Table 4.7: Performance indicators for the new process designs.

Indicator	REF	Design A	Design B
$F_{\text{mag,mean}}$ [%]	0.218	0.208	0.062
$F_{\text{mag,max}}$ [%]	2.857	2.679	0.92
$T_{\text{bed,mean}}$ [°C]	49.98	50.83	49.65
$T_{\text{bed,max}}$ [°C]	177.83	180.05	177.43
Q_{fossil} [MW]	15.06	14.55	14.08
Q_{el} [MW]	0	5.36	5.36
E_{tot} [kWh/ton _p]	33.46	44.24	43.21
A_{grate} [m ²]	315	308	315

Table 4.8 shows the process constraint values which are within the limits. The evaporation rate, r_{evap} , is at the maximum limit. This occurs in the top layer of the bed in the beginning of the DDD zone.

Table 4.8: Process constraints for the new process designs.

Constraint	REF	Design A	Design B	Limit
Δp_{bed} [Pa]	7260	7485	7485	8000
T_{fan} [°C]	348.1	285.43	282.98	400
T_{grate} [°C]	480.8	491.24	491.16	500
r_{evap} [kg/m ³ /s]	2.329	2.5	2.5	2.5

4.3 Plasma torches

This section describes the results from the simulations of plasma torches applied to the straight-grate process. A plasma torch case study is established which is used to analyze the effect of different plasma working gases and working gas flows. Finally, an optimization is made which proposes two methods for improving the energy efficiency of the process after implementation of plasma torches.

4.3.1 Plasma torch case study

The calculated parameters for the plasma torch case study include total heating power requirement for the firing zones, the number of plasma torches and flow rate increase, presented in Table 4.9. The number of torches is only used to estimate the total working gas flow rate.

Table 4.9: Calculated parameters for the plasma torch case study.

Parameter	Value
Total power required [MW]	15.06
Number of plasma torches	8.86
Total air flow [Nm^3/s]	119.39
Total working gas flow [Nm^3/s]	0.62
Flow rate increase [%]	0.52

For the plasma torch case study, a working gas of air is used with a flow rate of $250 \text{ Nm}^3/\text{h}$ per torch. This means that the flow rate of the process gas increases but the composition is not affected. A flow rate of $250 \text{ Nm}^3/\text{h}$ is relatively low in comparison to the air flows in the firing zones, as can be seen in Table 4.9. This means that the introduction of working gas into the process gas only has a marginal effect that is unlikely to affect the performance of the process as a whole to a significant degree.

The performance of the plasma torch case is compared with the reference case in Figure 4.13 and 4.14. Some temperature deviations can be seen in the firing zones, however, the curves are more or less identical. The magnetite mass fraction decreases slightly faster for the plasma torch case compared to the reference case. The final magnetite content in the bottom layer is 2.50 % as can be seen in Table 4.10, which is 0.35 % lower than for the reference case. This indicates a small performance improvement, which can mostly be explained by the increased amount of oxygen in the process gas due to the lack of combustion. When oxygen working gas is used instead of air, the magnetite content becomes 2.41 %, which is a further improvement of 0.09 %.

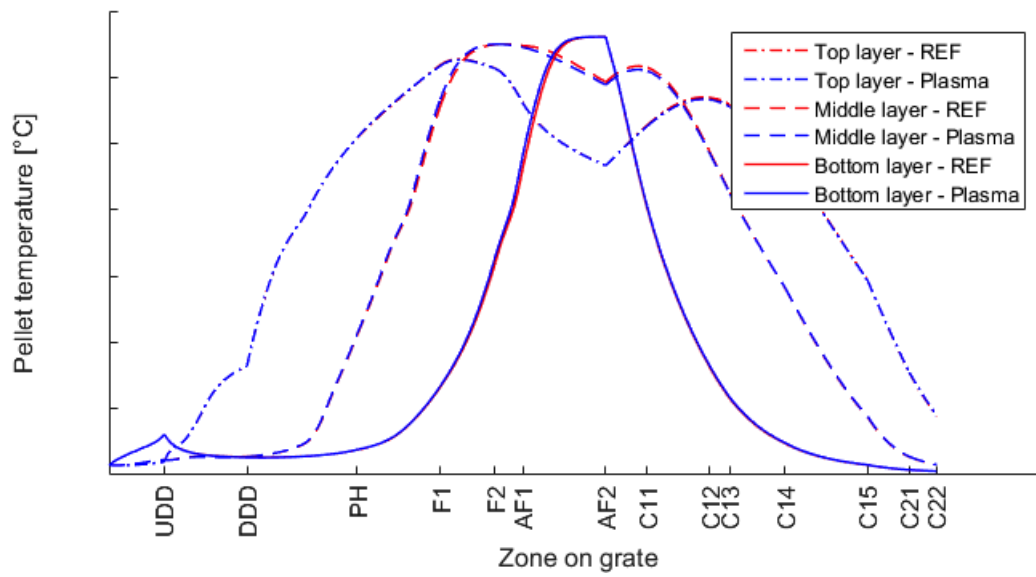


Figure 4.13: Pellet temperature throughout the process for the reference case and the plasma torch case.

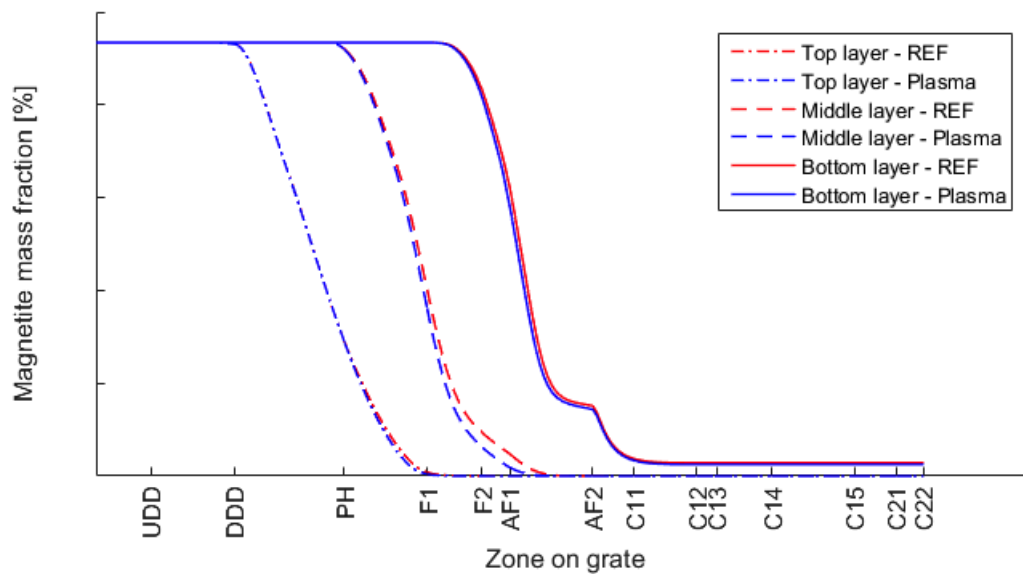
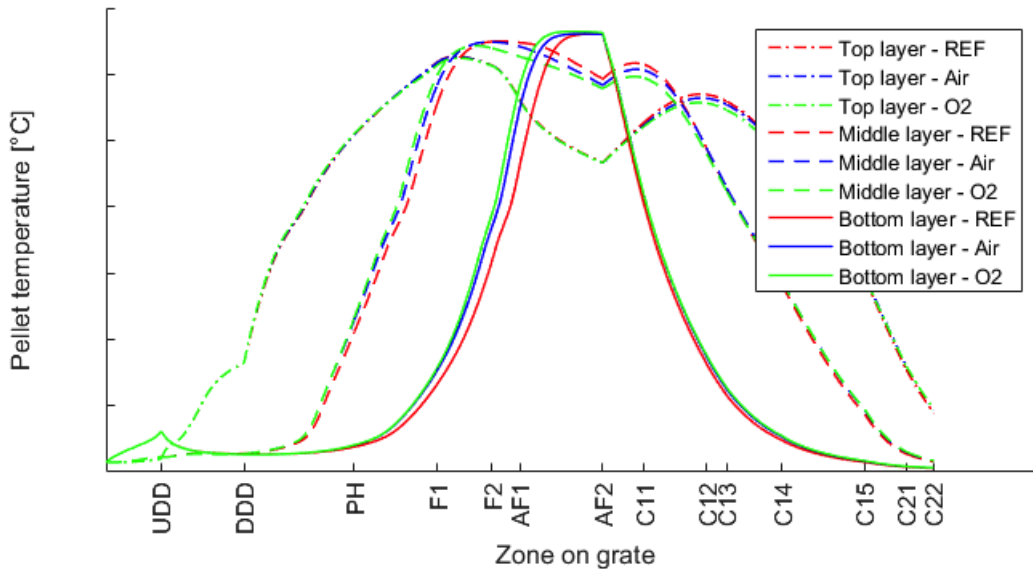


Figure 4.14: Magnetite mass fraction throughout the process for the reference case and the plasma torch case.

Table 4.10: Performance indicators for the plasma torch case study.

Indicator	REF	Plasma
$F_{\text{mag,mean}}$ [%]	0.218	0.173
$F_{\text{mag,max}}$ [%]	2.857	2.504
$T_{\text{bed,mean}}$ [°C]	49.98	50.53
$T_{\text{bed,max}}$ [°C]	177.83	179.10
Q_{fossil} [MW]	15.06	0
Q_{el} [MW]	0	14.40
E_{tot} [kWh/ton _p]	33.46	32.00

In order to achieve significant changes to the process conditions, higher working gas flow rates are required. To study the effects of different working gases the flow rates are increased by a factor of ten to 2500 Nm³/h per torch, keeping the same torch power. This results in a process gas flow rate increase of around 5.2 %. Cases with air, N₂, O₂ and CO₂ as working gas are simulated. It is found that all of the gases except O₂ gives similar results. Therefore, only air and O₂ are presented in Figure 4.15 and 4.16. As can be seen in Table 4.11, the maximum magnetite content at the end of the process is 2.28 % for air but decreased even further to 0.60 % for oxygen. This indicates that using pure oxygen as working gas in the plasma torches is a good choice since it increases the oxidation rate and improves the quality of the pellets. However, increasing the oxygen content in the process gas also leads to a higher temperature of the finished pellets and a higher grate temperature. The maximum grate temperature is 543 °C which is slightly above the constraint.

**Figure 4.15:** Pellet temperature throughout the process for the plasma torch cases with increased flow rates.

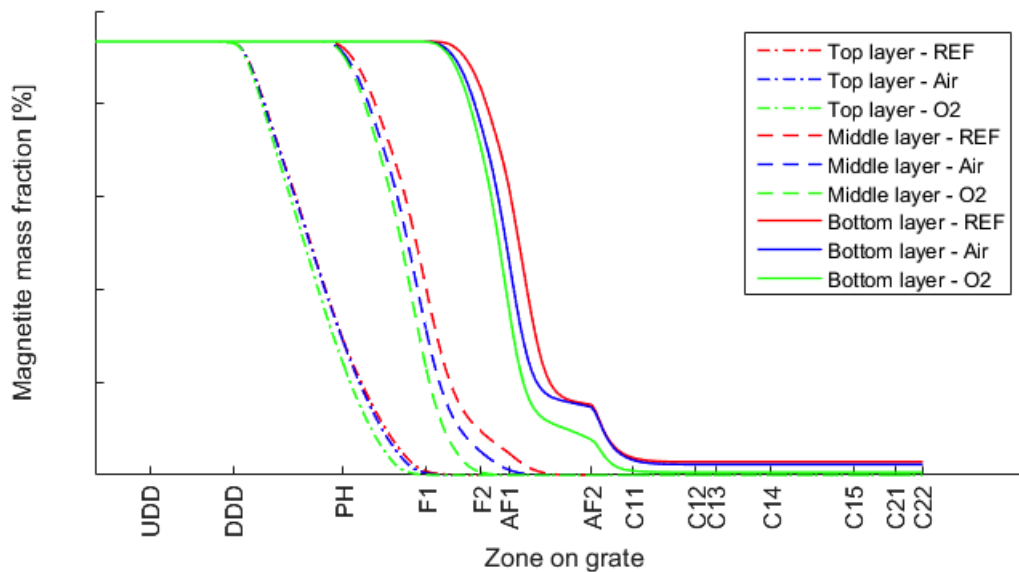


Figure 4.16: Mass fraction of magnetite throughout the process for the plasma torch cases with increased flow rates.

Table 4.11: Performance indicators for the plasma torch cases with increased flow rate.

Indicator	REF	Air	O ₂
$F_{\text{mag,mean}}$ [%]	0.218	0.146	0.028
$F_{\text{mag,max}}$ [%]	2.857	2.278	0.599
$T_{\text{bed,mean}}$ [°C]	49.98	53.86	54.63
$T_{\text{bed,max}}$ [°C]	177.83	188.05	188.97
Q_{fossil} [MW]	15.06	0	0
Q_{el} [MW]	0	15.05	16.33
E_{tot} [kWh/ton _p]	33.46	33.45	36.28

The results show that plasma torches can be implemented in the straight-grate process without any major changes, with positive effects pellet quality and only small changes in energy consumption. Using pure oxygen as plasma gas should be considered, but using regular air is also a good alternative. Oxygen is more expensive than air since producing it requires energy. However, air has the potential to produce NO_x in the plasma arc which may be a problem and this will be discussed further in Section 4.4.

4.3.2 Optimization of plasma torch case

The first strategy for optimization of the plasma torch case is to lower the mass flow of gas in the C15-PH zones. The PH zone has the largest energy requirement and thus a large potential for improvement in terms of energy efficiency. This results in lower energy consumption but also a lower magnetite conversion. The mass flow was lowered by around 11 % until $F_{\text{mag,mean}}$ reached the same value as the reference case. This resulted in a decreased energy consumption of 18 % compared to the reference case with the same pellet quality.

The process can also be optimized with respect to the production rate. An increased production rate leads to a faster process with less time in each zone and thus lower magnetite conversion. In a similar way, the production rate is increased until the magnetite content is identical to the reference case. The production rate could then be increased by around 3 % before reaching the same magnetite content. This also gives a similar energy consumption as the first optimization strategy, however, an increase in the maximum bed temperature is observed. With a faster process, the bottom layer is exposed to high temperatures during a shorter time period, which might affect the sintering process negatively. The optimized versions of the plasma torch case are presented in Table 4.12, where Opt1 is the case with decreased C15-PH mass flow and Opt2 is the case with increased production rate.

Table 4.12: Performance indicators for the optimization of the plasma torch case.

Indicator	REF	Opt1	Opt2
$F_{\text{mag,mean}}$ [%]	0.218	0.218	0.218
$F_{\text{mag,max}}$ [%]	2.857	2.961	2.972
$T_{\text{bed,mean}}$ [°C]	49.98	55.05	56.12
$T_{\text{bed,max}}$ [°C]	177.83	179.10	201.91
Q_{fossil} [MW]	15.06	0	0
Q_{el} [MW]	0	12.32	12.33
E_{tot} [kWh/ton _p]	33.46	27.39	26.61
P_{rate} [ton _p /h]	450	450	463.5

4.4 Nitrogen oxide formation

In this section, the results from the Chemkin simulations of the plasma torch are presented. As previously described, three simulation models are used; the no-mixing case (NoMix), the mixing case with a predefined temperature profile (MixTP) and the mixing case where the energy equation is solved to calculate the temperature profile (MixEE).

The results from all of the three simulation cases are presented in Appendix B. For each case, plots have been produced showing the temperature profile, NO concentration, NO mass flow and NO production over the reactor. Plots have also been produced showing the mole fractions for all chemical compounds involved in the reactions and the rate of production for the reactions that either produce or reduce NO.

For all of the cases, it can be discussed if it is really a plasma if gas molecules are still present. There is always some degree of ionization in a plasma which affects the chemical reactions. This behaviour is not captured by the present model and it is therefore unclear whether plasmas can be accurately described by reaction modelling. Another uncertainty is the effect of radiation. For this model the plasma torch is assumed to be adiabatic, meaning that convective cooling is dominating over radiation. However, if gas radiation is significant, this will also affect the absolute amount of NO formation.

4.4.1 No-mixing case

The NoMix case is used primarily to study the production of NO from the plasma gas itself. NO is only produced from the plasma if it contains both nitrogen and oxygen atoms. Therefore, production of NO is expected only in the case when air is used as plasma gas. Other common plasma gases such as N_2 , Ar, He and CO_2 does not produce NO from the plasma, however, NO formation is expected when the hot plasma gas mixes with air.

The plots that are relevant to the NoMix case are presented in Appendix B.2. It is clear from these simulations that the NO concentration is highest in the beginning of the reactor after around 5 cm. This is the point where the plasma gas is heated by the electric arc up to 5000 °C causing an extremely rapid temperature increase, see Figure 4.17. The mole fraction of NO reaches over 10 % at this point due to the Zeldovich reactions, Reaction B.1 and B.2. The NO concentration then decreases to around 2 % at the end of the plasma zone since the Zeldovich reactions are reversed, reducing the NO concentration. During the heating of the plasma gas, the maximum NO production occurs at a temperature of 4000 °C. At higher temperatures, the NO formation decreases, eventually becoming negative at temperatures close to 5000 °C.

In the initial part of the cooling zone Reaction B.1 and B.2 more or less balance each other. However, there are some differences causing the wave shape in the NO plot, see Figure 4.18. Finally, at lower temperatures Reaction B.3 and B.5 takes over. These reactions produce and consume NO_2 from NO at an equal rate, resulting in no net change in NO concentration. There is a high concentration of oxygen radicals throughout most of the reactor, while only a small amount of nitrogen radicals are present in the plasma zone.

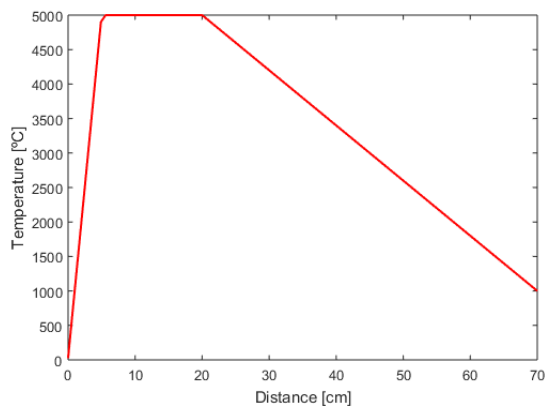


Figure 4.17: Temperature profile for the NoMix case.

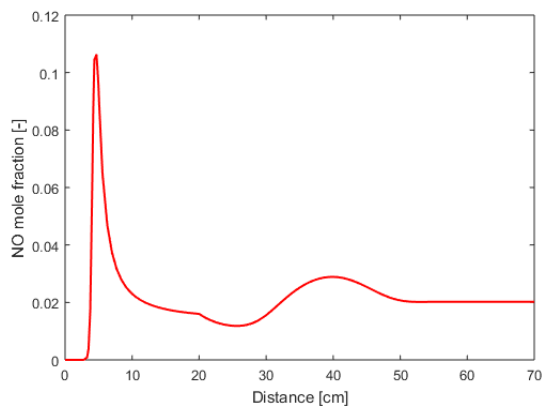


Figure 4.18: NO concentration for the NoMix case.

4.4.2 Mixing case (temperature profile)

The second case is used to study the production of NO from the mixing process. The MixTP case uses the same temperature profile as the NoMix case but the geometry is adapted as described in section 3.4. The plasma gas is argon, and air is mixed into the plasma with a total ratio of 10:1. The mixing occurs with an equal distribution from the 20 cm point until the end of the reactor, successively increasing the mass flow in the reactor from 10 to 110 g/s.

The results from the MixTP case can be seen in Appendix B.3. As expected, the concentration of NO starts to increase as the mixing starts and in this case reaches slightly over 4 %. The concentration stays at this level for some time before starting to decrease after around 40 cm, finally reaching a concentration of 1.6 %, see Figure 4.19. Formation of NO occurs between 3000 and 5000 °C and the highest rate of production occurs at temperatures close to 5000 °C, see Figure 4.20. The minimum temperature for NO formation seems to be around 3000 °C.

The NO production is again dominated by the Zeldovich reactions in the high-temperature region. However, the rate of production for these reactions is significantly lower than for the NoMix case meaning that the other reactions become more important in comparison. The decrease of the NO concentration is mostly caused by the dilution with air, however, some NO is also destroyed by chemical reactions in the temperature interval between 2000-3000 °C. After 40 cm, most of the reactions are reversed. This leads to a decrease in NO mass flow that can be seen towards the end of the reactor. The results show that both the heating of the plasma and the mixing can produce significant amounts of NO, up to levels of a few percent if the temperature decrease is linear.

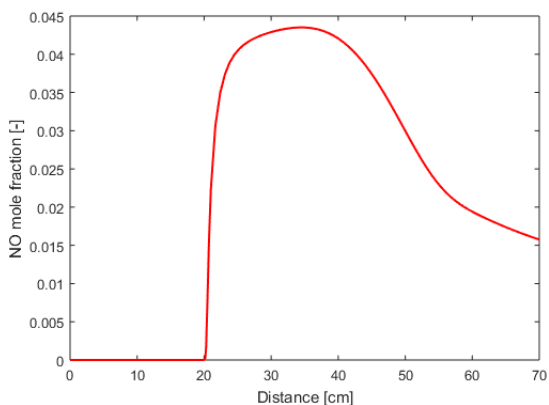


Figure 4.19: NO concentration for the MixTP case.

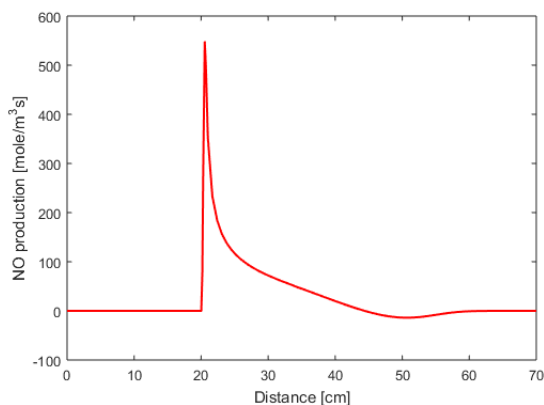


Figure 4.20: NO production for the MixTP case.

4.4.3 Mixing case (energy equation)

The results of the simulations for the MixEE case are presented in Appendix B.4. The calculated temperature profile differs significantly from the linear temperature profile used previously, see Figure 4.21. It decreases fast in the beginning of the mixing zone, reaching a temperature of less than 2000 °C within the first 5 cm. The decrease then slows down and reaches an outlet temperature of around 1300 °C.

Since thermal NO production is rapid at high temperatures, the residence time in the temperature interval where NO is formed is much shorter in these simulations. NO formation only occurs in a very short section of the reactor at the beginning of the mixing zone, see figure 4.22. This leads to a significantly lower concentration of NO than in the two former cases. The maximum NO concentration is only around 0.8 %, while the outlet concentration is close to 0.1 %. The reversion of the NO-producing reactions occur earlier and the radicals are barely visible in comparison to the O₂ and N₂ concentration.

In this case, NO is formed almost exclusively by the Zeldovich reactions. There is no destruction of NO through chemical reactions, the NO that has been formed is stable throughout the rest of the reactor. The reduction of the NO concentration is thus only due to dilution with air. NO is formed at temperatures above 2000 °C and the maximum rate of production occurs at around 4000 °C. However, it is reasonable to assume that the formation would continue to increase with temperature if the residence time was longer. Since NO formation increases with temperature, faster cooling in the high-temperature region should be beneficial in order to reduce NO formation. As the NO formation is limited to a very small area with the highest temperature, another interesting option is to mix the plasma gas with an inert gas before mixing it with air. For example, introducing a 10 g/s flow of argon from 20 to 25 cm gives less than 1 ppm NO in the outlet gas. NO reduction strategies will be discussed further in Section 4.4.6.

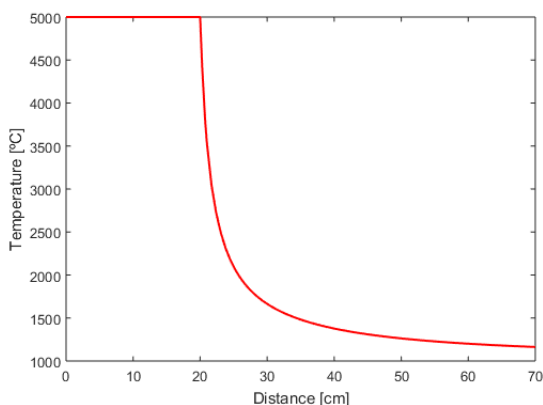


Figure 4.21: Temperature profile for the MixEE case.

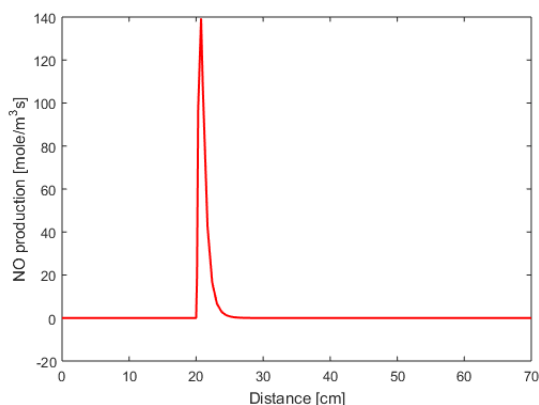


Figure 4.22: NO production for the MixEE case.

4.4.4 Model validation

In order to assess the reliability of the results, the simulation models are validated against experimental tests and the results are presented in Table 4.13. The NoMix case shows higher NO concentration for more air, however, the NO concentration is 10-20 times higher than in the experiments. For the MixTP case, the working gas composition has barely any effect on NO concentration. Some NO is produced in the plasma zone but an absolute majority of the NO is produced in the mixing zone. However, for the MixEE case the NO production in the plasma zone dominates and determines the final NO concentration. Out of the three simulation models, the MixEE case matched best with experiments.

Since the amount of mixing air in the experiments is not known, this value can be varied in order to match the experimental results. The adapted mixing case (MixAdapt) is the MixEE case where the amount of mixing air was increased from 100 g/s to 215 g/s, giving an air-to-plasma ratio of 21.5. The MixAdapt case gives results that are very similar to the experiments, where only the concentration for 100% air is off by around 300 ppm. This means that the experimental results can be reproduced using the simulation model that has been developed in this project which is a good indication that the model is relatively accurate and that the results are trustworthy.

Table 4.13: Comparison of NO concentration [ppm] between the experiments and the simulation models with different amounts of air in CO₂ working gas.

Air [%]	Experiments	NoMix	MixTP	MixEE	MixAdapt
3	303	7058	17222	857	299
6	402	9961	17227	1066	404
9	482	11612	17231	1237	489
100	1856	21639	17464	5149	2243

4.4.5 Sensitivity analysis

The sensitivity analysis is performed for the MixEE case since this shows the most resemblance to experiments. According to Figure 4.23, increased plasma temperature results in a higher NO volume fraction. If the plasma temperature is 3000 °C, there is practically no residence time at temperatures above 2000 °C, resulting in a low NO concentration. Significant amounts of NO are produced when the plasma temperature reaches over 4000 °C and the concentration continues to increase with the temperature above this. Since high temperatures are one of the most important properties of a plasma torch, it may not be possible to alter the temperature in order to lower the NO formation. As can be seen in Figure 4.24, the mixing zone length also affects the NO formation but the effect is not as large. Mixing the same amount of air in a longer zone gives a longer residence time and the temperature drops slower. The NO concentration increases with a longer mixing zone but seems to reach a maximum value of around 1500 ppm. This indicates that it is important to achieve good mixing between the plasma gas and the air in order to keep the mixing zone short and the NO concentration low.

4. Results and discussion

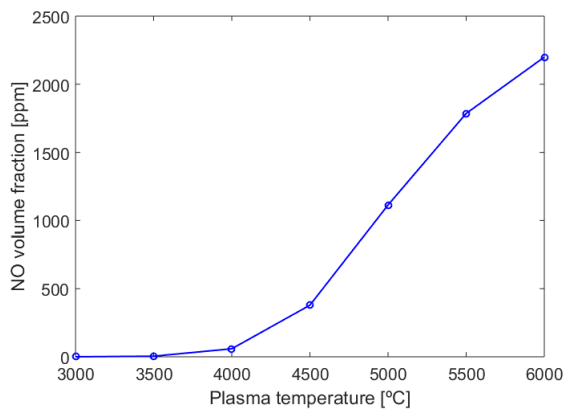


Figure 4.23: Effect of plasma temperature on NO concentration.

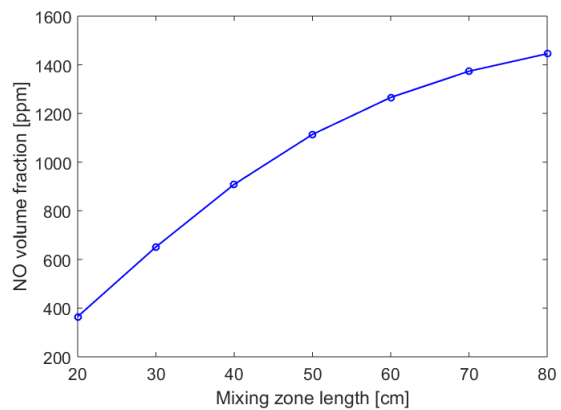


Figure 4.24: Effect of mixing zone length on NO concentration.

The parameter that has the largest impact on the NO concentration is the air-to-plasma ratio (the amount of mixing air in relation to plasma gas). The effect of air to plasma ratio on NO concentration and NO formation can be seen in Figure 4.25 and 4.26. At an air to plasma ratio of 1, the NO concentration reaches over 10 000 ppm (1 %). When more cooling air is introduced into the reactor, the velocity of the gas increases resulting in shorter residence time and less time at high temperatures. Another effect of introducing more air is that the overall temperature level in the reactor is decreased, which has the same effect. Since the total flow rate is changed, the NO concentration does not provide information about the total amount of NO produced. Therefore, a second plot is produced where the mass flow of NO is calculated by relating the mass fraction of NO to the total mass flow. This plot shows a similar trend where less air gives more NO, however, the relationship is more linear instead of exponential.

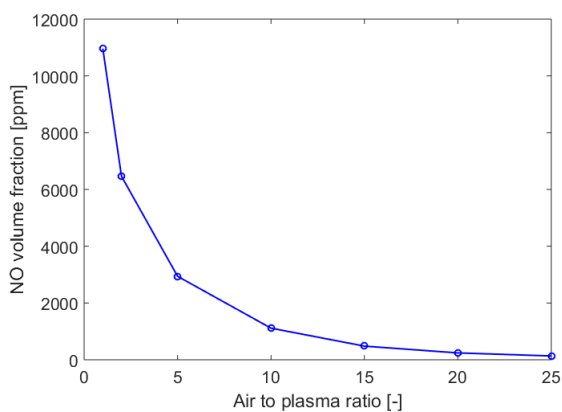


Figure 4.25: Effect of air to plasma ratio on NO concentration.

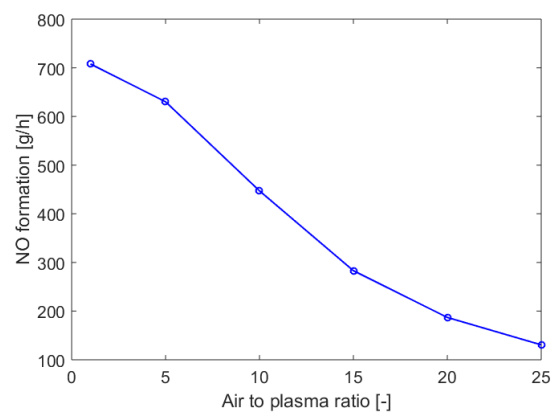


Figure 4.26: Effect of air to plasma ratio on NO formation.

Finally, the plasma flow rate is varied while the air to plasma ratio is kept the same. The effect of plasma gas flow on NO concentration and NO formation can be seen in Figure 4.27 and 4.28. The trends are similar to what can be seen for the air to plasma ratio. However, at plasma flow rates lower than 10 g/s, the NO concentration increase but the NO formation starts to decrease. The flow rate of 250 Nm³/h used in the plasma case study corresponds to a plasma gas flow of around 85 g/s. According to Figure 4.27, the NO volume fraction is then less than 50 ppm.

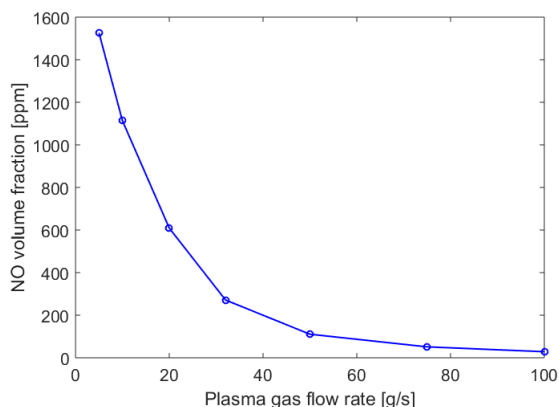


Figure 4.27: Effect of plasma gas flow rate on NO concentration.

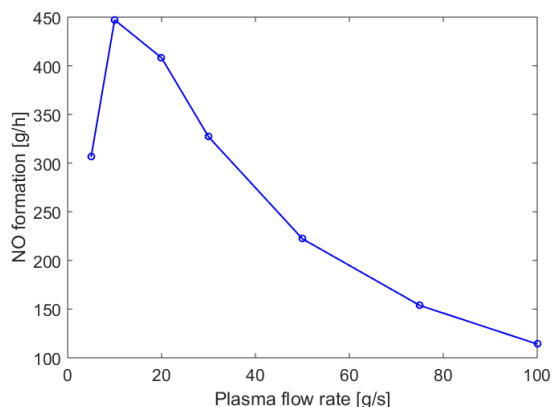


Figure 4.28: Effect of plasma gas flow rate on NO formation.

4.4.6 Working gases and NO reduction

Simulations are performed to show the effect of the plasma working gas on the formation of NO. The temperature profile is defined according to the results from the MixEE case since the program sometimes automatically adjusted the temperature to a lower level. The results from the working gas simulations are presented in Figure 4.29. The results show that both more nitrogen and oxygen atoms in the working gas seem to increase the amount of NO that is produced. Some of the differences can also be explained by the difference in molar mass, for example, 10 g/s is a smaller molar flow for Ar due to the larger molar mass compared to the other compounds. Hydrogen produces almost no NO since the hydrogen atoms react with NO to form OH according to reaction 2.8. Other than hydrogen, argon and carbon monoxide are the gases that produce the least amounts of NO.

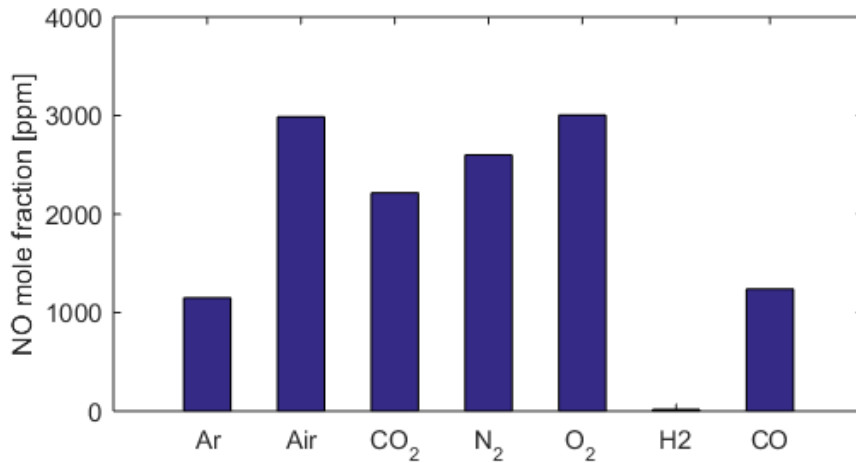


Figure 4.29: NO mole fraction for common plasma working gases.

NO reduction is studied through simulations of reburning and oxygen reduction. The results from these simulations are presented in Figure 4.30. The results show that reburning is the more effective out of the two strategies, achieving lower NO concentrations for all methane flowrates. For low methane flow rates, oxygen reduction through combustion even increases the NO concentration. The reason why oxygen reduction does not work as expected is that the oxygen atoms are not removed from the gas, but instead used to form H₂O molecules. At high temperatures, these water molecules will dissociate into oxygen and hydrogen radicals. Since oxygen radicals are present, NO formation is expected.

In these simulations, a methane flow rate of around 3 g/s seems to be optimal for reburning. Adding more than 3 g/s does not have any significant effect on the NO concentration. When methane is combusted, hydrocarbon radicals are formed that will react and destroy NO. The combustion of methane produces its own nitrogen oxides, however, the concentrations are much lower than those from the plasma torch, resulting in a net reduction of NO. A reduction of up to 65% is achieved in the simulations, indicating that reburning could be an effective measure for reduction of nitrogen oxides from plasma torches.

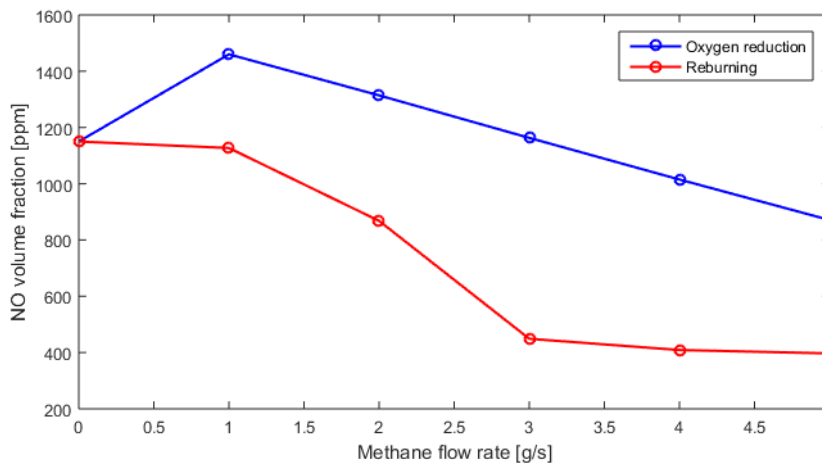


Figure 4.30: Effect of methane flow rate for the two reduction strategies.

5

Conclusions

This project investigates the potential of replacing fossil fuel burners with electric heating in the straight-grate process by modifying a previously developed process model. The evaluation is based on a reference case with performance indicators and process constraints provided by LKAB for the straight-grate unit MK3. The results show that implementation should be possible for both plasma torches and microwaves with mostly positive effects on performance indicators and without running into process constraints. The only performance indicator that requires attention is the NO_x emissions from plasma torches.

Results from simulations with microwave heating correlated well with previous experience of microwave-assisted drying of iron ore pellets in lab scale, providing legitimacy to the results. Implementing microwaves did not significantly affect the performance parameters directly evaluated by the process model. Recondensation of water vapour in the bed could be avoided, indicating less deformation and clogging of pellets due to over-wetting. Design modifications utilizing the benefits of microwave heating allowed for a 7 m^2 reduction of the drying section while reducing the fossil power demand by almost 1 MW and reducing the maximum magnetite content of pellets by almost 2 %. However, around 5 MW of electricity is needed for microwave generation, decreasing the overall energy efficiency. There is a limited emission reduction potential in this application which could be viable if electricity is readily available at low cost with a low emission footprint.

Implementation of plasma torches may be an alternative for electrification of the straight-grate process and can decrease the CO_2 emissions from the process significantly. Retrofitting plasma torches in place of fossil fuel burners in a pelletizing plant with a 40 MW thermal input has the potential to reduce CO_2 emissions by up to 140 000 ton per year. It has been concluded that the implementation of plasma torches in the straight-grate process only has a small effect on process parameters and energy consumption. With plasma torches, there will not be any combustion reaction and thus no combustion products in the process gas. This leads to slightly higher oxygen content in the gas which results in a higher oxidation rate of the pellets. There will also be an introduction of an external plasma forming gas which increases the process gas flow and changes its composition. However, this will only affect the process conditions significantly at very high flow rates. With increased oxidation, the process can be optimized, for example towards decreased energy consumption or increased production rate.

The only negatively affected performance indicator for the plasma torches is the NO_x emissions. Reaction modelling in Chemkin was used to study the formation of nitrogen oxides from plasma torches applied to the straight-grate process. A simplified reactor model was developed with a plasma zone and a mixing zone. In conclusion, the results show that significant amounts of NO is produced when hot plasma gas mixes with air. The formation of NO is dominated by the thermal NO mechanism (Zeldovich reactions) and the reaction rate increases exponentially with temperature. Validation using previous experiments shows that the MixEE case gives results that most closely resembles reality. If the flow of mixing air is increased by 115 %, the experimental results can be reproduced with good accuracy. This model was therefore used in a sensitivity analysis and to study the effects of different plasma gases and NO reduction strategies. The sensitivity analysis showed that higher plasma temperature, longer mixing zone and lower flow rates generally lead to increased NO formation. Reburning was the most promising out of the studied reduction strategies, with NO reduction of up to 65 % in the simulations.

5.1 Recommendations for future work

The possibilities of utilizing the BedSim model to study the effects of implementing microwaves and electric plasma torches have been thoroughly investigated in this study. Further work in this area should instead be experimental tests to prepare for practical implementation. The focus should be on evaluating the data from the experiments and comparing it to the modelling results. The experiments will also be important in order to study parameters that can not be simulated in the bed model such as sintering, pellet strength and gas mixing. This will hopefully lead to an increased understanding of the process and proposals for concepts that are ready for full-scale testing.

Further investigations should be performed towards the implementation of microwaves focusing on evaluating under which circumstances microwave implementation would be viable from a financial and emission reduction point of view. An initial financial analysis would indicate if the reduced emissions due to less fossil fuel use and improved product quality can outweigh the increased total power demand of the process. If microwaves prove to be financially viable, the next step would be to perform practical tests with lab scale equipment using varying frequency and power intensity to further evaluate the possibilities and limitations of microwave implementation.

The possibility of using microwaves in combination with downdraft drying should also be investigated. Microwaves could possibly be used in combination with a gas flow of low-grade heat in the DDD zone which would cool the higher layers of the bed to prevent them from overheating and transport heat to the lower layers of the bed. This method could potentially be more energy efficient than microwaves in combination with UDD since the heat provided by the microwaves would be transported down through the bed by the downdraft gas flow. The bed would then be able to retain the heat provided by the microwaves through the process to a larger extent.

For plasma torches, there are some important details that can not be simulated with the process model. One example is the mixing process of the plasma and the recirculated air. Since the plasma is much hotter than a combustion flame it becomes more important for the process gas to be homogeneous before reaching the pellet bed. This could otherwise lead to uneven oxidation of the pellets. Due to this, the mixing process should be studied further through fluid dynamics simulations or practical experiments. When finally implementing plasma torches in the real process, it will be a good idea to begin by replacing only one pair of burners. In this way, the investment cost can be spread out and changes in pellet quality can be evaluated. If no major changes are observed, more burners can be replaced until eventually the process operates with plasma torches only.

It is also important to remember that there are many uncertainties regarding the NO simulations. First of all, reaction modelling might not be able to accurately describe the behaviour of plasma. At extremely high temperatures the particles become ionized which affects the chemical reactions. However, to which degree this would affect the results compared to normal gas-phase reaction kinetics is still unclear and needs to be studied further. Secondly, more data of different types of plasma torches including dimensions, mass flows and plasma temperatures would allow for simulations that can be used to better predict the absolute amounts of NO formation. Due to these uncertainties, it would be a good idea to measure the production of nitrogen oxides from plasma torches in a test rig before implementation. The NO formation could then be measured for different operating conditions to find out what works best in practice.

5.2 New process concept

As a final part of this project, a new process concept is proposed where both microwaves and plasma torches are utilized to supply the energy to the process. When working on the electrification of the process, it is important to have a holistic view of the entire steel production chain. This concept is an integration between a straight-grate pelletization plant and a direct-reduction plant. It is a futuristic vision of how new technologies could be combined in order to produce CO₂-neutral steel. The new process concept is presented in Figure 5.1.

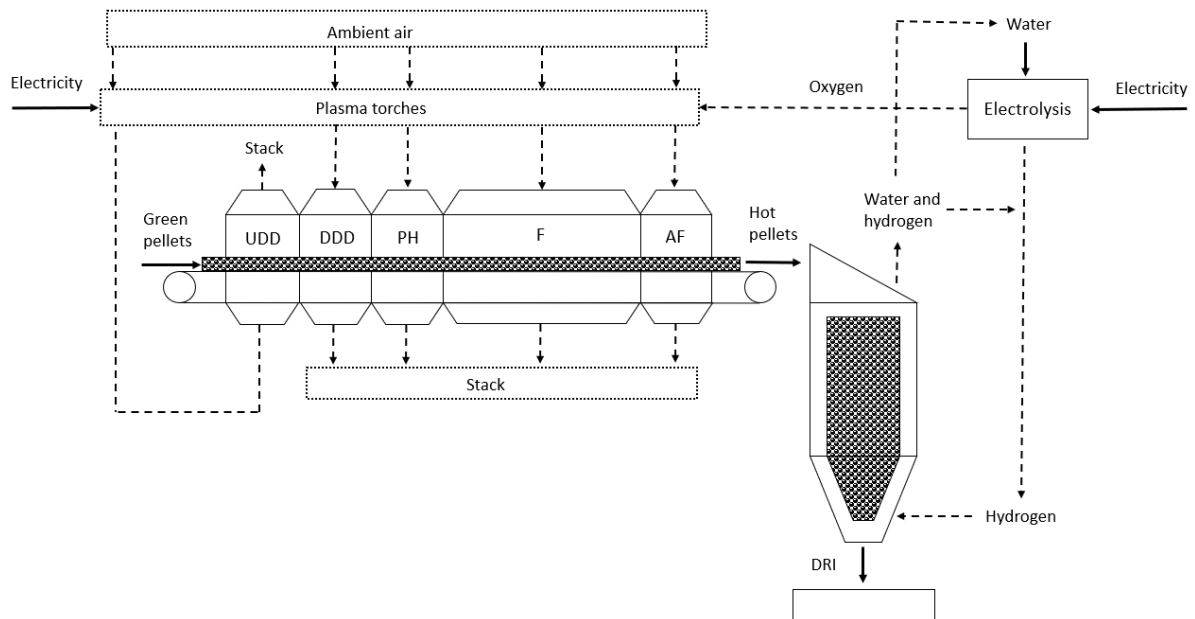


Figure 5.1: Principal design of the new process concept for pelletization and direct-reduction of iron ore.

The concept consists of a travelling grate with a drying and firing section but no cooling section. Instead, the pellets are fed directly into the direct-reduction process where they are reduced by a flow of hydrogen gas. Iron is reduced when it is heated to a temperature of 800 - 1200 °C in the presence of a reducing gas, for example hydrogen gas. Since the pellets already have a high temperature when they enter the direct-reduction process, less heat has to be supplied in order to heat up the reducing gas resulting in lower energy consumption. Waste heat from the pelletization process can also be used in the direct-reduction to improve energy efficiency even further.

At the same site, electrolysis of water is performed in order to produce pure oxygen and hydrogen gas. Electrolysis is a process where electricity is used to split up water molecules into its components, oxygen and hydrogen. The oxygen gas can then be used as plasma working gas while the hydrogen gas can be used for direct-reduction of the iron ore pellets. This reduces the need to store leftover gas from the electrolysis, as it can be pumped directly to the process. As described in the plasma case study, supplying extra oxygen to the process gas will increase the magnetite conversion, resulting in increased pellet quality.

Since there is no cooling section, it will not be possible to recirculate heat in the pelletizing unit. All of the heat instead have to be supplied from plasma torches and microwaves. Microwaves are used in the UDD zone to reduce problems related to over-wetting of pellets in the higher layers of the bed. In the DDD zone, microwaves are used in combination with a low-temperature flow of air, preferably waste heat from some other part of the process. The microwaves heat the higher layers of the bed while the downward flowing air absorbs heat from the higher layers and transport the heat downwards into the bed. For a process with the same production rate as the reference case, the total amount of heat that has to be supplied is around 240 MW. This is a considerable increase compared to the original straight-grate process and would require several large, high power torches.

In this concept, the heat requirement is practically moved from the direct-reduction to the pelletization process but the net energy requirement of the overall process should be similar. However, heat losses and leakage of air in the recirculation will no longer be a problem. A straight-grate without cooling zones also leads to much lower grate area resulting in a lower initial investment costs for the plant. A final advantage is that the transportation between the pelletizing plant and the steel production plant is eliminated, resulting in lower transportation costs and emissions.

This concept makes it is possible to produce totally CO₂-neutral steel if the direct-reduced iron is then finally refined in an electric arc furnace. There are however still many questions that have to be answered. What is the pellet strength in its hot state? Will the pellets be able to keep their shape when being loaded into the direct-reduction unit? What amounts of hydrogen and oxygen gas are required? Many questions still have to be answered before this concept can become a reality.

Bibliography

- [1] United Nations Framework Convention on Climate Change (2015). Adoption of the paris agreement. Article 4, ss. 22.
- [2] Naturvårdsverket (2012). Underlag till en färdplan för ett sverige utan klimatutsläpp 2050. Report 6537, ss. 3-4.
- [3] EU (2016). Directive 2016/2284 on the reduction of national emissions of certain atmospheric pollutants.
- [4] LKAB (2017a). Annual and sustainability report. Luleå: LKAB.
- [5] LKAB (2017b). Sustainability goals. <https://www.lkab.com/en/sustainability/our-sustainability-work/sustainability-goals/> [2019-02-04].
- [6] LKAB, SSAB and Vattenfall (2019). Hybrit - towards fossil-free steel. <http://www.hybritdevelopment.com/> [2019-05-13].
- [7] LKAB (2017a). Mining. <https://www.lkab.com/en/about-lkab/from-mine-to-port/mining/> [2019-01-29].
- [8] LKAB (2017b). Processing. <https://www.lkab.com/en/about-lkab/from-mine-to-port/processing/> [2019-01-29].
- [9] Stjernberg, J., Isaksson, O. and Ion, J.C. (2015). The grate-kiln induration machine - history, advantages, drawbacks, and outline for the future. *Southern African Institute of Mining and Metallurgy*, vol. 115, 2, pp. 137–144.
- [10] Nordgren, S. (2010). Energy analysis of pelletising in a straight grate induration furnace. Luleå: Luleå University of Technology.
- [11] Encyclopaedia Britannica (1998). Blast furnace. <https://www.britannica.com/technology/blast-furnace> [2019-04-30].
- [12] Eurotherm (2019). Blast furnace and stoves. <https://www.eurotherm.se/blast-furnace-and-stoves> [2019-04-30].
- [13] Fruehan et al. (2000). Theoretical minimum energies to produce for steel for selected conditions. Pittsburgh: Carnegie Mellon University.

- [14] Nilsson, J. (2018). LKAB's straight grate process: Examining new process concepts. Master's thesis, Chalmers University of Technology.
- [15] Biermann, M. (2016). Reassessment of the grate unit of the grate-kiln process for the iron ore production at LKAB. Master's thesis, Chalmers University of Technology.
- [16] Yurev, B.P. and Spirin, N.A. (2011). Oxidation of iron-ore pellets. *Steel in Translation*, vol. 41, 5, pp. 400–403.
- [17] Forsmo et al. (2008). Mechanisms in oxidation and sintering of magnetite iron ore green pellets. *Powder technology*, vol. 183, 2, pp. 247–259.
- [18] Haaf, M. (2016). Thermodynamic process evaluation of a rotary kiln unit at LKAB. Master's thesis, Chalmers University of Technology.
- [19] Hartman et al. (1996). Predicting the rate of thermal decomposition of dolomite. *Chemical engineering science*, vol. 51, 23, pp. 5229–5232.
- [20] Haque, K.E. (1999). Microwave energy for mineral treatment process - a brief review. *International journal of mineral processing*, vol. 57, 1, pp. 1–24.
- [21] Agrawal et al. (1999). Full sintering of powdered-metal bodies in a microwave field. *Nature*, vol. 399, pp. 668–678.
- [22] El Khaled et al. (2018). Microwave dielectric heating: Applications on metals processing. *Renewable and sustainable energy reviews*, vol. 82, 3, pp. 2880–2892.
- [23] Athayde, M., Cota Fonseca, M. and Covcevich Bagatini, M. (2018). Iron ore pellet drying assisted by microwave: A kinetic evaluation. *Mineral processing and extractive metallurgy review*, vol. 39, 4, pp. 266–275.
- [24] Sun, J., Wang, W. and Yue, Q. (2016). Review on microwave-matter interaction fundamentals and efficient microwave-associated heating strategies. *Materials*, vol. 9, 4.
- [25] Athayde, M., Covcevich Bagatini, M. and Cota Fonseca, M. (2018). Novel drying process assisted by microwave to iron ore pelletizing. *Materials research*, vol. 21, 5.
- [26] Taylor, P. and Pirzada, S. (1994). Thermal plasma processing of materials: A review. *Advanced Performance materials*, vol. 1, 1, pp. 35–50.
- [27] Venkatramani, N. (2002). Industrial plasma torches and applications. *Current Science*, vol. 83, 3, pp. 254–262.
- [28] Nunes Szente, R. (1995). Industrial applications of thermal plasmas. *AIP Conference Proceedings*, vol. 345, 1, pp. 487–494.
- [29] Gomez et al. (2009). Thermal plasma technology for the treatment of wastes: A critical review. *Journal of Hazardous Materials*, vol. 161, 2-3, pp. 614–626.
- [30] Zhukov, M.F. and Zasyplin, I.M. (2006). *Thermal Plasma Torches : Design, Characteristics, Application*. Cambridge International Science Publishing.

- [31] Camacho, S.L. (1988). Industrial-worthy plasma torches: State-of-the-art. *Pure and Appl. Chem.*, vol. 60, 5, pp. 619–632.
- [32] Westinghouse Plasma Corporation (2015). Industrial plasma systems. <http://www.alternrg.com/wp-content/uploads/2015/04/WPC-Plasma-Torches-Public.pdf> [2019-02-25].
- [33] Rao, L., Rivard, F. and Carabin, P. (2013). Thermal plasma torches for metallurgical applications. *4th International Symposium on High-Temperature Metallurgical Processing*.
- [34] Zhang, R., Tie, X., and Bond, D.W. (2003). Impacts of anthropogenic and natural nox sources over the us on tropospheric chemistry. *Proceedings of the National Academy of Sciences*, vol. 100, pp. 1505–1509.
- [35] Edland, R. (2017). *NOx Formation in Rotary Kilns for Iron Ore Pelletization*. PhD thesis, Chalmers University of Technology.
- [36] Rose, J. (1994). Acid rain: current situation and remedies vol. 4. Yverdon: Gordon and Breach.
- [37] Krupa, S.V. and Manning, W.J. (1988). Atmospheric ozone: Formation and effects on vegetation. *Environmental Pollution*, vol. 50, pp. 101–137.
- [38] Zeldovich, Y., Frank-Kamenetskii, D. and Sadonikov, P. (1947). Oxidation of nitrogen in combustion. Publishing House of the Acad of Sciences of USSR.
- [39] Uhm, H.S., Cho, S.C., Park, I.G. and Hong, M.S. (2008). Reduction of plasma nitrogen oxides by flames of hydrocarbon fuel. *Journal of the Korean Physical Society*, vol. 52, 6, pp. 1800–1803.
- [40] Echterhof, T., Gruber, J. and Pfeifer, H. (2011). Measurements and simulation of nox formation in the electric arc furnace. *Conference: 2nd International Conference Clean Technologies in the Steel Industry*.
- [41] Wilhelmsson, B. (2019). NOx formation in plasma generator. FoU Report 190001, Projekt: CemZero.

A

Process parameter calculations

A.1 Power requirement of microwaves

The study by Athayde et al [25] states that a constant power supply, Q_{potgrate} , of 10 kW was used for microwave generation. It is not clearly stated if the power requirement was measured from the wall electricity socket or if it was the actual microwave output. For these calculations it was assumed that the power requirement was measured from the wall socket. The power intensity q_{potgrate} was calculated according to Equation A.1. The pellet mass, m_{pellets} , and density, ρ_{pellets} , was 45 kg and 5260 kg/m³ respectively. The bed depth, l_{bed} , was 0.37 m. The complementary data collected from the LKAB input data was the voidage factor of the bed, Φ , which was 0.41.

$$q_{\text{potgrate}} = \frac{Q_{\text{potgrate}}}{A_{\text{potgrate}}} = \frac{Q_{\text{potgrate}}}{\frac{m_{\text{pellets}}/l_{\text{bed}}}{(1-\Phi)\rho_{\text{pellets}}}} = 255.17 \left[\frac{\text{kW}}{\text{m}^2} \right] \quad (\text{A.1})$$

The power intensity q_{potgrate} together with the 21 m² surface area of the UDD zone from the reference case was used to calculate the electric power requirement, Q_{el} , for microwave generation for the real process according to Equation A.2. Q_{Micro} was then added to the performance indicator Q_{net} , which represents the power requirement of the entire process.

$$Q_{\text{el}} = q_{\text{potgrate}} \cdot A_{\text{UDD}} = 5.36 \left[\text{MW} \right] \quad (\text{A.2})$$

A.2 Evaporation rate

The evaporation rate, r_{evap} , was calculated using the output file O.Data_BGH2O. This file stores the values of the mass flow of steam through the bed per square meter, $\dot{m}_{\text{H}_2\text{O}}$ [kg/m²/s], calculated by the BedSim file. The output file O.Data_BGH2O contains one value for each vertical position in the bed in every horizontal position of the grate. The values are accumulated in flow direction. The amount of steam released between two vertical positions in the bed is therefore calculated according to Equation A.3, where y [m] represents vertical position in the bed.

$$r_{\text{evap},i} = \frac{\dot{m}_{\text{H}_2\text{O},i} - \dot{m}_{\text{H}_2\text{O},i-1}}{y_i - y_{i-1}} \left[\frac{\text{kg}}{\text{m}^3 \cdot \text{s}} \right] \quad (\text{A.3})$$

The evaporation rate was calculated for each vertical position in the bed in each horizontal position along the grate in the zones where moisture was still present. The maximum evaporation rate in each zone was then acquired to determine if it was within the constraint limit.

A.3 Gas moisture saturation

The moisture content of the gas leaving the UDD/Micro section was calculated according to Equation A.4 and A.5. Equation A.4 summarizes the moisture which is evaporated in the microwave zones and expresses it as an average across the number of UDD zones. The average amount of water evaporated in the microwave zones was then added to the moisture content of the gas leaving the UDD sections, according to Equation A.5, in order to calculate which moisture content that the gas would have if the UDD and microwave heating was in the same zone.

$$\dot{m}_{\text{H}_2\text{O} \text{avg}, \text{micro}} = \frac{\sum [X_{\text{H}_2\text{O}, \text{out}} \cdot \dot{m}_{\text{gas}, \text{out}} - X_{\text{H}_2\text{O}, \text{in}} \cdot \dot{m}_{\text{gas}, \text{in}}]_{\text{micro}}}{n_{\text{UDD zones}}} \left[\frac{\text{kg}}{\text{s}} \right] \quad (\text{A.4})$$

$$m_{\text{H}_2\text{O}, i} = \frac{\dot{m}_{\text{H}_2\text{O} \text{avg}, \text{micro}} + [X_{\text{H}_2\text{O}, i} \cdot \dot{m}_{\text{gas}, \text{out}, i}]_{\text{UDD}}}{\dot{m}_{\text{gas}, \text{out}, i} \cdot (1 - X_{\text{H}_2\text{O}, i})} \left[\frac{\text{kg}_{\text{H}_2\text{O}}}{\text{kg}_{\text{dry gas}}} \right] \quad (\text{A.5})$$

The calculated moisture content was then compared to the maximum moisture carrying capacity of air at the temperature of the gas as it leaves the UDD zone.

A.4 Pressure drop

The pressure drop across the bed in each zone was calculated using the output file O.Data_BPDRIP which stores one value for every vertical position in the bed in every horizontal position along the grate. The value stored in each position is the pressure difference between the actual pressure in the position and atmospheric pressure. The average pressure drop over the bed height in a zone was calculated according to Equation A.6, where Δp is the pressure drop across the bed and \dot{m}_{gas} is the mass flow through the bed.

$$\Delta p_{\text{bed}} = \frac{\sum_t \Delta p(t) \cdot \dot{m}_{\text{gas}}(t)}{\sum_t \dot{m}_{\text{gas}}(t)} \text{ [Pa]} \quad (\text{A.6})$$

A.5 Mean magnetite mass fraction

The mean magnetite mass fraction in the bed at the outlet of the process, $F_{\text{mag,mean}}$, was calculated using the output file O.Data_BMAG. This file stores the magnetite content of the pellets for every vertical position in the bed in each horizontal position along the grate. The last row of this file represents the magnetite content in the outlet of the process.

Since the vertical positions are not spaced equally, a weighted average has to be calculated. First the magnetite mass fraction in each cell is calculated as the average of the two closest points according to Equation A.7. The mean mass fraction of magnetite in the bed is then calculated through Equation A.8, where $\Delta y_{\text{cell},i}$ is the height of cell i .

$$F_{\text{mag,cell},i} = \frac{F_{\text{mag},i} + F_{\text{mag},i+1}}{2} \left[\frac{\text{kg}_{\text{mag}}}{\text{kg}_{\text{p}}} \right] \quad (\text{A.7})$$

$$F_{\text{mag,mean}} = \frac{\sum_i F_{\text{mag,cell},i} \cdot \Delta y_{\text{cell},i}}{\sum_i \Delta y_{\text{cell},i}} \left[\frac{\text{kg}_{\text{mag}}}{\text{kg}_{\text{p}}} \right] \quad (\text{A.8})$$

A.6 Mean bed temperature

The mean temperature of the bed at the outlet of the process, $T_{\text{bed,mean}}$, was calculated using the output file O.Data_BMTEMP. The last row of this file represents the temperature of the pellets at the outlet of the process. In a similar way to the magnetite mass fraction, a weighted average was calculated through Equation A.9 and A.10.

$$T_{\text{bed,cell},i} = \frac{T_{\text{bed},i} + T_{\text{bed},i+1}}{2} \text{ [}^\circ\text{C]} \quad (\text{A.9})$$

$$T_{\text{bed,mean}} = \frac{\sum_i T_{\text{bed,cell},i} \cdot \Delta y_{\text{cell},i}}{\sum_i \Delta y_{\text{cell},i}} \text{ [}^\circ\text{C]} \quad (\text{A.10})$$

A.7 Energy balance

The power requirement and energy consumption of the process was calculated according to Equations A.11 and A.12 where p_{rate} [ton_p/h] is the production rate, $m_{\text{gas},i}$ [kg/kg_p] is the gas mass flow of firing zone i and $\Delta h_{\text{gas},i}$ [J/kg] is the enthalpy difference of the gas over zone i . The fossil fuel demand can be calculated as the net heat demand minus the heat demand from electricity, see Equation A.13.

$$E_{\text{tot}} = \sum_i \frac{\dot{m}_{\text{gas},i} \cdot \Delta h_{\text{gas},i}}{3.6} \left[\frac{\text{Wh}}{\text{ton}_p} \right] \quad (\text{A.11})$$

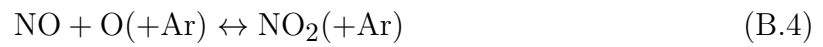
$$Q_{\text{net}} = E_{\text{tot}} \cdot p_{\text{rate}} \left[\text{W} \right] \quad (\text{A.12})$$

$$Q_{\text{fossil}} = Q_{\text{net}} - Q_{\text{el}} \left[\text{W} \right] \quad (\text{A.13})$$

B

Nitrogen oxide plots

B.1 NO reactions



B.2 No-mixing case

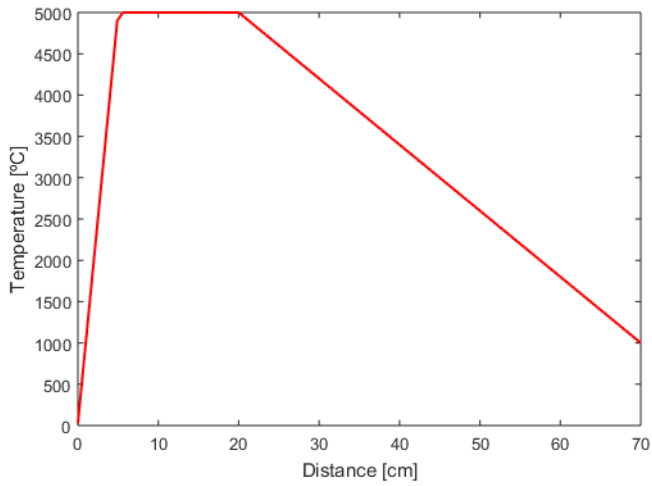


Figure B.1: Temperature profile for the NoMix case.

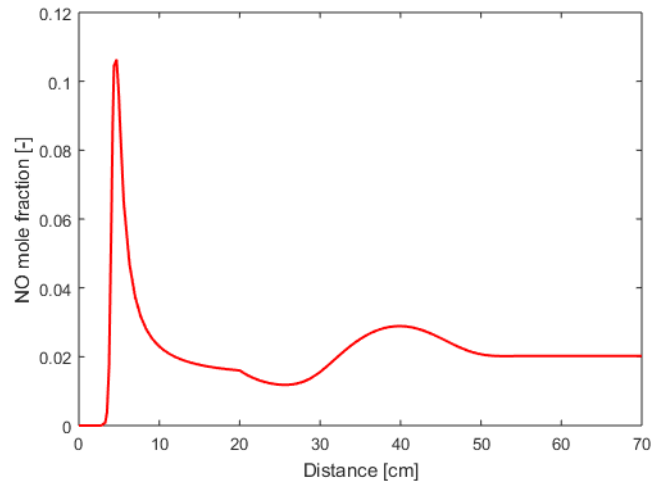


Figure B.2: NO concentration for the NoMix case.

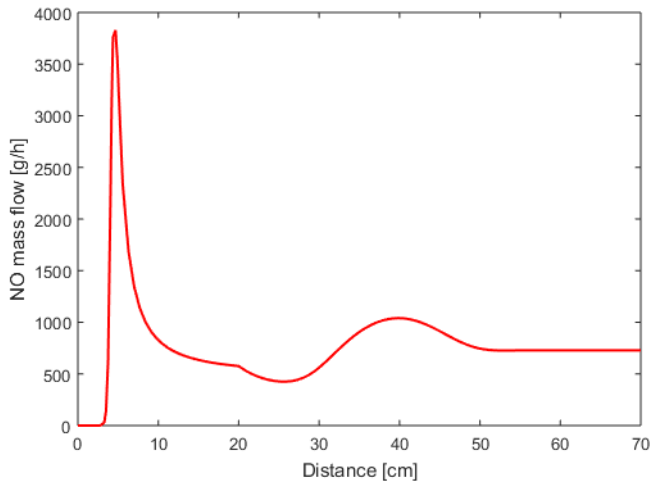


Figure B.3: NO mass flow for the NoMix case.

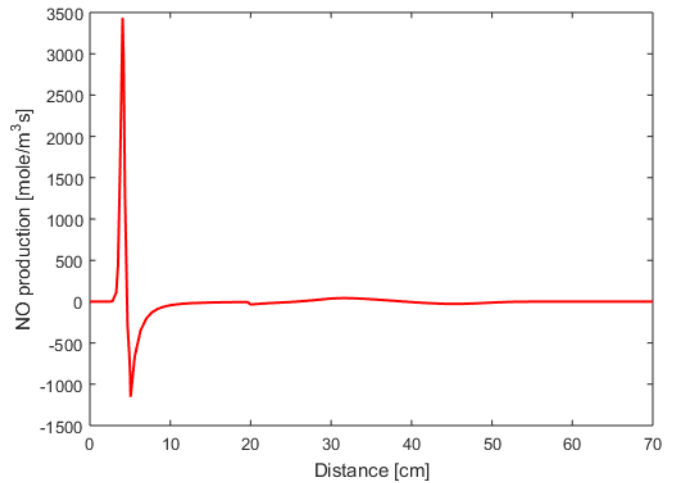


Figure B.4: NO production for the NoMix case.

B. Nitrogen oxide plots

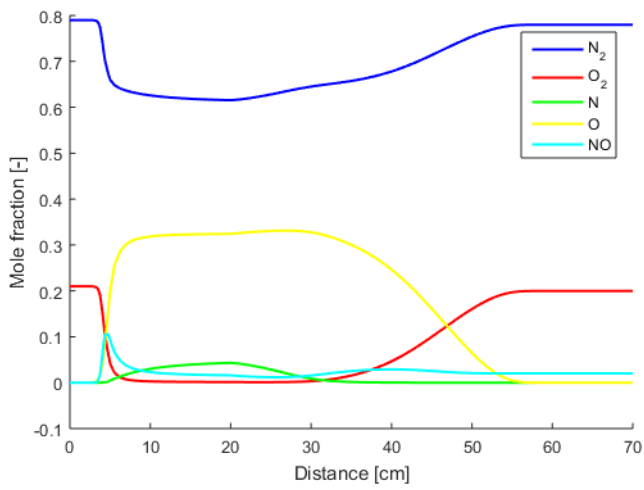


Figure B.5: Species concentration for the NoMix case.

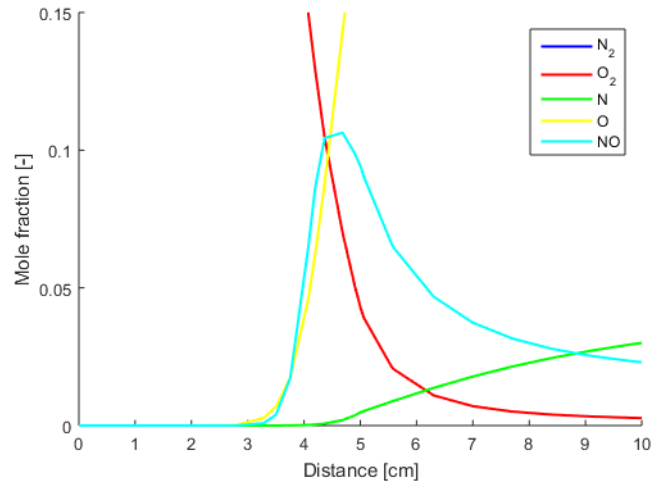


Figure B.6: Close-up of Figure B.5.

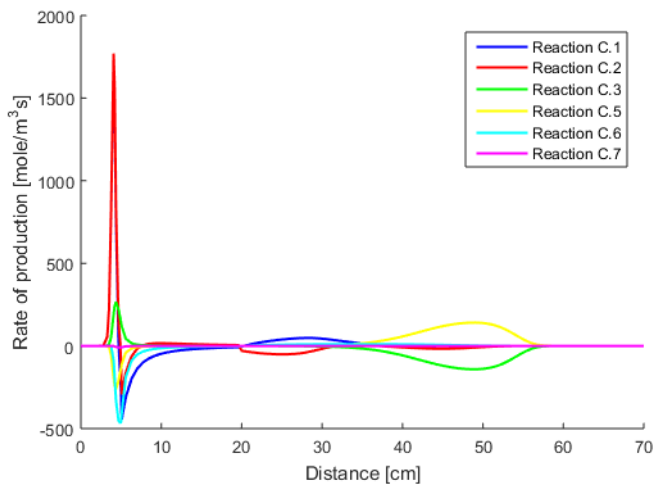


Figure B.7: Rate of production for the NoMix case.

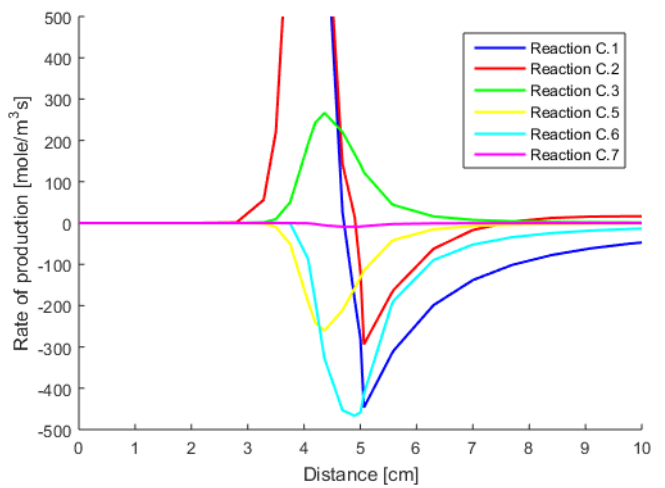


Figure B.8: Close-up of Figure B.7.

B.3 Mixing case (temperature profile)

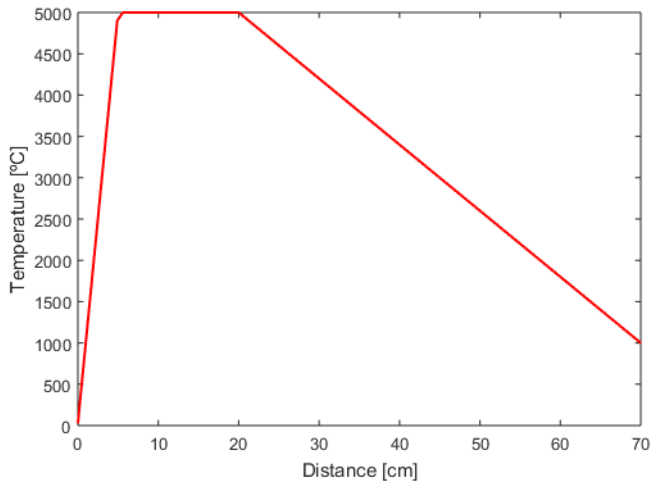


Figure B.9: Temperature profile for the MixTP case.

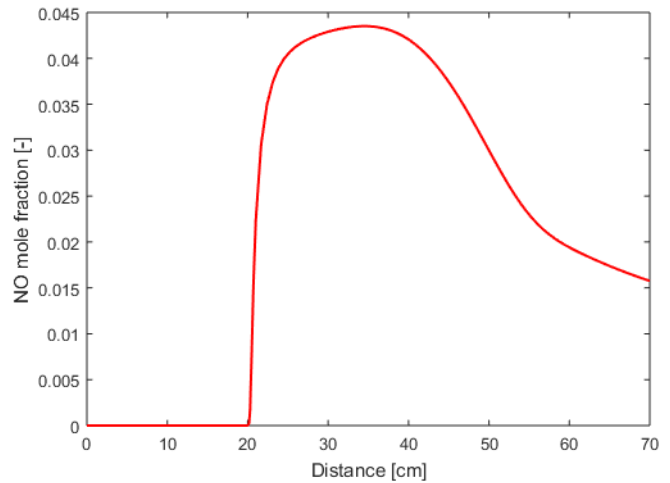


Figure B.10: NO concentration for the MixTP case.

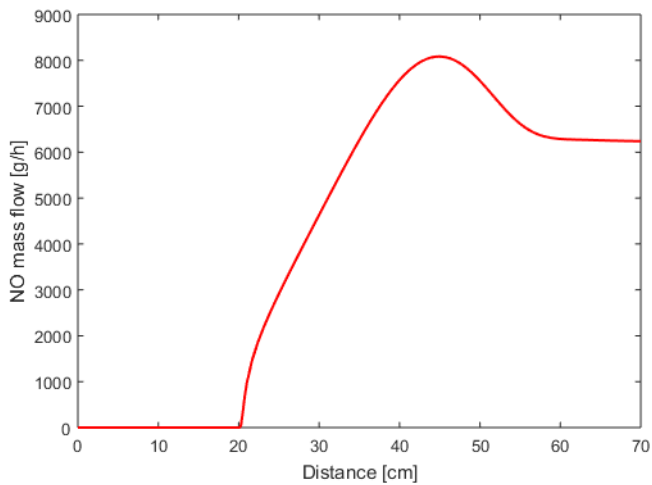


Figure B.11: NO mass flow for the MixTP case.

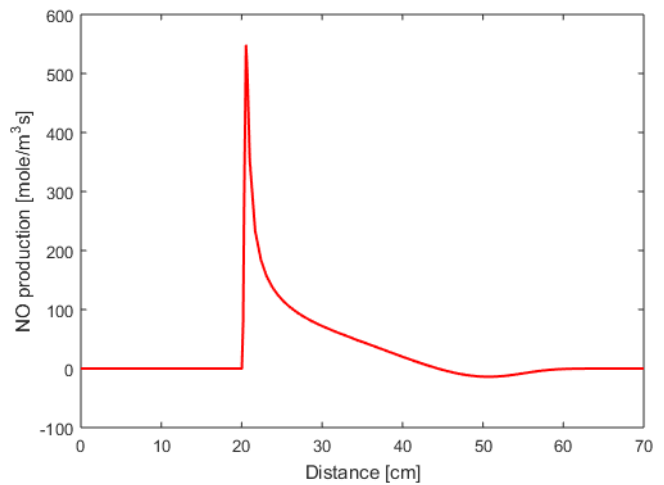


Figure B.12: NO production for the MixTP case.

B. Nitrogen oxide plots

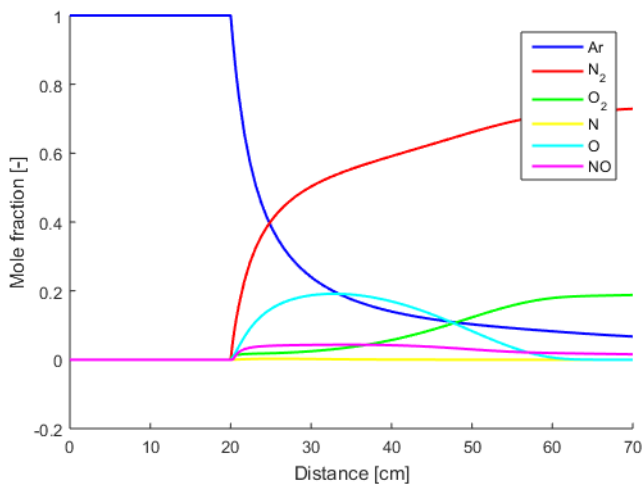


Figure B.13: Species concentration for the MixTP case.

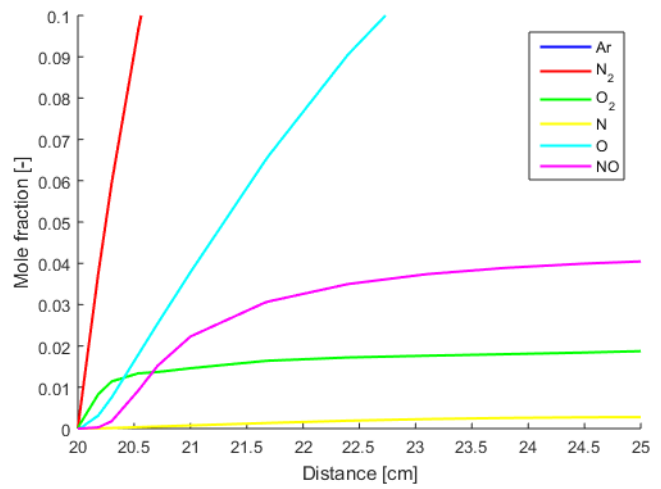


Figure B.14: Close-up of Figure B.13.

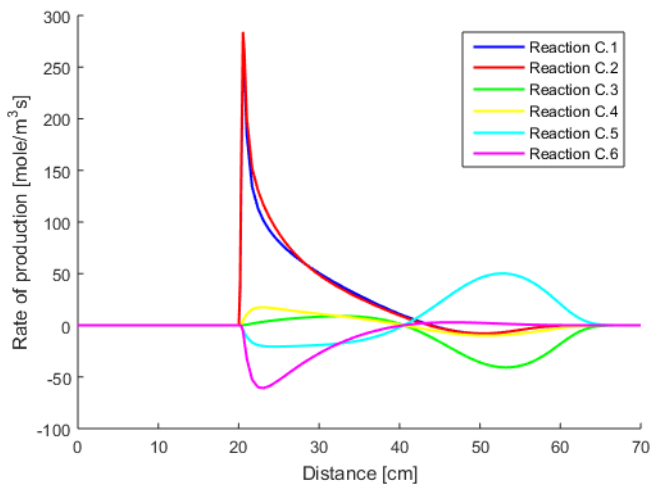


Figure B.15: Rate of production for the MixTP case.

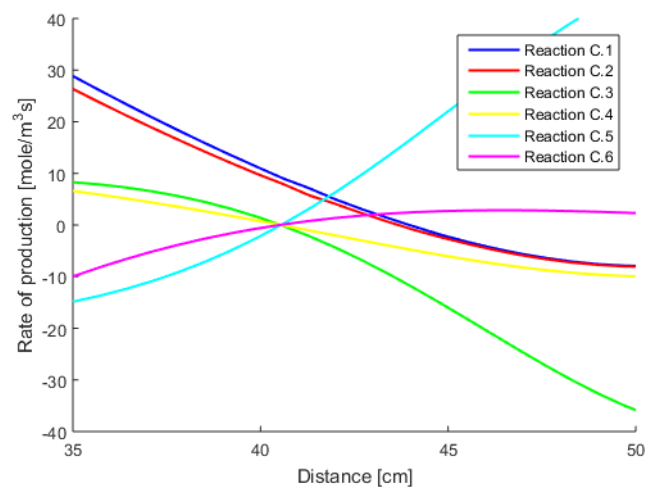


Figure B.16: Close-up of Figure B.15.

B.4 Mixing case (energy equation)

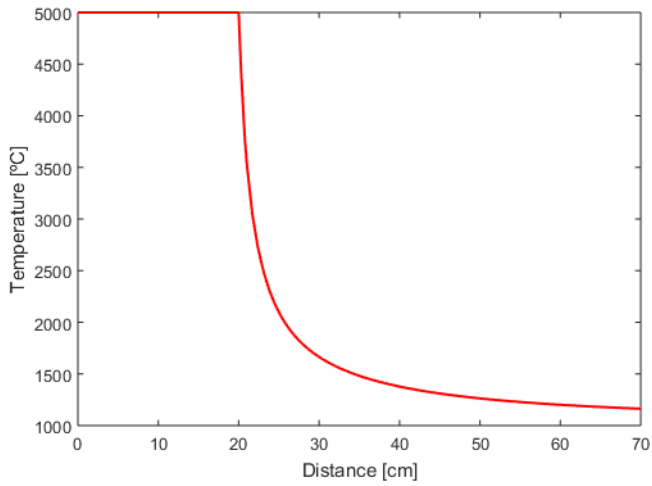


Figure B.17: Temperature profile for the MixEE case.

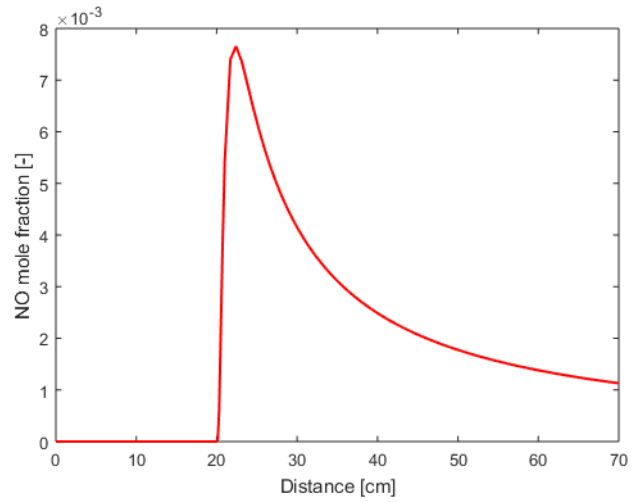


Figure B.18: NO concentration for the MixEE case.

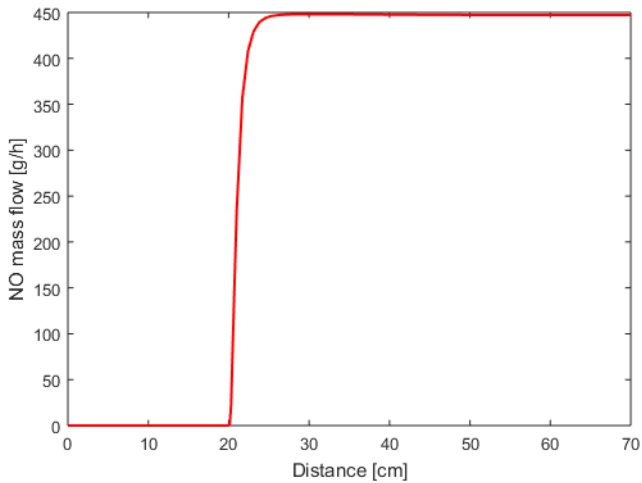


Figure B.19: NO mass flow for the MixEE case.

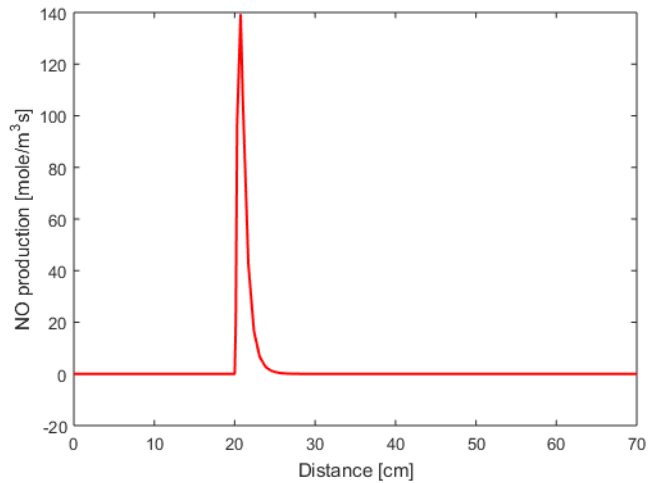


Figure B.20: NO production for the MixEE case.

B. Nitrogen oxide plots

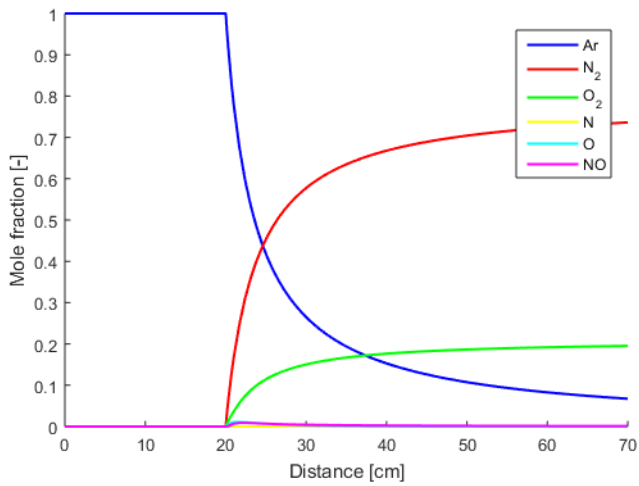


Figure B.21: Species concentration for the MixEE case.

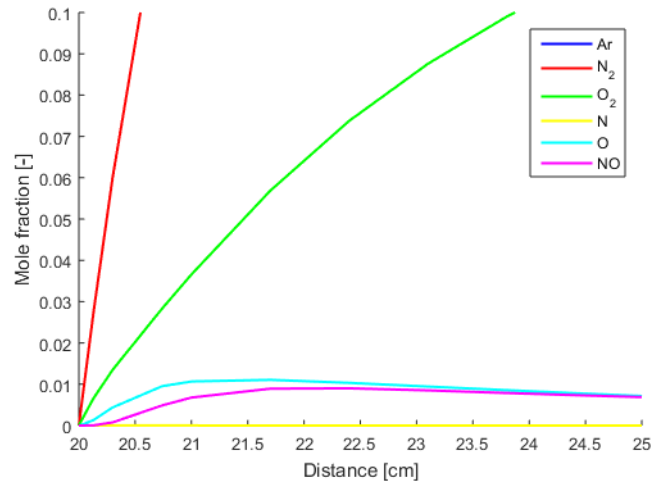


Figure B.22: Close-up of Figure B.21.

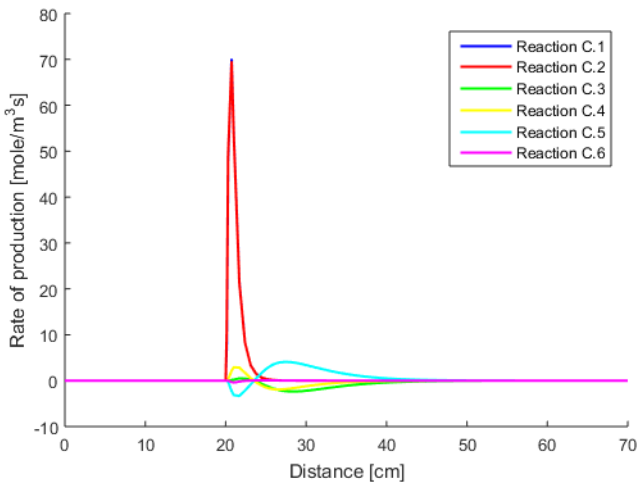


Figure B.23: Rate of production for the MixEE case.

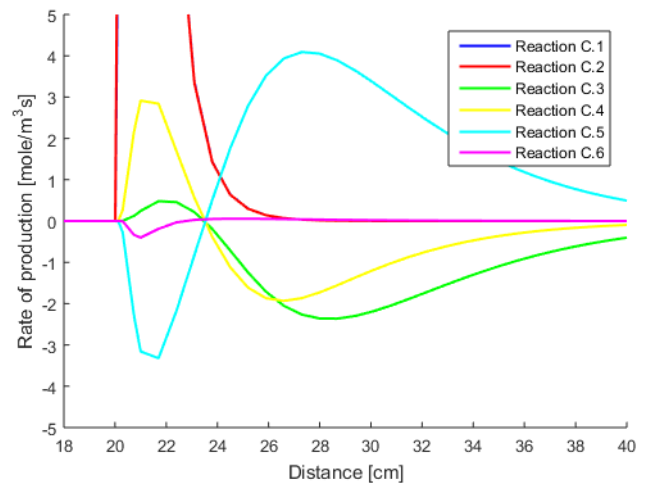


Figure B.24: Close-up of Figure B.23.